A computational multi-component method for modeling the evolution of size distribution functions and its application to cosmic dust grains

von

Dipl.-Phys. Daniel Krüger
aus Berlin

Vom Fachbereich 4 (Physik)
der Technischen Universität Berlin
zur Verleihung des akademischen Grades
Doktor der Naturwissenschaft
genehmigte Dissertation

Berlin 1997
D 83

Promotionsausschuß

Vorsitzender: Prof. Dr. P. Zimmermann
Berichter: Prof. Dr. E. Sedlmayr
Prof. Dr. S. Hess
Priv. Doz. Dr. J. P. Kaufmann

Tag der mündlichen Prüfung: 16.09.1997

Abstract

A general method for modeling the evolution of size distribution functions in stationary one-dimensional flows is derived without making prior assumptions about the particular physical processes involved. Various physical and chemical processes acting differently on particles of different size can be treated simultaneously. Furthermore, the particles are not assumed to be comoving but are allowed to exhibit size-dependent hydrodynamical velocities.

The numerical method is applied to several test problems where analytical solutions are known. It is found to be both highly accurate and computationally efficient. This is because the size distribution is discretized on a Lagrange-like grid which moves in size space according to the evolution of selected sample particles. Furthermore, a suitable discretization of the source term for particle coagulation guarantees that physical conservation laws like mass conservation are strictly obeyed.

The multi-component method is applied to model the formation and processing of cosmic dust grains considering three different astrophysical scenarios. First, dust formation in the cool envelopes around C-stars is investigated within the framework of a self-consistent model of a stationary dust driven wind. It is found that the consideration of drift results in a considerable distortion of the size distribution as compared to the case of zero drift velocity. Generally, there are less but larger grains if drift is included. The difference in characteristic quantities such as the increase of the mean grain mass and the dust-to-gas ratio injected into the ISM or the decrease of the dust optical depth due to dynamical dilution may amount to 50% for low mass loss models.

In a second application, dust growth and coagulation are treated in their mutual dependence. After identifying the two fundamental parameters determining the relative importance of either process a grid of model caluclations is presented. It is found that continuous growth processes always are very rapid as long as there is condensable material left in the gas phase. On the other hand, coagulation can lead to the formation of massive aggregates provided that the product of gas density and available time is sufficiently large. The efficiency of dust coagulation is maximum when the relative velocity between dust particles is equal to the critical velocity for sticking of the constituting grains of the dust aggregates.

Last not least, dust destruction in a protostellar accretion shock is investigated. The final grain size distribution after processing by the shock is computed as well as the shape of inbetween size distributions during grain processing. Essentially, it is found that large grains above a certain limit size a_{vap} remain almost unscathed while those below a_{vap} completely vaporize. In the case of an MRN distribution of silicate grains 38% of the total dust mass is returned to the gas phase for a shock velocity of 50 km/s.

The presented multi-component method is in no way restricted to the description of cosmic dust grains. In fact, there is a wide range of problems that can be cast in a form such that this new method is applicable.

Contents

List of Figures

List of Tables

Introduction

Dust is an omnipresent component of the interstellar medium (ISM). It is found, for instance, in the winds of late-type stars and thought to be responsible for the heavy mass loss of these objects. In fact, late-type stars — especially cool red giants — provide by far the largest contribution to the stellar mass injection rate into the ISM (Gehrz 1989), and thus can be regarded as the main sites of cosmic dust formation.

Once formed, existing grains may be processed in a variety of ways, both destructive and non-destructive. Interstellar shock waves, for one example, lead to mechanical and chemical sputtering, even complete vaporization (see Seab (1987) and Draine (1995) for a review). Furthermore, intense UV-fields and cosmic rays may change the chemical structure of the solid material (Ogmen & Duley (1988), Jenniskens et al. (1993), Bernstein et al. (1995)). On the other hand, grains in quiescent molecular clouds are coated by ice-mantles and, given sufficient time, tend to coagulate forming larger aggregates. Due to the volatile nature of such ice-mantles and the aggregates being prone to shattering even by moderately strong shock waves these processes can be classified as processing rather than formation.

Evolution of the dust component comes to a temporary halt only after the grains have been incorporated in meteoritic and cometic material or within other solar system bodies provided that the body is not large enough to experience significant radioactive heating as is known to have occured on the parent bodies of several classes of meteorites.

So, dust is also intimately linked with the question of the origin of life, since every theory of star and planetary system formation has to account for the role of dust as a cooling agent during cloud collapse and as constituting material of planets.

In summary, it can be said that dust plays a key role in the cosmic cycle of matter, and the structure, composition and size distribution of cosmic dust grains are of considerable importance for the understanding of many astrophysical issues. Unfortunately, observation yields little direct information about the nature of the dust and the life cycle of grains. A consistent modeling of the most important cosmic dust production and processing sites seems necessary to supplement observations and make possible their correct interpretation.

Consequently, we are in need of a detailed knowledge of the physical and chemical processes the dust grains are involved in, as well as efficient computational methods to describe these processes and the dust component itself.

There already exist a variety of methods that mainly concentrate on the description of certain aspects of dust formation and processing. A short overview will be given here as far as I am aware of their publication and without claim to completeness.

Gail & Sedlmayr (1984, 1988) have developed a rapid moment method to calculate dust formation and growth. This method was successively improved by including evaporation (Gauger et al. 1990), the treatment of heterogeneous and core-mantle grains (Dominik et al. 1993) and a formalism to derive the shape of the grain size spectrum (Dominik et al. 1989). However, for growth or destruction processes to be included in this scheme their grain size dependence has to vary proportional to some integer power of the grain radius a. Furthermore, the treatment of discontinuous processes which eliminate grains from the size distribution function is not possible. Thus, coagulation or fragmentation due to grain-grain collisions cannot be described by means of the moment method. Due to its rapidity the moment method could be successfully applied to model dust formation in the circumstellar envelopes of red giants (see the references above), novae (Beck et al. 1992) and supernovae (Woitke 1992).

In another approach Monte Carlo simulations are used to determine the grain size distribution (e.g. Daniels & Hughes 1981). Astrophysical applications include the modeling of cometary dust-tails (Fulle 1992) and grain processing in the ISM (Liffman & Clayton 1989, Liffman 1990). In principle, the use of Monte Carlo techniques allows for the treatment of virtually any desired growth or destruction process. However, such calculations require a large amount of computing time. It thus seems difficult to use these stochastic computer simulation methods in combination with iterative solution schemes for e.g. the hydrodynamic equations describing the astrophysical object under consideration.

The effects of grain-grain collisions on the grain size distribution are described by an integro-differential equation (Smoluchowsky 1917). This coagulation equation has been solved analytically in the steady state case (Dorschner 1982, Hayakawa & Hayakawa 1988). Elaborate time-dependent numerical calculations have been performed by several authors, e.g. Kessel'man & Frolov (1986), Mizuno et al. (1988), Wetherill & Stewart (1989) and Ohtsuki et al. (1990).

An advanced method for the description of dust processing in contracting protostellar clouds has been presented by Rossi et al. (1991), including a simultaneous treatment of grain-grain collisions *and* grain growth. Unfortunately, their approach has not been studied further. A similar method has been used by McKee et al. (1987) and Jones et al. (1994, 1996) to model grain destruction in shocks in the ISM.

All of the methods mentioned above either assume the center of mass of the dust component to be comoving with the gas or even treat the dust-gas mixture as a one-fluid, i.e. under the assumption of negligible net motion of the grains relative to the bulk of the gas (position coupling). With respect to the modeling of non-destructive processes there is another frequent shortcoming namely an incapability to simultaneously treat both continuous grain growth by accretion of gas particles and clustering of grains due to coagulation.

One aim of this thesis is to provide a general method of describing dust formation and processing and a corresponding numerical scheme that allows for the *simultaneous* consideration of a multitude of processes acting on the grains in case of a stationary one-dimensional (1D) flow. The grains are *not* assumed to be position coupled to the gas and a size-dependent, directed drift velocity is explicitly allowed for inducing effects such as the dynamical dilution of the dust component (Krüger et al. 1994).

In Chapter 1 a special differential form of a balance or conservation equation for the grain size distribution function is derived. A corresponding computational multi-component scheme is presented in Chapter 2 including some details on efficient implementation. Chapter 3 comprises some test calculations of the presented numerical method for cases where analytic solutions are — at least partly — known. First, grain sputtering behind dense shocks is investigated. Further test calculations have been performed for the coagulation equation in cases of simple coalescence rates.

Part II of this thesis is dedicated to the application of the presented multi-component method to several astrophysical problems. First, dust formation in the cool envelopes or red giant stars is investigated within the framework of a stationary dust driven wind model (Chapter 4). Special attention is paid to the influence of grain drift motion on the evolution of the size distribution. In Chapter 5 grain growth and dust coagulation under astrophysical conditions are treated simultaneously in their mutual dependence. By calculating a grid of models the space of relevant parameters is surveyed in order to determine the domains where either process dominates. As a last exemplary station of the life cycle of grains dust vaporization in a protostellar accretion shock is modeled in Chapter 6.

Finally, some brief conclusions are given at the end of this thesis, trying also to put the presented multi-component method in a wider perspective with regard to simulating the evolution of size distribution functions in general.

Part I

The multi-component method

Chapter 1

Evolution of the grain size distribution function

In this chapter a general equation for the value of the size distribution function as modified by different processes affecting the dust component will be derived. The dust particles are assumed to be characterized by a single, quasi-continuous parameter. In the following this parameter will be identified with the grain radius a, although other choices, e.g. the grain mass or volume are also conceivable. If the grains are, for instance, spherical and of uniform chemical composition, they can in fact be characterized by this sole parameter a.

Concerning the chemical and physical processes acting on the dust grains it will in the following be distinguished between *continuous* and *discontinuous* processes, respectively. Discontinuous processes abruptly change the size of the affected grains and/or alter their *number*, e.g. coagulation, shattering or (possibly complete) vaporization. Such processes are usually caused by grain-grain collisions.

In contrast, continuous processes are incessantly acting on the surface of a grain, slowly eroding or covering the outermost layer of the grain and thus smoothly changing its size. These processes include mechanisms such as homogeneous or heterogeneous (chemical) growth, thermal evaporation, chemical and mechanical sputtering etc. (cf. e.g. Gauger et al. 1990). Usually, continuous processes are those arising from interaction of the grain with the gas phase.

1.1 Flow assumptions and topology

A stationary flow is considered, and it is assumed that an appropriate coordinate system (p, q, r) can be chosen such that the flow is symmetric with respect to p and q. The sole independent variable is designated by r (1D formulation). Simple examples of such a flow geometry are a plane-parallel shock wave or a spherically symmetric outflow or infall, respectively. The description of thin viscous accretion disks is also possible. The hydrodynamics of such disks are considered one-dimensional, because the flow is independent of the angular coordinate and the coordinate perpendicular to the disk can often be discarded.

In order to mimic certain two-dimensional flows, e.g. collimated bipolar outflows, an equivalent quasi-spherical model can be adopted (Ruden et al. 1990). By means of this simplification of more complicated flow geometries the otherwise prohibitive computation of, for instance, non-equilibrium chemistry and dust formation is made possible.

The set of state variables describing the gas and the velocities $\vec{v}_{\rm d}(a,r)$ of grains with radius a are assumed to be known or obtained otherwise, i.e. by the solution of the corresponding equations.

1.2 The size evolution of a sample grain

Refraining from discontinuous processes, the net growth of a single dust grain of spatial dimension d and radius a consisting of N monomers is described by (Gauger et al. 1990)

$$\frac{{\rm d}N}{{\rm d}t} = \frac{1}{\tau_{\rm net}(N,t)} N^{\frac{d-1}{d}} \tag{1.1}$$

or, equivalently,

$$\frac{{\rm d}a}{{\rm d}t} = \frac{1}{\tau_{\rm net}(a,t)} \frac{a_0}{d} \tag{1.2}$$

where $\tau_{\rm net}^{-1}$ denotes the net growth rate and a_0 is the hypothetical radius of a monomer. $\tau_{\rm net}^{-1}$ comprises all types i of continuous processes to be considered and is simply given by

$$\tau_{\rm net}^{-1} = \sum_i \tau_i^{-1}. \tag{1.3}$$

In the stationary case Eq. (1.2) for the grain growth can be written as

$$\frac{{\rm d}a}{{\rm d}r} = \frac{1}{v_{\rm d}(a,r)} \frac{1}{\tau_{\rm net}(a,r)} \frac{a_0}{d} \tag{1.4}$$

where $v_{\rm d}(a,r)$ is the velocity component in r-direction of a grain of radius a. In the following the grain radius a will be refered to as grain "size" in order to avoid confusion with the independent variable r.

There are essentially two possibilities of modeling grain "creation" (cf. also Fig. 1.1): First, a dust particle of size a_* may be injected at the base r_0 of the flow, where the calculation starts. This will be the case when the processing of a given grain

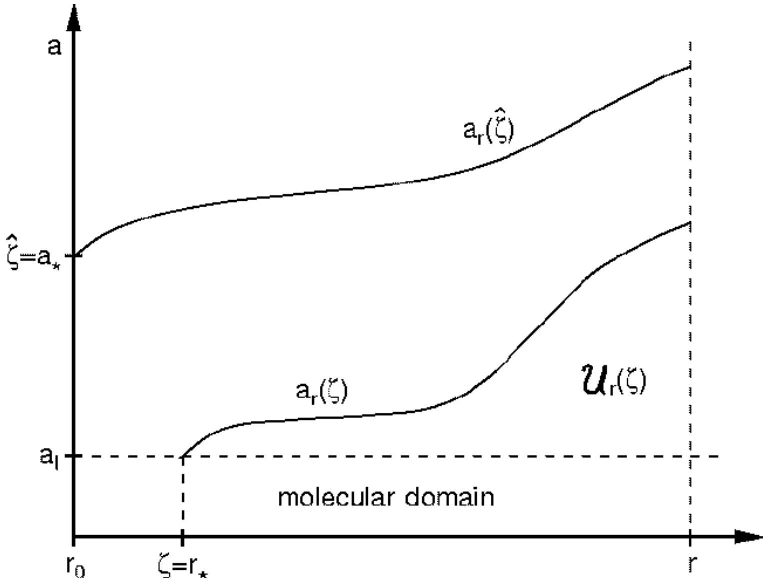

Figure 1.1: Size evolution $a_r(\zeta)$ of sample grains injected with size $\hat{\zeta} = a_*$ at r_0 or condensed from the gas phase at $\zeta = r_*$ with initial size a_ℓ, respectively. Also depicted is the subset $\mathcal{U}_r(\zeta)$ (see text).

size spectrum (e. g. that of the ISM) is to be investigated. On the other hand, for explicitly modeling grain *formation*, e.g. in the cool envelopes of red giants, small clusters condense out of the gas phase at $r = r_*$ (this process is refered to as nucleation). Introducing a lower limit a_ℓ of the size of macroscopic particles the dust component can be separated from the molecular domain and the growth species (cf. Gauger et al. 1990). If a cluster exceeds the size a_ℓ it is considered a newly created dust particle.

In order to keep a uniform notation and since both cases may occur in the same flow, the combined parameter ζ is introduced which is equal to either a_* or r_* depending on the specific model of grain "creation". The parameter ζ thus characterizes the initial condition upon "creation" of a grain.

At position r in the flow a specific sample grain will have grown to a size $a_r(\zeta)$ given by integration of Eq. (1.4)

$$a_r(\zeta) = a_* + \frac{a_0}{d} \int_{r_*}^{r} \frac{1}{v_\mathrm{d}(a_{r'}(\zeta), r')} \frac{1}{\tau_\mathrm{net}(a_{r'}(\zeta), r')} \mathrm{d}r' \tag{1.5}$$

where $r_* \equiv r_0$ if the particle is merely injected at the base of the flow and $a_* \equiv a_\ell$ for $r_* > r_0$, i.e. in case of nucleation. Equation (1.5) is well defined as long as $a_r(\zeta) \geq a_\ell$, otherwise the considered sample grain will be regarded as removed from the dust component by destructive continuous processes, e.g. due to evaporation.

It is important to notice here that in a stationary flow any grain created at a position $\hat{r}_* > r_*$ further downstream than an exemplary reference grain or with a smaller initial size $\hat{a}_* < a_*$ will at no point be larger than this reference grain, since as soon as it has grown up to the size of the reference grain all continuous growth and destruction processes for the two grains will be equal. In other words, grains can not "overtake" one another with respect to their size.

1.3 The fundamental balance equation

As stated above a stationary 1D flow is considered in a spatial domain

$$\mathcal{V} = [p_0; p_{\max}] \times [q_0; q_{\max}] \times [r_0; r_{\max}] \equiv \mathcal{P} \times \mathcal{Q} \times \mathcal{R}. \tag{1.6}$$

Let $f(a, r)$ be the size distribution of dust particles such that $f(a, r)\mathrm{d}a$ equals the number of particles per unit spatial volume in the grain size interval between a and $a + \mathrm{d}a$. In the four-dimensional vector space

$$\mathcal{W} = [a_\ell; a_{\max}] \times \mathcal{V} \equiv \mathcal{A} \times \mathcal{V} \tag{1.7}$$

the following balance or conservation equation holds for the size distribution function f in any subset $\mathcal{U} \subseteq \mathcal{W}$

$$\int_{\mathcal{U}} \nabla \bullet (\vec{u}(a, r) f(a, r))\, \mathrm{d}\mathcal{U} = \int_{\mathcal{U}} q(a, r)\, \mathrm{d}\mathcal{U} \tag{1.8}$$

where in the 1D formulation the nabla operator ∇ collapses to $(\partial/\partial a, 0, 0, \partial/\partial r)$ and $\vec{u} = (\dot{a}, \dot{p}, \dot{q}, \dot{r})$ denotes the four-velocity of grains in the vector space $\mathcal{W}$. Discontinuous processes creating or destroying grains of size a at r are described by the source term $q(a, r)$.

The volume element $\mathrm{d}\mathcal{U}$ of the four-dimensional vector space is given by

$$\mathrm{d}\mathcal{U} = \mathrm{d}a\, \mathrm{d}x\, \mathrm{d}y\, \mathrm{d}z \tag{1.9}$$

$$= \mathrm{d}a \left| \frac{\partial(x, y, z)}{\partial(p, q, r)} \right| \mathrm{d}p\, \mathrm{d}q\, \mathrm{d}r \tag{1.10}$$

where x, y, z signify cartesian coordinates. In order to perform the integration within a specific coordinate system (p, q, r) of the Jacobian determinant Δ of the corresponding spatial transformation is needed

$$\Delta = |J| = \left| \frac{\partial(x, y, z)}{\partial(p, q, r)} \right|. \tag{1.11}$$

In the 1D case this determinant can be factorized into two parts $\Delta_{p,q}$ and Δ_r. For spherical symmetry (i. e. $(p,q,r) = (\theta,\phi,r)$) for instance, $\Delta_{\theta,\phi} = \sin\theta$ and $\Delta_r = r^2$.

The balance equation (1.8) can thus be rewritten in the following way

$$\begin{aligned}&\int_p \mathrm{d}p \int_q \mathrm{d}q\, \Delta_{p,q} \cdot \int_a \mathrm{d}a \int_r \mathrm{d}r\, \nabla \bullet (\vec{u}(a,r) f(a,r))\Delta_r \\ &= \int_p \mathrm{d}p \int_q \mathrm{d}q\, \Delta_{p,q} \cdot \int_a \mathrm{d}a \int_r \mathrm{d}r\, q(a,r)\Delta_r \qquad (1.12)\end{aligned}$$

where the first double integrals on both sides are identical and can be omitted.

Now consider a specific subset $\mathcal{U}_r(\zeta) \subseteq \mathcal{W}$ chosen such that its upper boundary with respect to $\mathcal{A}$ is given by the size of a sample grains $a_r(\zeta)$ (cf. Fig. 1.1 showing a projection of $\mathcal{U}$ onto $\mathcal{A} \times \mathcal{R}$). Formally, $\mathcal{U}_r(\zeta)$ is given by

$$\mathcal{U}_r(\zeta) = \{(a,r') \mid r' \in [r_*; r] \wedge a \in [a_\ell; a_{r'}(\zeta)]\} \times \mathcal{P} \times \mathcal{Q} \qquad (1.13)$$

This choice of a trajectory $a_{r'}(\zeta)$ of a sample grain as one of the boundaries of $\mathcal{U}_r(\zeta)$ has the advantage that no flux of dust particles crosses that boundary of $\mathcal{U}_r(\zeta)$ (cf. Sect. 1.2). Refraining from discontinuous processes, grains are entering or leaving the subset $\mathcal{U}_r(\zeta)$ only via the boundaries where the dust particles are created and across the boundary at r where the size distribution function is to be evaluated.

By means of the Gauss law the balance equation (1.8) or (1.12), respectively, then reads

$$\begin{aligned}&\Delta_r \int_{a_\ell}^{a_r(\zeta)} \mathrm{d}a'\, v_\mathrm{d}(a',r) f(a',r) - \Delta_{r_0} \int_{a_\ell}^{a_*} \mathrm{d}a'\, J_0(a') - \int_{r_*}^{r} \mathrm{d}r'\, J_\ell(r')\Delta_{r'} \\ &= \int_{r_*}^{r} \mathrm{d}r'\, \Delta_{r'} \int_{a_\ell}^{a_{r'}(\zeta)} \mathrm{d}a'\, q(a',r') \qquad (1.14)\end{aligned}$$

where the flux-like quantities $J_0(a) \equiv v_\mathrm{d}(a,r_0) f(a,r_0)$ and $J_\ell(r) \equiv \dot{a}|_{a_\ell} f(a_\ell,r)$ were introduced. The latter can be identified with the rate of nucleation or evaporation, respectively, as defined by Gail & Sedlmayr (1988). The second term on the l. h. s. of Eq. (1.14) is equal to zero if the sample grain has been created by condensation from the gas phase at $r_* > r_0$. In the absence of discontinuous processes the integral on the r. h. s. vanishes.

In order to arrive at an expression for the value of the distribution function $f(a,r)$ Eq. (1.14) is formally differentiated with respect to ζ, noting that some limits of the integrals also depend on ζ. This finally yields the special differential balance or conservation equation for the grain size distribution

$$\begin{aligned}&-\Delta_{r_0} \frac{\mathrm{d}a_*}{\mathrm{d}\zeta} J_0(a_*) + \Delta_{r_*} \frac{\mathrm{d}r_*}{\mathrm{d}\zeta} J_\ell(r_*) + \Delta_r \frac{\mathrm{d}a_r(\zeta)}{\mathrm{d}\zeta} v_\mathrm{d}(a_r(\zeta),r) f(a_r(\zeta),r) \\ &= \int_{r_*}^{r} \mathrm{d}r'\, \Delta_{r'} \frac{\mathrm{d}a_{r'}(\zeta)}{\mathrm{d}\zeta} q(a_{r'}(\zeta),r') \equiv Q(a_r(\zeta),r). \qquad (1.15)\end{aligned}$$

If the sample grain has been "created" by injection, i.e. if $\zeta \equiv a_*$, the second term on the l. h. s. vanishes and $\mathrm{d}a_*/\mathrm{d}\zeta = 1$, while for a sample grain condensed at $r_* > r_0$ the first term is identical to zero and $\mathrm{d}r_*/\mathrm{d}\zeta = 1$.

In principle, the size distribution f can be calculated from this equation at any point r and for every size $a = a_r(\zeta)$. However, as $a_r(\zeta)$ is actually an integrated quantity (cf. Eq. (1.5)) depending on $a_{r'}(\zeta)$ for $r' < r$, Eq. (1.15) represents an integro-differential equation and the derivatives of $a_r(\zeta)$ are not readily obtained. The computational multi-component scheme presented in Sect. 2 comprises the evaluation of these derivatives by finite differences on a non-uniform $a_r(\zeta_i)$-grid which is moving in the grain size space $\mathcal{A}$. This grid is constructed by following the size evolution of a large, variable number of grains injected at r_0 and/or originating from appropriately chosen radii $r_* = r_i$.

1.4 Processes affecting the grain size distribution

As stated above it is distinguished between continuous and discontinuous processes acting on a grain. In this subsection it will be briefly described how these classes of processes can be taken into account in the general balance equation. For a review of grain growth and destruction processes see, for example, Seab (1987).

1.4.1 Continuous processes

The treatment of continuous processes such as growth or sputtering is an inherent feature of the approach presented above. These processes are taken into consideration by simply including their corresponding grain growth or reduction rates, respectively, in Eq. (1.4) for the evolution of a sample grain size. The derivative of this sample grain size directly affects the value of the distribution function via the basic Eq. (1.15).

General expressions for the rates of grain growth and evaporation as well as chemical sputtering have been derived by Gauger et al. (1990). Applying their concepts, Dominik et al. (1993) specifically investigated the continuous processes for anorganic grains. A physical description of carbonaceous grain growth has been presented by Krüger et al. (1996). The necessary modifications of the sticking efficiencies due to drift motion of the grains relative to the gas can be found in Krüger & Sedlmayr (1997) (cf. also Chapter 4). Regarding the destructive continuous processes Lenzuni et al. (1995) reviewed the thermodynamics and the kinetics of chemisputtering and sublimation. Furthermore, Tielens et al. (1994) reanalyzed grain sputtering and provided thermal and nonthermal (or mechanical) sputtering yields based upon extensive laboratory studies.

1.4.2 Discontinuous processes

Grain processing due to discontinuous processes such as coagulation, (possibly complete) vaporization or shattering is represented by a source term $q(a,r)$ in Eq. (1.15). Unfortunately, there seems to be little experimental data on reaction probabilities or yields available (cf. Seab 1987). However, Tielens and coworkers have made impressive progress studying grain-grain collisions by means of analytical models. Coagulation, for example, has been thoroughly investigated by Chokshi et al. (1993) and Dominik & Tielens (1997). Tielens et al. (1994) determine the fraction of a grain vaporized by a grain-grain collision. Furthermore, in a recent paper by Jones et al. (1996) the fragment size distribution resulting from grain shattering is related to the relative velocity and grain sizes of projectile and target.

Here, an expression for $q(a,r)$ corresponding to coagulation is stated as an exemplary source function. Actually, $q(a,r)$ is a Boltzmann type collision term accounting for gains and losses from the size range $[a; a + \mathrm{d}a]$. According to Völk et al. (1980) it is of the form

$$\begin{aligned} q(a,r) = &-f(a,r)\int_{a_\ell}^{a_{\max}} \mathrm{d}a'\, f(a',r)\Omega(a,a',r) \\ &+ \frac{1}{2}\int_{a_\ell}^{a} \mathrm{d}a'\, f(a',r)f(\bar{a},r)\left(\frac{a}{\bar{a}}\right)^2 \Omega(a',\bar{a},r) \end{aligned} \tag{1.16}$$

where $\bar{a}^3 \equiv a^3 - a'^3$ due to mass conservation. The reaction frequency $\Omega(a,a',r)$ per unit density is given by the product of the collisional cross-section and the r.m.s. of the sticking probability α and the relative velocity v_{rel} of the grains

$$\Omega(a,a',r) = \pi(a+a')^2\langle[\alpha(a,a',r)v_{\mathrm{rel}}(a,a',r)]^2\rangle^{1/2}. \tag{1.17}$$

In the limit case of high size dependent drift velocities in r-direction $v_{\mathrm{rel}}(a,a',r) = v_{\mathrm{d}}(a,r) - v_{\mathrm{d}}(a',r)$. In the opposite case of vanishing drift in r-direction, v_{rel} may be given by isotropic relative velocities due to a Brownian motion of the grains or turbulent gas motion (cf. Völk et al. 1980). Please note, however, that according to the results of Chokshi et al. (1993) the sticking probability of colliding grains is zero for $|v_{\mathrm{rel}}| > v_{\mathrm{cr}} \sim 10^2$ cm s^{-1} (cf. Chapter 5 for a more detailed discussion of this point).

1.5 Summary

In this chapter a differential form of a balance or conservation equation for the grain size distribution function was derived. In contrast to other approaches on the subject of grain processing, this equation is not only applicable in those regimes where either growth or coagulation dominates the evolution of the size distribution. Instead, all processes acting on the grains can be treated simultaneously, also taking into account that grains of different size may move and be processed differently. This makes possible a more detailed treatment of such effects as the size dependence of grain temperature and charge on the processing of the distribution function. Moreover, distinct spatial geometries and symmetries of the flow can be taken into account as long as there is only one independent spatial coordinate.

Chapter 2

The computational multi-component scheme

So far the presented approach was completely analytic; no errors due to discretization etc. have been introduced during the derivation of the fundamental balance or conservation equation (1.15). However, in order to evaluate this equation, i.e. to calculate the size distribution at r and for $a = a_r(\zeta)$, one has to calculate the derivatives of $a_r(\zeta)$ with respect to ζ. To do this, one follows the size evolution of a large number of sample grains, i.e. for each sample grain an ordinary differential equation (ODE) of type (1.4) is integrated advancing the solution with increasing r. In this way a moving, non-uniform grid in grain size space $\mathcal{A}$ is constructed, its points being identified with the momentary sizes $a_r(\zeta_i)$ of sample grains.

If nucleation or complete thermal evaporation of grains is to be considered, the number of sample grains and, hence, the number of ODE's to be solved successively increases or decreases, respectively. The grid in grain size space $\mathcal{A}$ then not only varies in position but also in size.

2.1 Grid generation

It is obviously difficult to give some general advice on an appropriate choice of grid points since this strongly depends on the specific problem to be solved. In case of the mere processing of a given size distribution, i.e. if all sample grains are injected at the base r_0 of the flow and no further nucleation takes place, a logarithmically spaced a_i-grid serving as initial conditions $a_{*,i}$ for the system of ODE's of type (1.4) (henceforth called grid point equations) should suffice. The number of grid points I, i.e. the dimension of the system of ODE's, then depends on the desired resolution.

If, additionally or instead, nucleation is to be treated the number of grid points I is not constant anymore. During the integration of the grid point equations their number is successively incremented whenever one chooses to add a new grid point $a_r(\zeta_i)$ at $r_i \equiv r_{*,i}$. This is done to account for the continuous increase of the number density of grains due to condensation of small clusters from the gas phase.

There are several possible criteria to decide whether a new grid point should be added: for example, whenever the state variables of the gas have changed by a certain fraction or whenever a certain amount of dust has been newly formed. An estimate for the expected final size $a_\infty(r_i)$ of a grains formed at r_i may also serve as a useful guide. For example, Dominik et al. (1989) derived a final grain size estimate in quickly expanding flows

$$a_\infty(r) \approx \left(\frac{\mathrm{d}\tau_{\mathrm{net}}(r)}{\mathrm{d}r}\right)^{-1} \Big/ v_{\mathrm{d}}(r) a_0 \tag{2.1}$$

where τ_{net} and v_{d} have been assumed to be independent of the grain size a by these authors.

Now, given the availability of a final grain size estimate, a new grid point is added when the estimated final size of a grain condensing at the momentary position r is smaller than a certain fraction of the estimated final size of the previous sample grain created at r_I

$$\log a_\infty(r_I) - \log a_\infty(r) > \delta \quad \rightarrow \quad \texttt{create grid point} \tag{2.2}$$

The value of δ is chosen according to the desired resolution of the grain size distribution at infinity. In order to achieve a final number $I_{\max}$ of grid points one puts

$$\delta = \frac{\log a_\infty(r_1) - \log a_\ell}{I_{\max} - 1} \tag{2.3}$$

corresponding to a roughly logarithmically equidistant grid in grain size space $\mathcal{A}$ at the end of computation.

As stated in Sect. 1.2 sample grains may also be removed from the gas phase due to destructive continuous processes like sputtering or thermal evaporation. This will happen, for instance, in the accretion disks around protostellar objects (cf. Chapter 6). In this case, the number I of grid equations will be successively decremented as the smaller grains are destroyed.

$$a_r(\zeta_I) < a_\ell \quad \rightarrow \quad \texttt{remove grid point} \tag{2.4}$$

Since the grain size grid points are identified with the momentary size $a_r(\zeta_i)$ of sample grains, the grid points move through the grain size space $\mathcal{A}$ according to the evolution of the dust component and the size distribution function f should always be well resolved. In the rare case where neighbouring grid points become too far apart or too close, finer or coarser resolution can be easily achieved by insertion or removal, respectively, of grid points.

Concerning the insertion of grid points this remapping or rezoning procedure involves simple linear interpolation of the grain size distribution function at the desired new grid point $a_r(\hat{\zeta})$. This introduces discretization errors of second order in the grain size separation $a_r(\zeta_i) - a_r(\zeta_{i+1})$ as do all other numerical schemes employed in the presented multi-component approach. The corresponding initial parameter $\hat{\zeta}$ of the new sample grain is obtained through integration of Eq. (1.4) backward in r-direction until $r = r_0$ or $a_r(\hat{\zeta}) = a_\ell$.

2.2 Numerical differentiation by finite differences

The relevant derivatives in the fundamental balance equation (1.15) can now be approximated by the analytic derivative of the Lagrange interpolating polynomial of degree two passing through the set of points $\{\zeta_j, a_r(\zeta_j)\}$ with $j = i-1, i, i+1$

$$\begin{aligned}\frac{\mathrm{d}a_r(\zeta_i)}{\mathrm{d}\zeta_i} &= -\frac{h_i}{h_{i-1}(h_{i-1}+h_i)}a_r(\zeta_{i-1}) + \frac{h_i - h_{i-1}}{h_i h_{i-1}}a_r(\zeta_i) \\ &+ \frac{h_{i-1}}{h_i(h_{i-1}+h_i)}a_r(\zeta_{i+1}) \end{aligned} \tag{2.5}$$

where $h_i \equiv \zeta_{i+1} - \zeta_i$. At the first and at the last grid point ($i = 1$ and $i = I$, respectively) the set of points is adjusted by choosing $j = 1, 2, 3$ and $j = I-2, I-1, I$ yielding similar formulae. The discretization error of this finite difference scheme is of second order in h_i.

Obviously, I has to be larger than 2 for this scheme to be applied at all. Thus, in case of an initially dust-free medium no information about the size distribution can be obtained during the initiation of the multi-component method. Consequently, the first three grid points should be generated in rather quick succession after the onset of nucleation.

2.3 Discontinuous processes

For the treatment of discontinuous processes due to grain-grain collisions the computational quantity $Q(a_r(\zeta_i), r)$ in the fundamental balance equation (1.15) needs to be calculated. This is most efficiently done by solving one additional ODE per grid point, namely

$$\frac{\mathrm{d}Q(a_r(\zeta_i), r)}{\mathrm{d}r} = \Delta_r \frac{\mathrm{d}a_r(\zeta_i)}{\mathrm{d}\zeta_i} q(a_r(\zeta_i), r) \tag{2.6}$$

where the derivative of $a_r(\zeta_i)$ with respect to ζ_i is evaluated as described in Sect. 2.2. The initial value of Q at the time of grid point creation is always zero.

An appropriate discretization of the physical source function $q(a_r(\zeta_i), r)$ depends on the considered discontinuous process. As an example, an efficient method for numerically treating dust coagulation will be presented.

2.3.1 Discretization of the coagulation source term

The analytic form of the corresponding source function q has already been given in Sect. 1.4.2, where the grain radius a was used to characterize the dust particles. As has been emphasized before (cf. page 7), other choices such as grain mass or volume are equally possible. It is up to the user to decide which parameter renders the formulation of the considered problem most appropriate. With regard to coagulation, the grain mass m is most suitable, since the mass of a grain resulting from coagulation is just given by the sum of the masses of the colliding grains. Equation (1.16) then has the form (Smoluchowsky 1917)

$$\begin{aligned} q(m,r) &= -f(m,r)\int_{m_\ell}^{m_{\max}} \mathrm{d}m'\, f(m',r)\Omega(m,m',r) \\ &\quad + \frac{1}{2}\int_{m_\ell}^{m} \mathrm{d}m'\, f(m',r)f(m-m',r)\Omega(m',m-m',r) \qquad (2.7) \\ &\equiv q^{(-)}_{\mathrm{coag}}(m,r) + q^{(+)}_{\mathrm{coag}}(m,r) \qquad (2.8) \end{aligned}$$

where $q^{(-)}_{\mathrm{coag}}(m,r)$ and $q^{(+)}_{\mathrm{coag}}(m,r)$ denote the loss and the gain term describing the removal and creation of grains of mass m, respectively.

The first integral is easily discretized by means of the extended trapezoidal rule

$$\begin{aligned} & q^{(-)}_{\mathrm{coag}}(m_r(\zeta_i),r) = -f(m_r(\zeta_i))\cdot \\ &\quad \Big\{ f(m_r(\zeta_1),r)\,\Omega(m_r(\zeta_i),m_r(\zeta_1),r)\,[m_r(\zeta_1)-m_r(\zeta_2)]/2 \\ &\quad + \sum_{j=2}^{I-1} f(m_r(\zeta_j),r)\,\Omega(m_r(\zeta_i),m_{r(\zeta_j)},r)\,[m_r(\zeta_{j-1})-m_r(\zeta_{j+1})]/2 \\ &\quad + f(m_r(\zeta_I),r)\,\Omega(m_r(\zeta_i)m_r(\zeta_I),r)\,[m_r(\zeta_{I-1})-m_r(\zeta_I)]/2 \Big\}. \qquad (2.9) \end{aligned}$$

The discretization error of this rule is of second order in grain mass separation $m_r(\zeta_i)-m_r(\zeta_{i+1})$. Thus, the proposed discretization scheme is accurate to the same order as the numerical differentiation scheme (cf. Sect. 2.2).

In order to keep the notation simple, the following abbreviations will be used in the remainder of this section

$$\begin{aligned} m_r(\zeta_i) &\equiv m_i \\ f(m_r(\zeta_i),r) &\equiv f_i \\ \Omega(m_r(\zeta_i),m_r(\zeta_j),r) &\equiv \Omega_{ij} \\ [m_r(\zeta_1)-m_r(\zeta_2)]/2 &\equiv \Delta m_1 \\ [m_r(\zeta_{i-1})-m_r(\zeta_{i+1})]/2 &\equiv \Delta m_i \qquad i=2,\ldots,I-1 \\ [m_r(\zeta_{I-1})-m_r(\zeta_I)]/2 &\equiv \Delta m_I \end{aligned}$$

where the quantity Δm_i can be regarded as the support of the i-th segment of the continuous distribution function. Equation (2.9) now reads

$$q^{(-)}_{\rm coag}(m_i, r) = -f_i \sum_j f_j \Omega_{ij} \Delta m_j \tag{2.10}$$

Efficient computation of the *gain* term $q^{(+)}_{\rm coag}(m, r)$ is more difficult due to the fact that the mass $\bar{m} \equiv m - m'$ will generally not coincide with an actual sample grain mass. Employing the above approach of directly discretizing the integral is possible in principle. However, this involves some interpolation of f on the grain size grid m_i in order to determine, for example, the value of $f(\bar{m}, r)$.

Here, another approach[1] is taken which sets out from a more basic formulation of the Boltzmann type collision term $q^{(+)}_{\rm coag}$ than given in Eq. (2.7)

$$\begin{aligned} & q^{(+)}_{\rm coag}(m, r)\mathrm{d}m\,\mathrm{d}r = \\ & \quad \frac{1}{2} \int_{m'} \int_{m''} f(m', r)\mathrm{d}m'\, f(m'', r)\mathrm{d}m''\, \omega(m', m'' \to m)\mathrm{d}m\,\mathrm{d}r. \end{aligned} \tag{2.11}$$

The abstract quantity $\omega(m', m'' \to m)$ is the transition rate of grains of masses m' and m'' into one grain of mass m not necessarily equal to $m' + m''$. However, due to mass conservation m *is* always equal to $m' + m''$ in the case of coagulation. Thus, the transition rate ω is related to the reaction frequency Ω (cf. Eq. (1.17)) by

$$\omega(m', m'' \to m) = \Omega(m', m'')\delta(m - m' - m'') \tag{2.12}$$

where δ denotes the standard Dirac distribution.

Equation (2.11) is equivalent to textbook definitions of the Boltzmann collision term for gas particles (e.g. Mihalas & Weibel Mihalas 1984), except for the fact that there is only one reaction product and not two post-collision particles as in the kinetic theory of gases. This effective elimination of half the coagulating grains is also the reason for the factor 1/2 on the r. h. s. of Eq. (2.11).

In order to resolve the Dirac distribution, Eq. (2.11) is multiplied with a piecewise linear shape function (hat function)

$$\Lambda_k(m) \begin{cases} 0 & : \quad m \le m_{k-1} \quad \text{or} \quad m \ge m_{k+1} \\ \frac{m - m_{k-1}}{m_k - m_{k-1}} & : \quad m_{k-1} < m \le m_k \\ \frac{m_{k+1} - m}{m_{k+1} - m_k} & : \quad m_k < m < m_{k+1} \end{cases} \tag{2.13}$$

[1] Actually, this approach also works for the discretization of the loss term $q^{(-)}_{\rm coag}$.

and integrated over m, i.e. $q_{\rm coag}(m,r)$ is sampled at the gridpoint m_k

$$\int_m \Lambda_k(m) q^{(+)}_{\rm coag}(m,r) {\rm d}m\,{\rm d}r = \frac{1}{2}\int_{m'}\int_{m''} f(m',r){\rm d}m'\, f(m'',r){\rm d}m''$$
$$\int_m \Lambda_k(m)\Omega(m',m'')\delta(m-m'-m''){\rm d}m\,{\rm d}r \tag{2.14}$$

Evaluation of the last integral yields $\Lambda_k(m'+m'')\Omega(m',m'')$, i.e. it is zero unless $m'+m''$ is bracketed by m_{k-1} and m_{k+1}. Now the remaining integrals in Eq. (2.14) are again approximated by means of the extended trapezoidal rule resulting in

$$q^{(+)}_{\rm coag}(m_k,r) = \frac{1}{2\Delta m_k}\sum_i\sum_j f_i\Delta m_i\, f_j\Delta m_j\, \Lambda_k(m_i+m_j)\Omega_{ij}. \tag{2.15}$$

From a computational point of view, the I^3 evaluations of Λ-functions needed to calculate $q^{(+)}_{\rm coag}$ for all k is somewhat awkward, involving the testing of many `if`-conditions. An efficient and more process-oriented way of implementing the gain term (2.15) is to compute $q^{(+)}_{\rm coag}(m_k,r)$ for all k in parallel by executing two nested loops over i and j. Each pair of coagulating grain masses m_i and m_j results in a grain of mass $m = m_i + m_j$ which is bracketed by a lower and an upper sample grain mass, denoted by m_{low} and m_{upp}, respectively, i.e. $m_{low} < m_i + m_j < m_{low+1} = m_{upp}$. The fractional contribution of this elementary process to each of the gain terms $q^{(+)}_{\rm coag}(m_{low},r)$ and $q^{(+)}_{\rm coag}(m_{upp},r)$ is proportional to the weights $\Lambda_{low}(m_i+m_j)$ and $\Lambda_{upp}(m_i+m_j)$. This procedure reduces the numerical effort to second order in I.

2.3.2 Observance of conservation laws

Obviously, coagulation does not conserve the number of grains as such. However, the number of grains eliminated from the size distribution function is always exactly double the number of grains created, which can be formally expressed as

$$\int_{m_\ell}^{m_{\rm max}} q^{(-)}_{\rm coag}(m,r) + 2q^{(+)}_{\rm coag}(m,r)\,{\rm d}m = 0. \tag{2.16}$$

In order to test the consistency of the proposed discretization scheme with regard to discontinuous processes, it will be shown that the criterion (2.16) is fulfilled when the integral is approximated by the extended trapezoidal rule. Inserting the discretized expressions for $q^{(-)}_{\rm coag}(m_k,r)$ and $q^{(+)}_{\rm coag}(m_k,r)$, Eqs. (2.10) and (2.15), it follows that

$$
\begin{aligned}
&\sum_k \left\{q^{(-)}_{\text{coag}}(m_k,r) + 2q^{(+)}_{\text{coag}}(m_k,r)\right\}\Delta m_k \\
&\quad= \; -\sum_k f_k\Delta m_k \sum_j f_j\Omega_{kj}\Delta m_j + \sum_k\sum_i\sum_j f_i\Delta m_i\, f_j\Delta m_j\, \Lambda_k(m_i+m_j)\Omega_{ij} \\
&\quad= \; -\sum_k\sum_j f_k\Delta m_k\, f_j\Delta m_j\, \Omega_{kj} + \sum_i\sum_j f_i\Delta m_i\, f_j\Delta m_j\, \Omega_{ij}\sum_k \Lambda_k(m_i+m_j) \\
&\quad= \; \sum_i\sum_j f_i\Delta m_i\, f_j\Delta m_j\, \Omega_{ij}\sum_k\left\{\Lambda_k(m_i+m_j)-1\right\} \\
&\quad= \; \sum_i\sum_j f_i\Delta m_i\, f_j\Delta m_j\, \Omega_{ij}\left\{\Lambda_{low}(m_i+m_j)+\Lambda_{upp}(m_i+m_j)-1\right\} \\
&\quad= \; 0 \qquad (2.17)
\end{aligned}
$$

where *low* and *upp* are the indices of those consecutive grid points which bracket $m = m_i + m_j$. This important result means, that the presented computational scheme consistently describes the evolution of the total grain number within the limitations of the second order approximation of the integral.

The conservation of the total mass of the dust component is expressed by an equation similar to Eq. (2.16)

$$\int_{m_\ell}^{m_{\max}} m q^{(-)}_{\text{coag}}(m,r) + m q^{(+)}_{\text{coag}}(m,r)\,\mathrm{d}m = 0. \qquad (2.18)$$

Proceeding in an analogous manner as above, it can be shown that mass conservation of the dust is an inherent property of the algorithm and thus numerically guaranteed

$$
\begin{aligned}
&\sum_k \left\{m_k q^{(-)}_{\text{coag}}(m_k,r) + m_k q^{(+)}_{\text{coag}}(m_k,r)\right\}\Delta m_k \\
&\quad= -\sum_k m_k f_k\Delta m_k \sum_j f_j\Omega_{kj}\Delta m_j + \sum_k \frac{m_k}{2}\sum_i\sum_j f_i\Delta m_i f_j\Delta m_j \Lambda_k(m_i+m_j)\Omega_{ij} \\
&\quad= -\sum_k\sum_j m_k f_k\Delta m_k f_j\Delta m_j\Omega_{kj} + \sum_i\sum_j f_i\Delta m_i f_j\Delta m_j\Omega_{ij}\sum_k\frac{m_k}{2}\Lambda_k(m_i+m_j) \\
&\quad= -\sum_i\sum_j m_i f_i\Delta m_i\, f_j\Delta m_j\,\Omega_{ij} + \sum_i\sum_j f_i\Delta m_i\, f_j\Delta m_j\,\Omega_{ij}\frac{m_i+m_j}{2} \\
&\quad= \sum_i\sum_j f_i\Delta m_i\, f_j\Delta m_j\,\Omega_{ij}\frac{m_j-m_i}{2} \\
&\quad= \sum_i\sum_{j<i} f_i\Delta m_i\, f_j\Delta m_j\left\{\Omega_{ij}\frac{m_j-m_i}{2} + \Omega_{ji}\frac{m_i-m_j}{2}\right\} \\
&\quad= 0 \qquad (2.19)
\end{aligned}
$$

since the reaction frequency for coagulation (1.17) is symmetric with respect to its grain size arguments.

2.4 Derived macroscopic quantities of the dust component

It is now possible to calculate the size distribution function by means of the fundamental balance equation (1.15). One only has to keep track of the evolution of the sample grain sizes $a_r(\zeta_i)$ and of the quantities $Q(a_r(\zeta_i), r)$ accounting for discontinuous processes and to take care of storing the quantities ζ_i and $\Delta_{r_0} J_0(a_i)$ or $\Delta_{r_i} J_\ell(r_i)$, respectively.

Given the size distribution f on the non-uniform grid $a_r(\zeta_i)$ any macroscopic quantity given as a linear functional of the grain size spectrum can be calculated by simple integration, e. g. the total dust opacity, the collisional drag force exerted by the drifting grains or the consumption rate of condensable material from the gas due to grain growth. The following equation holds for any macroscopic property $P_\mathrm{d}(r)$ of the dust component given the microscopic property $p(a, r)$ of a single grain of size a

$$\begin{aligned} P_\mathrm{d}(r) = {} & f(a_r(\zeta_1), r)\, p(a_r(\zeta_1), r)\, [a_r(\zeta_1) - a_r(\zeta_2)]/2 \\ & + \sum_{i=2}^{I-1} f(a_r(\zeta_i), r)\, p(a_r(\zeta_i), r)\, [a_r(\zeta_{i-1}) - a_r(\zeta_{i+1})]/2 \\ & + f(a_r(\zeta_I), r)\, p(a_r(\zeta_I), r)\, [a_r(\zeta_{I-1}) - a_r(\zeta_I)]/2 \end{aligned} \tag{2.20}$$

where the integral was approximated by the extended trapezoidal rule. The discretization error of this rule is of second order in grain size separation $a_r(\zeta_i) - a_r(\zeta_{i+1})$.

In Eq. (2.20) the size dependent microscopic properties of the grains are weighted by the distribution function and explicitly integrated. Thus, some commonly used simplifications concerning the calculation of dust properties become obsolete. For example, the opacity of the grains can be calculated by means of the exact formulation of Mie theory instead of assuming either the small or large particle limit.

More complicated, non-linear functionals of the grain size distribution function can be calculated in an analogous manner to Eq. (2.20) though they may involve some interpolation of f on the grain size grid $a_r(\zeta_i)$. Fortunately, linear interpolation (which again involves discretization errors of second order in grain size separation) is sufficient here.

2.5 Error estimation

The underlying fundamental principle of the presented approach is the flux conservation of the dust component (cf. Eq. (1.8))

$$\begin{aligned} \Delta_r \int_{a_\ell}^{a_\mathrm{max}} \mathrm{d}a'\, v_\mathrm{d}(a', r) f(a', r) = {} & \Delta_{r_0} \int_{a_\ell}^{a_\mathrm{max}} \mathrm{d}a'\, J_0(a') \int_{r_0}^{r} \mathrm{d}r'\, J_\ell(r') \Delta_{r'} \\ & + \int_{r_0}^{r} \mathrm{d}r'\, \Delta_{r'} \int_{a_\ell}^{a_\mathrm{max}} \mathrm{d}a'\, q(a', r'). \end{aligned} \tag{2.21}$$

It therefore seems plausible to define the estimated error $\epsilon(r)$ of the computational multi-component method by the deviation of the "theoretical" flux $j_{\rm tot}(r)$ given by the r. h. s. of Eq. (2.21) from the numerical grain flux $j_{\rm tot}^{\rm num}$ as calculated according to Eq. (2.20) with $p(a,r) \equiv v_{\rm d}(a,r)$, which represents the the l. h. s. of Eq. (2.21)

$$\epsilon(r) = |1 - j_{\rm tot}^{\rm num}(r)/j_{\rm tot}(r)|. \tag{2.22}$$

If this error exceeds or falls below some user-specified thresholds, grid points can be inserted or removed, respectively, in order to adjust the achieved accuracy of the multi-component method (cf. Sect. 2.1).

2.6 Summary

In this chapter a computational multi-component method for the efficient numerical solution of the fundamental balance equation (1.15) was derived. The essential idea was to discretize the size distribution on a Lagrange-like grid in grain size space which moves according to the size evolution of selected sample grains. In this way, the grid is self-adapting to the way the size distribution is evolving which seems more natural than the use of a static grid. The treatment of continuous changes in grain size is thus an inherent feature of the multi-compontent method, since such processes simply amount to an adjustment of the grid in grain size space.

Another distinguished feature of the presented method is that no attempt was made to approximate the size distribution function by a linear combination of simple box-car or square puls size distributions refered to as bins. Instead, the grain size spectrum is sampled at selected grid points only, which can be compared to the discretization approach taken in radiative transfer calculations. This allows for a straightforward inclusion of coagulation and other discontinuous processes.

Chapter 3

Test calculations

Having derived and implemented a new computational method, it is always advisable to test one's numerical procedures against known solutions (Lissauer & Stewart 1993). For this reason, some test calculations were performed with respect to both continuous and discontinuous processes. The presented calculations are not intended to give new astrophysical insights but rather serve as worked examples for the multi-component method and as a test for its validity. For more elaborate astrophysical applications see Part II of this thesis.

Although the treatment of continuous and discontinuous processes is investigated separately by means of different test problems, this is only done in order to allow for a direct comparison with known analytical solutions. In fact, the simultaneous treatment of both continuous and discontinuous processes is a major advantage of the multi-component method (cf. also Chapter 5).

3.1 Continuous processes

In this section, the computational multi-component method outlined in Chapter 2 is applied in a test calculation considering only continuous processes. A simple scenario is chosen for modeling the processing of a given grain size distribution due to mechanical sputtering behind a dense shock. Such shock processing of grains is a common astrophysical phenonemon, occuring e.g. in the ISM due to supernova blast waves (Seab & Shull 1983).

3.1.1 Adopted scenario

In order to discuss the effects of grain sputtering independent of a complicated hydro- and thermodynamical structure, a very simple model of a jump-type or J-type shock of velocity v_{s} will be used here. The results of Neufeld & Hollenbach (1994) who thoroughly investigated a dense shock of preshock density $n^0_{\langle\mathrm{H}\rangle} = 10^9$ cm^{-3} and $v_{\mathrm{s}} = 50$ km s^{-1} are adopted and slightly simplified. After the immediate jump of the gas velocity v_{g} to $1/4\ v_{\mathrm{s}}$ behind the shock front, the gas further decelerates as it cools.

The initial grain velocity $v_\mathrm{d}(a,0)$ just behind the shock is given by v_s. According to the results of Neufeld & Hollenbach (1994) no significant deceleration of the grains takes place for $N_\mathrm{H} < 10^{16}$ cm^{-2} where

$$N_\mathrm{H} = \int n_{\langle\mathrm{H}\rangle}\,\mathrm{d}l \tag{3.1}$$

is the column densities of hydrogen nuclei behind the shock front. Similarly, it turns out (cf. Sect. 3.1.6) that grain sputtering is negligble in this region.

Hence, the computation is started at $N_\mathrm{H} \approx 10^{16}$ cm^{-2}. The value of the gas velocity for smaller column densities does not influence the outcome of the calculations, since grain deceleration and sputtering sets in at $N_\mathrm{H} \approx 10^{16}$ cm^{-2}.

According to the results of Neufeld & Hollenbach (1994) the gas density is varying only slowly for 10^{16} cm$^{-2} \lesssim N_\mathrm{H} \lesssim 10^{21}$ cm^{-2}. Thus, a constant postshock density of hydrogen nuclei $n_{\langle\mathrm{H}\rangle} = 5\,10^{10}$ cm^{-3} is assumed in this region, corresponding to a gas velocity $v_\mathrm{g} = 1$ km s^{-1}. For $N_\mathrm{H} > 10^{21}$ cm^{-2} no further grain processing takes places and the computation is stopped.

3.1.2 Grain dynamics

In the present test calculation N_H takes the place of the independent flow variable r. Due to the plane-parallel geometry the transformation determinant $\Delta \equiv 1$.

For sufficiently high preshock densities the grains follow nearly linear trajectories and are stopped before they can be significantly accelerated by the betatron mechanism (Neufeld & Hollenbach 1994). Assuming the grains to be decelerated solely by collisional drag of the gas particles the equation of motion for a grain can be written as (cf. Woitke et al. 1993, henceforth WDS)

$$\frac{\mathrm{d}v_\mathrm{d}(a)}{\mathrm{d}N_\mathrm{H}} = -\frac{3\,1.4 m_\mathrm{u}}{4a\rho_\mathrm{s}}\frac{\left(v_\mathrm{d}(a) - v_\mathrm{g}\right)^2}{v_\mathrm{d}(a)} \tag{3.2}$$

where ρ_s denotes the mass density of the grain material and m_u is the atomic mass unit. In Eq. (3.2) and the remainder of this section the functional dependency of physical quantities on N_H is omitted.

3.1.3 Grain sputtering

The present test calculation is limited to the inclusion of mechanical sputtering as the sole processing mechanism of the grains. With N_H being the independent variable of the flow Eq. (1.4) for the grain size evolution can then be written as (cf. also WDS)

$$\frac{\mathrm{d}a}{\mathrm{d}N_{\mathrm{H}}} = -\pi a_0^2 \frac{v_{\mathrm{d}}(a) - v_{\mathrm{g}}}{v_{\mathrm{d}}(a)} \overline{Y}_{\mathrm{sp}} \frac{a_0}{d} \tag{3.3}$$

where $\overline{Y}_{\mathrm{sp}} \equiv \overline{Y}_{\mathrm{sp}}(v_{\mathrm{d}}(a) - v_{\mathrm{g}})$ denotes the mean sputtering yield, i.e. the number of lattice particles removed from the grain surface per incident gas particle.

As has been argued by WDS it suffices to take into account H, He and an artificial species (denoted by "C/N/O") for all metals in order to determine the mean sputtering yield. It is then given by

$$\overline{Y}_{\mathrm{sp}} = Y_{\mathrm{sp,H}} + \epsilon_{\mathrm{He}} Y_{\mathrm{sp,He}} + \epsilon_{\mathrm{CNO}} Y_{\mathrm{sp,CNO}} \tag{3.4}$$

where ϵ_i denotes the abundance of the sputtering species i relative to hydrogen. In this test calculation semianalytical yields derived from experimental data have been used (for details see Tielens et al. (1994) and references therein).

3.1.4 Initial grain size distribution and chemical composition of the gas phase

For the sake of simplicity the processing of spherical ice grains was investigated ($\rho_s \approx 1$ g/cm^{-3}, $a_0 = 1.9\,10^{-8}$ cm). These grains can also be imagined to consist of a small core coated by a thick layer of ice. The initial size distribution is given by

$$f(a) \propto a^{-3.5} \tag{3.5}$$

in the size range $10^{-2}\,\mu\mathrm{m} < a < 1\,\mu\mathrm{m}$ as suggested by the results of Mathis et al. (1977).

The adopted abundances of the sputtering species are $\epsilon_{\mathrm{He}} = 10^{-1}$ and $\epsilon_{\mathrm{CNO}} = 10^{-3}$.

3.1.5 Method of solution

Considering grain sputtering behind plane-parallel shocks the fundamental balance equation (1.15) simplifies to

$$f(a) = \frac{J_0(a_*)}{v_{\mathrm{d}}(a)} \Bigg/ \frac{\mathrm{d}a}{\mathrm{d}a_*} \tag{3.6}$$

For the multi-component method the size evolution of I sample grains is followed with their initial sizes $a_* = a_i$ chosen to be

$$\log_{10}(a_i/\mu\mathrm{m}) = -2 + 2[(i-1)/(I-1)]^2. \tag{3.7}$$

This corresponds to a modified logarithmic grid with higher resolution of the smaller grain sizes and thus accounts for the fact that 95% of the grains are smaller than $2.5\ 10^{-2}\,\mu$m.

The grid point equations (3.3) and the corresponding equations of motions (3.2) for the sample grains form a system of $2I$ ODE's. They are solved by means of an embedded, explicit fourth order Runge-Kutta scheme (Hairer et al. 1987). The calculations have been performed on a Silicon Graphics IRIS Indigo R 4000 workstation. The results presented below have been calculated with $I = 30$. This takes less than a second of computing time.

3.1.6 Results and discussion

Figure 3.1 shows the grain velocities v_{d} behind the shock front for three different initial grain sizes a_i. The well-known fact that the distance required to slow down the grains to approximately the gas velocity is proportional to their size (cf. WDS) is confirmed.

The size evolution of three sample grains relative to their initial size a_i is shown in Fig. 3.2. The larger a grain the longer it suffers from sputtering, since it maintains a significant drift velocity well beyond the shock front. However, the *relative* amount of dust material returned to the gas phase ($\sim 91\%$) is the same for all grains irrespective of their initial size. This has also been shown analytically by WDS.

The evolution of the grain size distribution $f(a)$ (multiplied by $a^{3.5}$ for convenience) is presented in Fig. 3.3 by a sequence of snapshots taken at various column densities N_{H} behind the shock. The final size distribution is obtained if all grains have decelerated to almost zero drift velocity. Compared to the initial size distribution the final distribution is shifted upwards due to the compression of the gas. The distribution is also shifted horizontally towards smaller grain sizes, since *all* grain sizes have been uniformly reduced by $\sim$ 55% due to sputtering. Actually, this particular relation between initial and final grain size distribution has already been obtained by purely theoretical insight (WDS), an agreement quite reassuring with regard to the validity of the presented multi-component method.

To summarize, in Fig. 3.3 the size distribution performs an upward movement combined with a shift to the left. Moreover, it does so in a certain order: sections of the distribution representing smaller grains (which are decelerated faster than larger ones) approach the final distribution at lower column densities. This is reflected in the snapshots for $N_{\mathrm{H}} = 10^{17}, 10^{18}, 10^{19}, 10^{20}$ cm^{-2}.

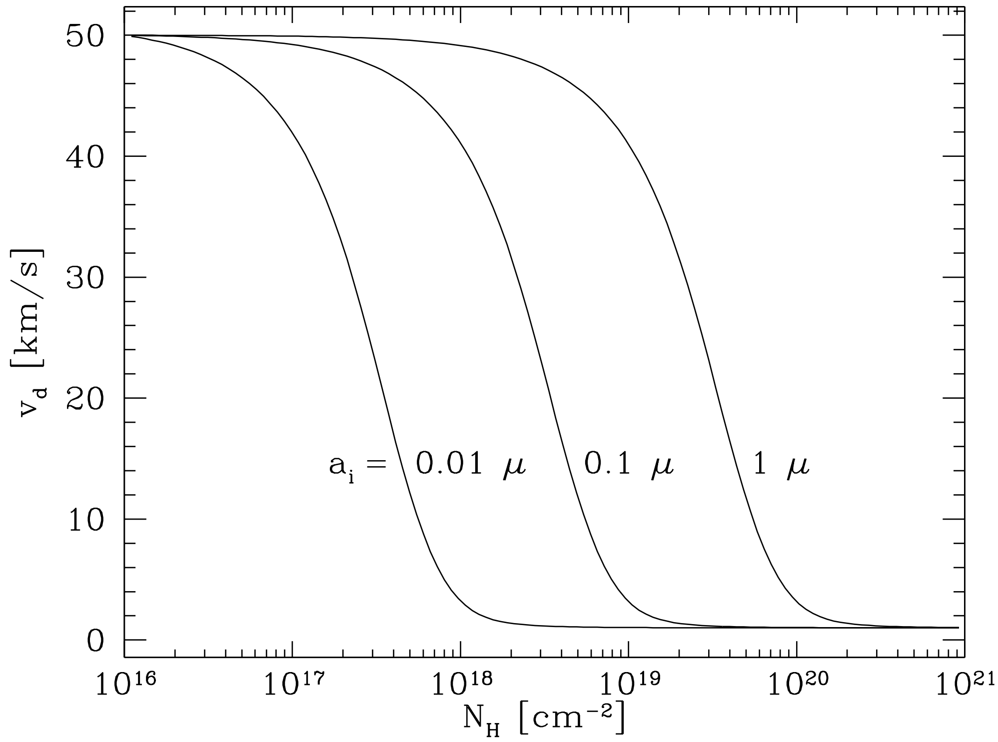

Figure 3.1: Grain velocities v_d behind the shock front for three dust particles of initial size $a_i = 0.01\,\mu$m, $0.1\,\mu$m and 1 μm.

The shape of these inbetween size distributions during grain deceleration and sputtering can be explained as follows: For every column density there is a grain size a such that the separation Δa of neighbouring grain sizes is temporarily increased, since grains smaller than a already almost completed the sputtering process while grains larger than a not yet experienced a significant change of size (cf. also Fig. 3.2). As a result, the derivative $\mathrm{d}a/\mathrm{d}a_*$ is large and, consequently, $f(a)$ is small (cf. Eq. (3.6)). This means that the corresponding section of the size distribution temporarily drops below the initial distribution. When the grains are decelerated to drift velocities smaller than about 10 km s^{-1} grain sputtering ceases. During the further deceleration of the grains the compression of the dust fluid, however, continues and the considered section of the distribution function rises towards the final distribution (cf. Eq. (3.6)).

Finally, Fig. 3.4 depicts the estimated local error ϵ as defined in Eq. (2.22) for three different numbers of grid points I. The maximum deviation from flux conservation does not accumulate towards the end of the calculation but rather occurs at $N_\mathrm{H} \sim 10^{18}$ cm^{-2}, when the majority of the grains, namely the small ones, are processed. However, this error only amounts to a few percent, even if as few as 10 grid points are distributed over the whole size spectrum.

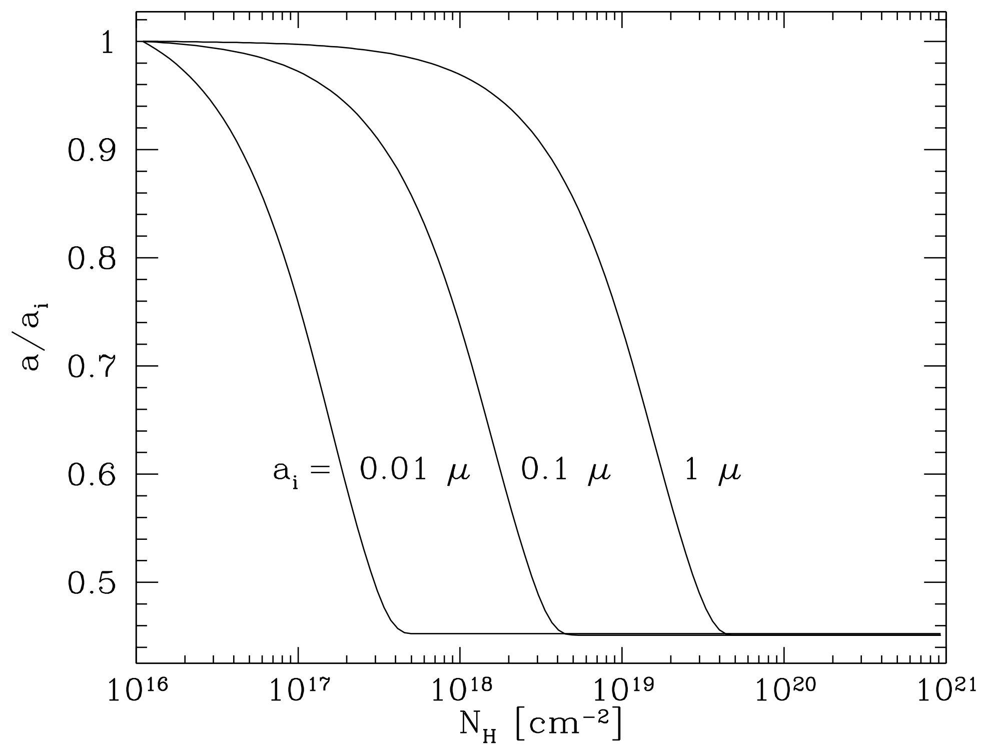

Figure 3.2: Size evolution of dust particles behind the shock front. The size is given relative to the initial size $a_i = 0.01\,\mu$m, $0.1\,\mu$m and $1\ \mu$m of the grains.

If the number I of grid points is increased, the mean separation in grain size space decreases accordingly in an reversely proportional manner. During the derivation of the computational multi-component scheme in Chapter 2 care was taken of all discretization errors being of second order in grain size separation. This can also be seen in Fig. 3.4 where a tenfold increase in the number of grid points leads to a reduction of the estimated local error by 10^2.

3.2 Discontinuous Processes

In order to construct a reasonable test problem for the numerical treatment of discontinuous processes as presented in Chapter 2, the fundamental balance equation (1.15) is simplified by refraining from the consideration of continuous processes (i.e. $a = a*$) and of nucleation (i.e. $J_\ell = 0$). Furthermore, a plane-parallel geometry as well as a constant dust velocity $v_{\rm d}$ in r-direction which is independent of grain size

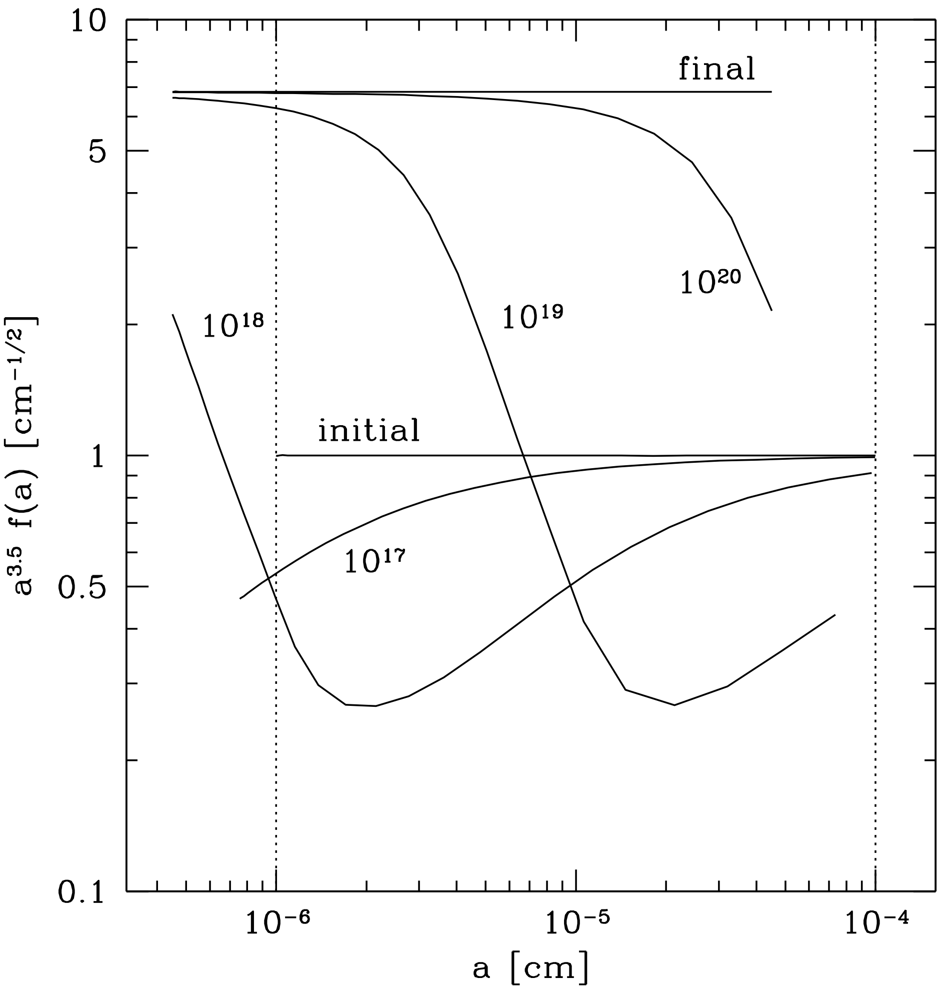

Figure 3.3: Snapshots of the grain size distribution (apart from an arbitrary scaling factor) multiplied by $a^{3.5}$ at four positions $N_{\rm H} = 10^m$ cm^{-2} behind the shock front. The initial and final size distributions are also depicted.

is adopted. The fundamental balance equation can then be written as

$$-J_0(a) + v_{\rm d} f(a,r) = \int_{r_*}^{r} {\rm d}r'\, q(a,r'). \tag{3.8}$$

Transforming from the independent variable r to the time t via ${\rm d}r = v_{\rm d}\,{\rm d}t$ and choosing the grain mass m to characterize the dust particles Eq. (3.8) reads

$$-J_0(m) + v_{\rm d} f(m,r) = \int_{t_*}^{t} {\rm d}t'\, v_{\rm d} q(m,t'). \tag{3.9}$$

If only coagulation is considered as sole discontinuous process (cf. Eq. 2.7), differentiating with respect to t yields the well-known coagulation equation (Smoluchowsky

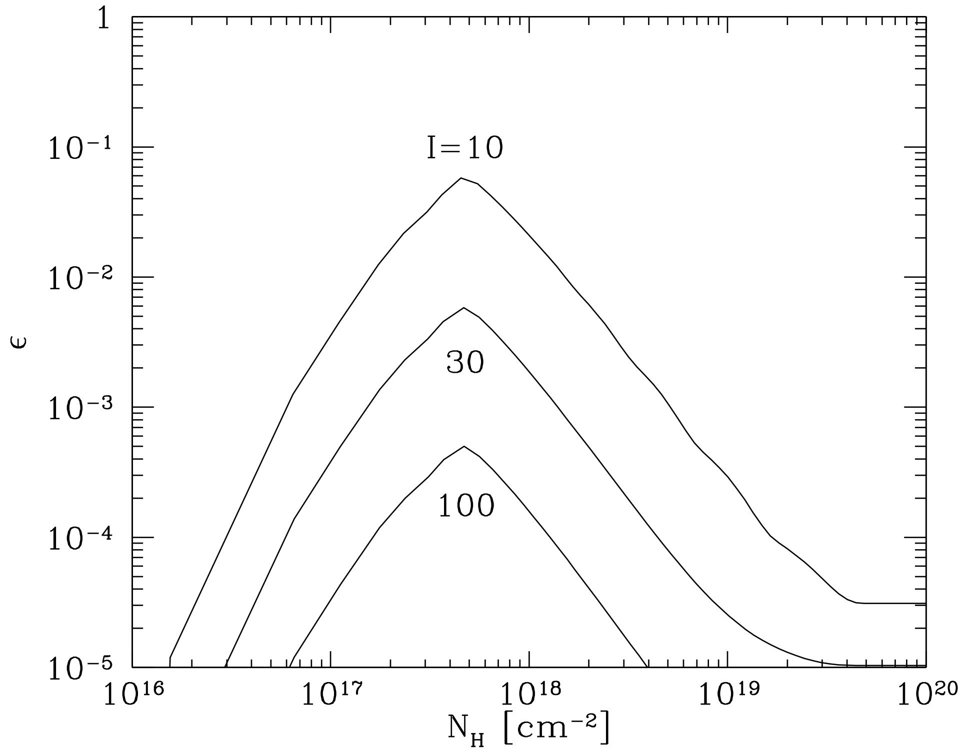

Figure 3.4: Estimated local error ϵ of the multi-component method for $I = 10$, 30 and 100 grid points

1917)

$$\begin{aligned}\frac{\mathrm{d}f(m,t)}{\mathrm{d}t} &= -f(m,t)\int_{m_\ell}^{m_{\max}} \mathrm{d}m'\, f(m',t)\Omega(m,m',t) \\ &\quad + \frac{1}{2}\int_{m_\ell}^{m} \mathrm{d}m'\, f(m',t)f(m-m',t)\Omega(m',m-m',t). \qquad (3.10)\end{aligned}$$

This coagulation equation has been widely studied by many authors, and analytical solutions have been found in several cases for simple forms of the reaction frequency Ω for certain initial distributions [1] (see Hayashi & Nakagawa (1990) for a summary). The few analytical solutions of the coagulation equation provide a rigorous test for the accuracy of any numerical algorithm used to model discontinuous processes. Two such solutions are the cases when $\Omega(m, m', t)$ equals a constant and when $\Omega(m, m', t)$ is proportional to the sum of the masses, $m + m'$.

[1] Unfortunately, none of these special cases represents realistic kernels of the integrals in Eq. (3.10), and they are not applicable to astrophysical problems.

3.2.1 Constant coagulation kernel

First, a constant reaction frequency $\Omega(m, m', t) \equiv \Omega$ and an initial size distribution at time $t_* = 0$

$$f(m, 0) = n_0 \delta(m - m_0) \tag{3.11}$$

are considered.

Analytic solution

The analytic solution is given by (Smoluchowski 1916)

$$f(m, t) = \sum_{k=0}^{\infty} n_0 g^2 (1 - g)^{k-1} \delta(m - k\, m_0) \tag{3.12}$$

with

$$g = (1 + \tau/2)^{-1} \tag{3.13}$$

where the normalized time is given by $\tau = \Omega n_0 t$. The solution (3.12) is zero unless m is an integer multiple of m_0, since coagulating particles of mass m_0 can only form particles of mass $k\, m_0$.

For large particles the relative separation between allowed particle masses becomes negligible and the size distribution can be regarded as quasi-smooth function

$$f(m, t) \approx m_0^{-1} n_0 g^2 (1 - g)^{m/m_0 - 1}, \qquad m \gg m_0. \tag{3.14}$$

Numerical solution

The coagulation equation (3.10) is equivalent to the standard equation (2.6) for treating discontinuous processes within the framework of the multi-component method, where the computational quantity Q is identified with the distribution function f and the independent variable r with the time t. The source function q was discretized as described in Sect. 2.3.1

$$\frac{\mathrm{d} f(m_k)}{\mathrm{d} t} = q^{(+)}_{\mathrm{coag}}(m_k, t) + q^{(-)}_{\mathrm{coag}}(m_k, t). \tag{3.15}$$

The grid points were distributed evenly spaced for $m \leq 10\, m_0$ and logarithmically beyond $10\, m_0$

$$m_k = \begin{cases} k\, m_0 & : \quad 0 \leq k \leq 10 \\ 1.3\, m_{k-1} & : \quad 10 < k \leq 50 \end{cases} \tag{3.16}$$

This choice of grid points accounts for the fact that for small particles only integer multiples of m_0 are possible particle masses, while for large masses these possible masses can be regarded as lying dense within the size space.

The 50 ordinary differential equations of type (3.15) were solved by means of an embedded, explicit fourth order Runge-Kutta scheme (Press et al. 1992). The calculation has been performed on a Pentium PC adopting dimensionless parameters

$$\Omega = n_0 = m_0 = 1.$$

Integration from $t_* = 0$ to $t = 10^4 \tau$ takes less than two seconds of computing time.

Figure 3.5 shows the evolution of the size distribution function. As can be seen in the upper panel, the agreement between the analytical and the numerical solution is very good except for the tail of the distribution function, where particle coagulation is artificially accelerated[2]. This discrepancy has also been observed by Ohtsuki et al. (1990). Wetherill (1990) claims to be able to work around this problem of numerical acceleration by creating new grid points at the high mass end of distribution only if the mass of the two colliding particles exceeds the mass of the largest grid point by a preassigned factor δ with values ranging from 1.1 to 1.2. It seems, however, that the absence of artificial runaway growth reported by this author is rather due to an extremely fine grid in grain size space, where the ratio of consecutive masses m_k is of the order of 1.1. In fact, it turns out that employing such a fine grid within the multi-component method also leads to complete agreement between the analytical and numerical solution.

In the lower panel of Fig. 3.5 $m^2 f$ is plotted on a linear scale and m on a logarithmic scale. In this plot the area below the curve for a given size interval $\Delta \log m$ corresponds to the mass contained in particles of this size, and the agreement between the analytical values and numerical modeling is excellent. This means that only a negligible part of the total mass is found in the mass range for which the inconsistencies described above occur.

A plot of the temporal evolution of macroscopic values derived from the size distribution (cf. Fig. 3.6) confirms this finding. The total mass

$$m_{\mathrm{tot}}(t) \equiv \int_0^\infty m f(m,t)\,\mathrm{d}m = n_0 m_0 \tag{3.17}$$

is numerically conserved as has been derived in Sect. 2.3.2. As expected, the number density of particles remaining at time t is also in complete agreement with the analytical expression reported by Wetherill (1990)

$$n_{\mathrm{tot}}(t) \equiv \int_0^\infty f(m,t)\,\mathrm{d}m = n_0 (1 + \tau/2)^{-1}. \tag{3.18}$$

[2]Note, however the logarithmic scaling of the ordinate

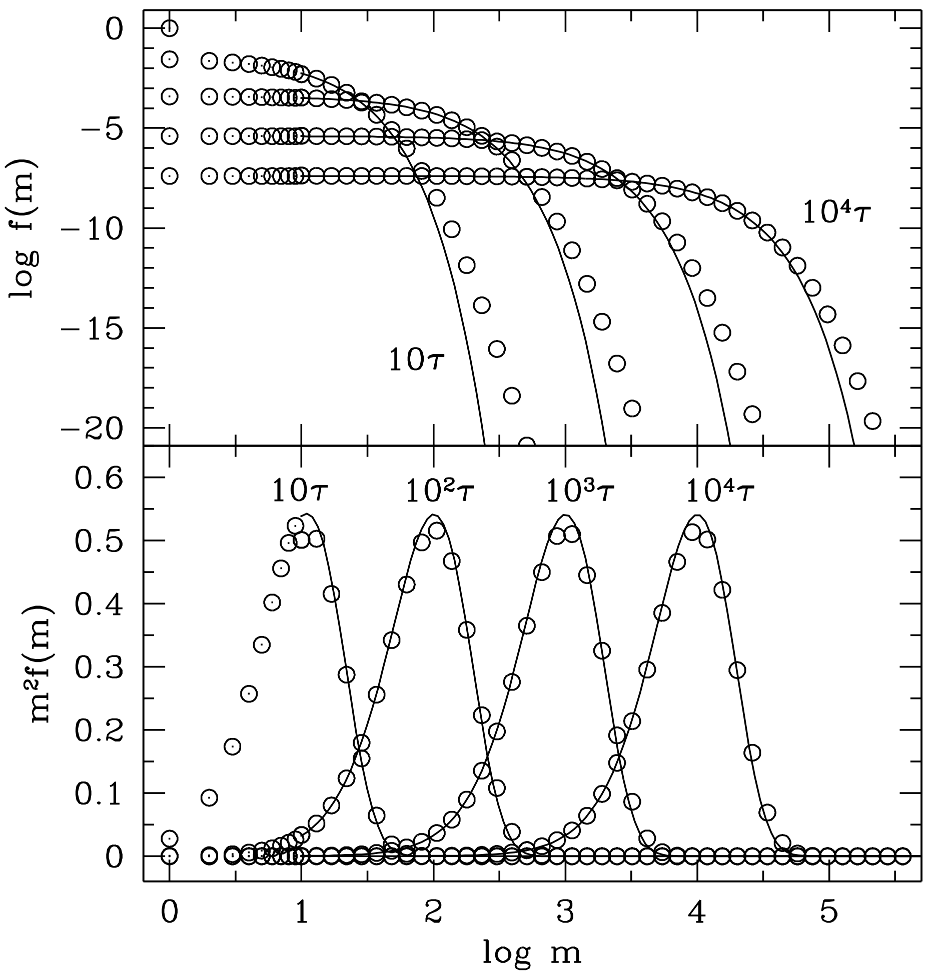

Figure 3.5: Comparison between numerical (open circles) and analytical (dots and solid curves) size distribution functions in the case of a constant coagulation kernel $\Omega(m, m', t) \equiv \Omega$ at five stages $t = 0, 10\tau, 10^2\tau, 10^3\tau, 10^4\tau$. For $\log m > 1$ the distribution is assumed to be quasi-smooth. In the lower panel the distribution function is multiplied by m^2.

3.2.2 Linear coagulation kernel

In this second case the reaction frequency is regarded as being proportional to the sum of the masses of the coagulating particles

$$\Omega(m, m', t) \equiv \alpha(m + m') \tag{3.19}$$

An initial steeply peaked exponential mass distribution at time $t_* = 0$ is adopted

$$f(m, 0) = \frac{n_0}{m_0} e^{-m/m_0}. \tag{3.20}$$

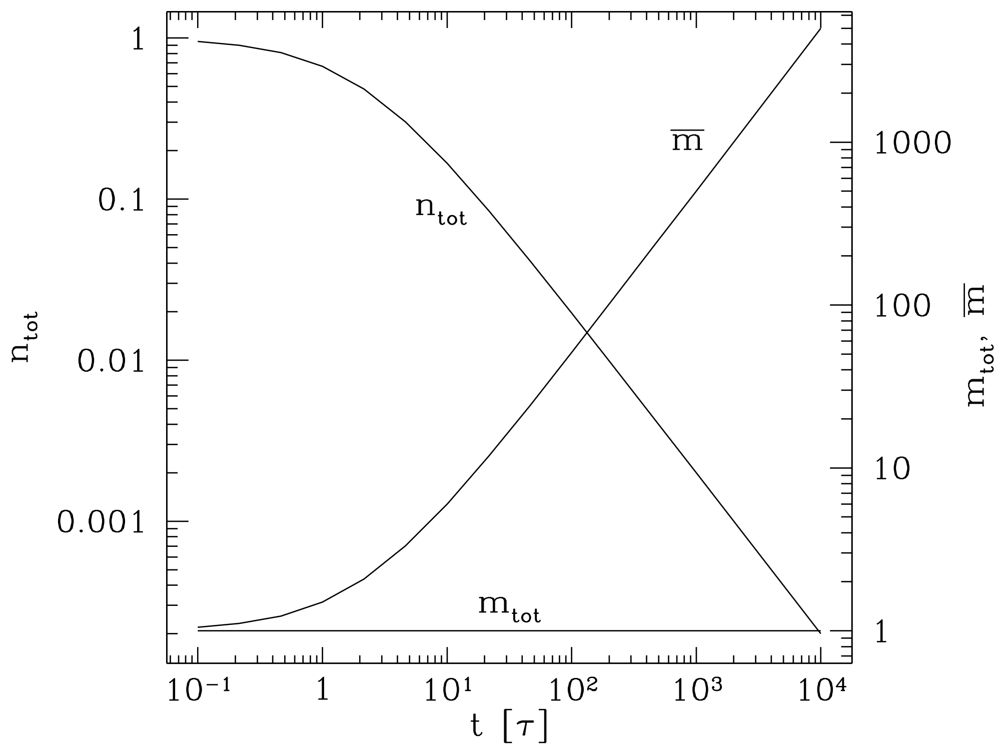

Figure 3.6: Temporal evolution of the total density $n_{\rm tot}$, the total mass $m_{\rm tot}$ and the mean mass $\bar{m} \equiv m_{\rm tot}/n_{\rm tot}$ in the case of a constant coagulation kernel $\Omega(m, m', t) \equiv \Omega$.

Analytic solution

The following analytic solution was found by Safronov (1962)

$$f(m,t) = \frac{n_0 g}{m\sqrt{1-g}} e^{-m/m_0(2-g)} I_1\left(2\frac{m}{m_0}\sqrt{1-g}\right) \tag{3.21}$$

where the fraction g of particles remaining at time t is given by

$$g = \exp(-\tau) \tag{3.22}$$

with the dimensionless time

$$\tau = \alpha n_0 m_0 t. \tag{3.23}$$

$I_1(x)$ is the first order modified Bessel function of the first kind.

Numerical solution

Discretization proceeded along the same lines as described in the previous section. For the size space a logarithmically equidistant grid starting at $m_{\min} = 10^{-2} m_0$ was used

$$m_k = \begin{cases} 10^{-2} m_0 & : \quad k = 1 \\ 1.2\, m_{k-1} & : \quad 1 < k \leq 200 \end{cases} \tag{3.24}$$

The large number of grid points was chosen in order to adequatly cover the large size space extending over 16 orders of magnitude (cf. Fig. 3.7).

The 200 ordinary differential equations of type (3.15) were again solved by means of an embedded, explicit fourth order Runge-Kutta scheme (Press et al. 1992). The calculation has been performed on a Pentium PC adopting dimensionless parameters

$$\alpha = n_0 = 1, \qquad m_0 = 100.$$

Integration from $t_* = 0$ to $t = 12\tau$ takes about ten seconds of computing time.

Figure 3.7 shows the evolution of the size distribution function. It can be seen in the upper panel, that the agreement between the numerical and the analytical solution is very good except for the tail of the distribution function, where pronounced discrepancies occur. This artificial acceleration of particle coagulation has also been noted by Ohtsuki et al. (1990).

In the lower panel of Fig. 3.7 $m^2 f$ is plotted on a linear scale and m on a logarithmic scale. An area obtained by integration of $m^2 f$ over an interval of the abscissa represents the mass contained in the interval. The agreement between the analytical values and numerical modeling is only fair. Still, the numerical solution satisfactorily represents the overall evolution of the bulk of the mass distribution.

This is confirmed by a plot of the temporal evolution of macroscopic values derived from the size distribution (cf. Fig. 3.8). The total mass is numerically conserved as has been derived in Sect. 2.3.2. As expected, the number density of particles remaining at time t is also in complete agreement with the analytical expression reported by Wetherill (1990)

$$n_{\mathrm{tot}}(t) = n_0 e^{-\tau}. \tag{3.25}$$

3.3 Summary

Several test calculations were performed in order to assess the validity and reliability of the computational multi-component method presented in Chapter 2. The

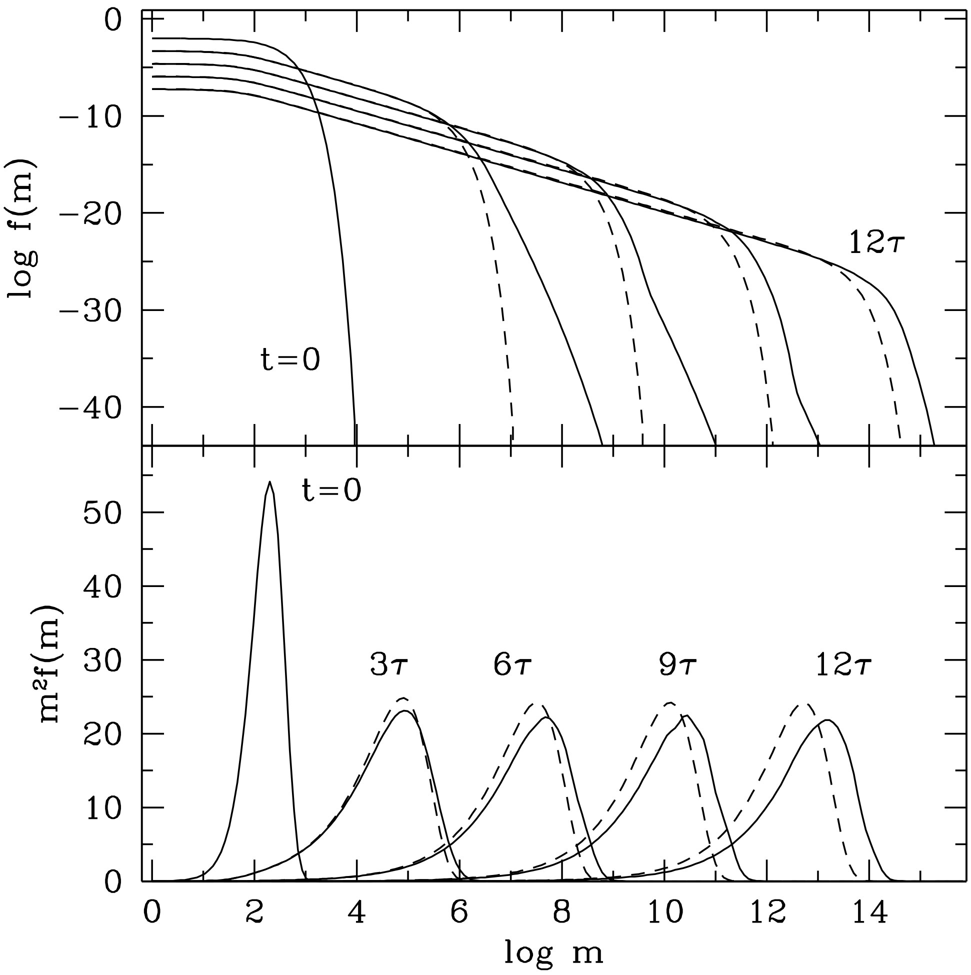

Figure 3.7: Comparison between numerical (solid curves) and analytical (dashed curves) size distribution functions in the case of a linear coagulation kernel $\Omega(m, m', t) \equiv \alpha(m + m')$ at five stages $t = 0, 3\tau, 6\tau, 9\tau, 12\tau$. In the lower panel the distribution function is multiplied by m^2.

corresponding code has proven to be very efficient and the results expected from a theoretical point of view could be reproduced in a satisfactory way.

The test calculation involving grain sputtering behind dense shocks additionally provided some physical insight of how exactly the grain size distribution evolves. With respect to discontinuous processes it was found that the temporal evolution of derived macroscopic quantities such as the total particle number and mass is exactly reproduced by the numerical scheme. However, the multi-component method suffers from the well-known artificial acceleration of particle coagulation which has been observed by Ohtsuki et al. (1990) for coarse mass-coordinate divisions.

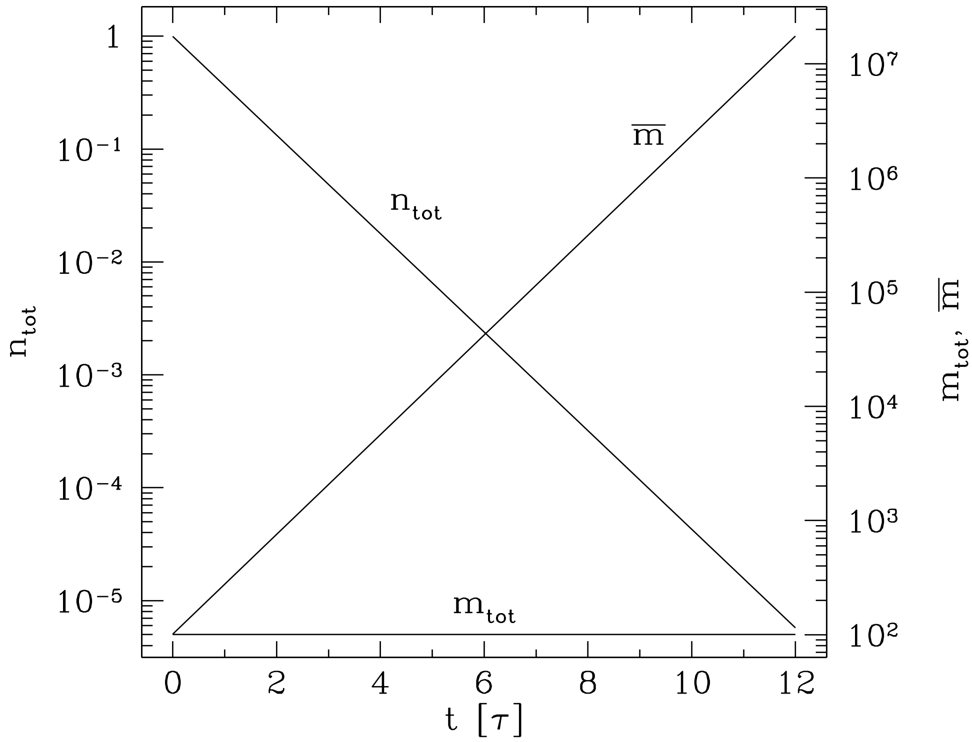

Figure 3.8: Temporal evolution of the total density $n_{\rm tot}$, the total mass $m_{\rm tot}$ and the mean mass $\bar{m} \equiv m_{\rm tot}/n_{\rm tot}$ in the case of a linear coagulation kernel $\Omega(m, m', t) \equiv \alpha(m + m')$.

In summary, a new and efficient method for the modeling of grain processing has been provided which seems capable of being applied to a wide range of astrophysical problems, e.g. dust formation in circumstellar dust shells (cf. Chapter 4), grain growth and coagulation under cosmic conditions (cf. Chapter 5), dust destruction in protostellar accretion shocks (cf. Chapter 6), the processing of chondrule precursor grains in the solar nebula and the formation of planetesimals.

Part II

Astrophysical applications

Chapter 4

Dust formation in stationary dust driven winds

It is now well established that dust is an important component of the extended atmospheres around late-type stars. A wealth of papers has been devoted to the investigation of the hydro- and thermodynamical role of dust in the circumstellar environment (see, e.g. the reviews of Lafon & Berruyer 1991, Sedlmayr & Dominik 1995 and references therein).

The art of modeling circumstellar dust shells (CDS) is very advanced and includes an elaborate treatment of time-dependent hydrodynamics (Bowen 1988, Fleischer et al. 1992), non-equilibrium chemistry (Nejad & Millar 1987, Beck et al. 1992), dust formation (Kozasa et al. 1984, Gail & Sedlmayr 1988), and radiative transfer (Rowan-Robinson & Harris 1982, Winters et al. 1994). However, the majority of models for CDS is still lacking a proper treatment of grain drift.

Those models which include grain drift concentrate on certain aspects, e.g. the momentum coupling of grains to the bulk of the gas (MacGregor & Stencel 1992, Krüger et al. 1994), the dynamical dilution of the dust component (Netzer & Elitzur 1993, Krüger et al. 1994) or the frictional heating due to drifting dust particles (Tielens 1983, Krüger et al. 1994).

Concerning the growth and nonthermal sputtering of drifting dust grains in circumstellar envelopes a first investigation was made by Kwok (1975). However, in his work all grains were assumed to have a uniform if time-dependent radius.

In contrast, Dominik et al. (1989) determined the entire distribution of grain sizes in self-consistent models for dust driven winds. In these models dust formation and growth were treated explicitly assuming, however, negligible drift and a dust growth rate independent of the grain size. Although the mere *effects* of drift on grain growth have already been investigated by Dominik et al. (1989) their method does not allow for a self-consistent treatment of these effects nor of nonthermal sputtering.

It is the aim of this chapter to expand these preliminary investigations by means of a general and self-consistent modeling procedure. Setting out from an investigation of how drift motion influences the formation and growth of dust particles in stellar winds, the shape of the resulting grain size spectrum is to be determined.

In Part I of this thesis a general computational scheme to describe the evolution of the grain size distribution in one-dimensional stationary flows in consideration of size dependent grain drift was provided. When combined with the well-known equations describing a dust driven wind (given, for example, in Krüger et al. 1994), this multi-component method permits a consistent modeling approach for dust driven winds in consideration of grain drift and yields results different from the preliminary ones of Dominik et al. (1989), once more proving the necessity of self-consistent modeling procedures.

In Sect. 4.1 the equations describing the formation and growth of drifting dust grains and the model of a dust driven wind are summarized. The computational scheme to calculate the size distribution and the method of solution for the wind model is described in Sect. 4.2. In Sect. 4.3 representative models of stellar winds around C-stars are presented and the influence of grain drift on the shape of the size distribution is discussed.

4.1 Basic equations

In this work the stellar wind is assumed to be stationary and spherically symmetric. Effects due to stellar rotation or magnetic fields are neglected.

Two components of the outflow are distinguished here, namely gas and dust. While the gas can in fact be treated as a single component because of the high thermal velocities and, hence, collision rates, the dust in turn is actually a multi-component medium. There is a size distribution of grains, each moving with a different drift velocity relative to the gas.

For the special case of uniform grain size, i.e. without treating the process of dust growth, the basic equations describing a spherical symmetric, stationary dust driven wind have already been stated, for instance, in Krüger et al. (1994). These equations are listed here for sake of completeness and some appropriate modifications made are indicated.

Grain formation and growth in consideration of a size dependent drift motion can be described by a special differential form of a balance or conservation equation for the grain size distribution function (cf. Chapter 1). Equation (1.15) was appropriately modified and is given in Sect. 4.1.2 in the context of a stellar outflow.

4.1.1 Equations for the gas

Conservation of mass, momentum and energy

Since the mass fraction of condensable matter in red giants is of the order 10^{-3} the mass flux of the gas is unaffected by dust formation, i.e. the mass flux is conserved.

Integration of the equation of continuity then yields

$$4\pi r^2 \rho_{\mathrm{g}} v_{\mathrm{g}} = \dot{M} \tag{4.1}$$

where the mass loss rate $\dot{M}$ is a constant and ρ_{g} and v_{g} denote the mass density and expansion velocity of the gas.

Neglecting selfgravitation of the shell the equation of motion for the gas in the case of a purely dust driven wind can be written as

$$\rho_{\mathrm{g}} v_{\mathrm{g}} \frac{\mathrm{d}v_{\mathrm{g}}}{\mathrm{d}r} + \frac{\mathrm{d}p}{\mathrm{d}r} = -\frac{GM_* \rho_{\mathrm{g}}}{r^2} + f_{\mathrm{drag}} \tag{4.2}$$

where p denotes the gas pressure, M_* is the stellar mass and f_{drag} is the collisional drag force exerted on the gas by radiatively accelerated dust grains (cf. Sect. 4.1.2).

The equation of state for a dilute gas is the ideal gas law

$$p = kT_{\mathrm{g}} \sum_i n_i \tag{4.3}$$

where n_i are the particle densities of the molecules contained in the gas as resulting from the treatment of the gas phase chemistry (cf. Sect. 4.1.1). In practice, only H, H_2 and He need to be considered.

By means of the equation of state (4.3) Eq. (4.2) can be cast in the form of a wind equation (Parker 1960)

$$(v_{\mathrm{g}}^2 - c_T^2) \frac{\mathrm{d}v_{\mathrm{g}}}{\mathrm{d}r} = v_{\mathrm{g}} \left[\frac{2c_T^2}{r} - \frac{GM_*}{r^2} + \frac{1}{\rho_{\mathrm{g}}} f_{\mathrm{drag}} - \frac{\mathrm{d}c_T^2}{\mathrm{d}r} \right]. \tag{4.4}$$

The wind equation has a critical or sonic point at the radius where v_{g} equals the isothermal sound velocity c_T of the gas. Special numerical techniques have to be invoked to deal with this internal singularity (cf. Sect. 4.2). If the pressure gradient in Eq. (4.2) is neglected and the solution of the flow equations is started at or beyond the sonic point, this problem does not arise.

In contrast to the work of Krüger et al. (1994), the energy balance of the gas is not treated in detail here. Instead, effective radiative relaxation of the bulk of the gas is assumed so that the gas temperature T_{g} is given by the radiative equilibrium (RE) temperature T_{rad} defined in Sect. 4.1.3. As a consequence, the gradient of the squared sound velocity in Eq. (4.4) is proportional to the gradient of T_{rad} if the variation of the mean molecular weight is assumed to be negligible.

A proper inclusion of the gas energy equation would not only obfuscate the influence of grain drift on dust formation and growth but also introduce a stiff component in the resulting large system of ordinary differential equations (cf. Sect. 4.2) therefore rendering an efficient numerical solution more difficult.

Gas phase chemistry

The concentrations of molecular species are of special importance for the formation of dust. For simplicity chemical equilibrium is assumed to prevail in the gas phase. Then the concentrations are simply determined by the elemental abundances ϵ_i relative to hydrogen and the local pressure and kinetic temperature of the gas. In this work the concentrations of 25 molecules formed from the elements H, He, O, C, N, Fe, Si, Mg, S, and Al are calculated according to Dominik (1992).

However, there are several mechanisms which lead to deviations from chemical equilibrium (for a discussion see Goeres et al. 1988). In the winds of M-stars, for example, the chemical non-equilibrium case has been thoroughly investigated by Beck et al. (Beck et al. 1992).

Krüger et al. (1996) found that the H/H_2 ratio is a decisive quantity for the determination of the dust growth efficiency (cf. Sect. 4.1.2). In the cooling stellar outflow this ratio will diminish due to H_2 formation via the following reactions

$$\begin{aligned} 3\,\mathrm{H} &\leftrightarrows \mathrm{H}_2 + \mathrm{H} && (4.5)\\ 2\,\mathrm{H} + \mathrm{H}_2 &\leftrightarrows 2\,\mathrm{H}_2 && (4.6)\\ \mathrm{CH} + \mathrm{H} &\leftrightarrows \mathrm{C} + \mathrm{H}_2 && (4.7) \end{aligned}$$

where the corresponding reaction kinetic data was taken from Millar et al. (1991) and Baulch et al. (1992).

At some point in the CDS, however, the decreasing density and temperature will give rise to a partly frozen chemistry, i.e. all timescales $\tau_{\mathrm{ch},i}$ of chemical reactions i leading to the formation of H_2 become larger than the hydrodynamical timescale $\tau_{\mathrm{exp}} \equiv r/v_{\mathrm{g}}$ (cf. Goeres et al. 1988). Therefore, the chemical equilibrium treatment of the gas phase chemistry is extended by including this important chemical nonequilibrium effect in the following way: In the expanding outflow the H/H_2 ratio is calculated from chemical equilibrium until the condition

$$\sum_{i=1}^{3} \tau_{\mathrm{ch},i}^{-1} < \tau_{\mathrm{exp}}^{-1} \qquad (4.8)$$

is fulfilled at $r = r_{\mathrm{frz}}$. For $r > r_{\mathrm{frz}}$ the H/H_2 ratio is set equal to that of r_{frz}, i.e. the atomic hydrogen concentration is frozen in.

Using the surface reaction rates given in Krüger et al. (1996) it is estimated that H_2 formation on grain surfaces always proceeds slowly compared to the hydrodynamical timescale. Thus, the H/H_2 ratio is not affected by the grain surface chemistry.

Due to the formation of grains, elements contributing to dust formation and growth are depleted from the gas phase. In case of pure carbon grains the corresponding decrease in the carbon abundance ϵ_{C} relative to hydrogen is taken into account by the following equation

$$\frac{1}{r^2}\frac{\mathrm{d}}{\mathrm{d}r}\left(r^2\epsilon_{\mathrm{C}}n_{\langle\mathrm{H}\rangle}v_{\mathrm{g}}\right) = -\mathcal{N}_{\mathrm{C}} \tag{4.9}$$

where $n_{\langle\mathrm{H}\rangle} = n_{\mathrm{H}} + 2n_{\mathrm{H}_2}$ denotes the total hydrogen density and $\mathcal{N}_{\mathrm{C}}$ is the rate of consumption of carbon atoms per volume due to dust growth (cf. Sect. 4.1.2).

4.1.2 Equations for the dust

The size evolution of a sample grain

Refraining from discontinuous processes arising, for instance, from grain-grain collisions the size evolution of a spherical grain of radius a in a stationary flow is given by (cf. Eq. (1.4))

$$\frac{\mathrm{d}a}{\mathrm{d}r} = \frac{1}{v_{\mathrm{g}} + v_{\mathrm{dr}}(a)}\frac{1}{\tau_{\mathrm{net}}(a)}\frac{a_0}{3} \tag{4.10}$$

where τ_{net}^{-1} denotes the net rate of grain size change and a_0 is the hypothetical radius of a monomer constituting the grain material (cf. Gail et al. 1984). $v_{\mathrm{dr}}(a)$ is the drift velocity of a grain of radius a (cf. Sect. 4.1.2). In the following the grain radius a is refered to as grain 'size' in order to avoid confusion with the independent radial variable r. As can be seen from Eq. (4.10) grain drift reduces the time available for efficient growth, since the grain is sped up on its trajectory outwards from the star and tends to 'drift away' from the growth region.

By introducing a lower limit a_ℓ of the size of macroscopic particles the dust component is separated from the molecular domain and the growth species (cf. Gauger et al. 1990). The value of a_ℓ corresponds to about 10^2 to 10^3 monomers. If a cluster exceeds the size a_ℓ at $r = r_*$ it is considered a newly created dust particle. At radius r such a grain will have grown to a size $a_r(r_*)$ given by integration of Eq. (4.10)

$$a_r(r_*) = a_\ell + \frac{a_0}{3}\int\limits_{r_*}^{r}\frac{1}{v_{\mathrm{g}} + v_{\mathrm{dr}}(a_{r'}(r_*))}\frac{1}{\tau_{\mathrm{net}}(a_{r'}(r_*))}\mathrm{d}r'. \tag{4.11}$$

The specific value adopted for a_ℓ has no influence on the outcome of our calculations.

The net rate of grain size change τ_{net}^{-1} usually comprises contributions from several different physical processes acting on the grain. In this work, grain growth and evaporation as well as erosion due to nonthermal sputtering is considered. The net rate is then given by the sum

$$\tau_{\mathrm{net}}^{-1} = \tau_{\mathrm{gr}}^{-1} - \tau_{\mathrm{ev}}^{-1} - \tau_{\mathrm{sp}}^{-1} \tag{4.12}$$

where $\tau_{\rm gr}$ and $\tau_{\rm ev}$ denote the characteristic growth and evaporation times, respectively, and $\tau_{\rm sp}^{-1}$ is the nonthermal sputtering rate. Each of these contributions will now be discussed in turn.

Grain growth. In CDS of carbon-rich AGB stars the dangling bonds of carbon atoms on a grain surface are expected to be saturated by hydrogen atoms. Growth reactions preferably occur via acetylene addition at temporary radical sites, where an H-atom has been abstracted (dehydrogenation). In a recent paper Krüger et al. (1996, henceforth KPS) argued that the resulting grain material will be amorphous diamond-like carbon, i.e. will have a large proportion of $\rm sp^3$ bonded carbon. They also devised a method of calculating the dehydrogenation probability p in dependence of the gas and the grain temperature, the $\rm H/H_2$ ratio and the drift velocity of the grain. According to KPS the grain growth rate can be written as

$$\tau_{\rm gr}^{-1} = 4\pi a_0^2 2 n_{\rm C_2H_2} v_{\rm rel}(a) p(a) \tag{4.13}$$

where $n_{\rm C_2H_2}$ is the particle density of acetylene and $v_{\rm rel}(a)$ is the average relative velocity between the grain and the growth species $\rm C_2H_2$.

Following Draine (1980), the following approximate expression for the increased average relative velocity due to the drift velocity $v_{\rm dr}(a)$ of a grain was used

$$v_{\rm rel}(a) = \left(\overset{\circ}{v}{}^2_{\rm C_2H_2} + v_{\rm dr}^2(a)/16\right)^{1/2}. \tag{4.14}$$

The average relative velocity in the hypothetical case of purely thermal motion (refered to by '$\circ$') is given by

$$\overset{\circ}{v}_{\rm C_2H_2} = \sqrt{\frac{kT_{\rm g}}{2\pi m_{\rm C_2H_2}}}. \tag{4.15}$$

where $m_{\rm C_2H_2}$ denotes the mass of an acetylene molecule.

From inspection of Eqs. (4.13) and (4.14) it follows that the growth rate may increase significantly if the grain is drifting relative to the gas since the collisional rate between grain and reacting species is increased. Furthermore, KPS showed that p increases for higher relative velocities $v_{\rm rel}$ since energetic hydrogen atoms colliding with the drifting grain tend to favour the abstraction of hydrogen from the grain surface.

On the other hand, it becomes increasingly difficult for a chemisorbed acetylene molecule to dissipate its surplus translational energy into the lattice, when the relative velocity is high (cf. the discussion in KPS). In order to account for this fact the growth rate is multiplied with a sticking efficiency

$$\alpha(v_{\rm rel}) = \exp\left[-\left(\frac{0.5 m_{\rm C_2H_2} v_{\rm rel}^2}{4E_{\rm b}}\right)^3\right] \tag{4.16}$$

where $E_b \approx 0.5$ eV can be regarded as a representative value for the binding (or chemisorption) energy of C_2H_2 on sp^3 carbon surfaces (cf. KPS and references therein). The adopted functional dependence of α is suggested by the results of molecular dynamic simulations of van-der-Waals particles (Head-Gordon & Tully 1992) and is also supported by theoretical considerations (cf. KPS and references therein).

In the process of chemisorption of C_2H_2 the triple bond between the two carbon atoms is broken. The resulting structure is then incorporated into the lattice by reconstruction or rearrangement (isomerization) processes and forms a new part of the grain surface. In the case of carbonaceous surfaces this take place on very short timescales from ps to μs (cf. KPS and references therein). At high dust temperatures $T_d \gtrsim 1600$ K, however, the timescale for desorption of the attached C_2H_2 molecule may be still shorter. In that case, Eq. (4.13) is no longer applicable and grain growth ceases.

Grain evaporation. At dust temperatures above ~ 1800 K the grain surface is nearly devoid of hydrogen and sublimation takes places through evaporation of C_i chain molecules. According to Lenzuni et al. (1995) the desorption rate is given by

$$\tau_{\rm ev}^{-1} = 4\pi a_0^2 \sum_i i \alpha_i \mathring{v}_{C_i} \frac{p_{{\rm sat},i}}{kT_d} \tag{4.17}$$

where α_i and $p_{{\rm sat},i}$ denote the evaporation coefficient and the vapor saturation pressure over the grain, respectively, of C_i. The corresponding thermodynamic data applicable to amorphous carbon grains are given in Lenzuni et al. (1995). In writing Eq. (4.17) the term corresponding to the reverse process, i.e. C_i attachment, was tacitly omitted, since it can be neglected at the low concentrations of C_i molecules encountered in CDS.

The spontaneous evaporation rate is unaffected by grain drift since it is an intrinsic property of the grain dependent on its internal temperature.

Nonthermal sputtering. As mentioned above, grain erosion due to nonthermal sputtering will also be included. It will become relevant when the drift velocity of a grain exceeds ~ 40 km s^{-1}. The corresponding rate of grain size reduction is given by (cf. also Sect. 3.1.3)

$$\tau_{\rm sp}^{-1} = \pi a_0^2 v_{\rm dr}(a)(n_{\langle {\rm H}\rangle} Y_{\rm sp,H} + n_{\rm He} Y_{\rm sp,He}) \tag{4.18}$$

where $Y_{{\rm sp},i}$ denotes the sputtering yield, i.e. the number of lattice particles removed from the grain surface per incident gas particle of species i, and n_i is the number density of that species. In case of solar chemical composition of the gas contributions to the sputtering of carbon grains from elements other than hydrogen and helium can be neglected (Woitke et al. 1993). In the present calculation semianalytical yields derived from experimental data (for details see Tielens et al. (1994) and references therein) have been used.

The grain size distribution function

It was shown in Chapter 1 that the value of the grain size distribution $f(a)$ at any radius r and for every grain size $a_r(r_*)$ can be calculated from the following differential balance or conservation equation

$$r^2[v_{\rm g} + v_{\rm dr}(a_r(r_*))]f(a_r(r_*))\frac{{\rm d}a_r(r_*)}{{\rm d}r_*} + r_*^2 J_\ell(r_*) = 0 \tag{4.19}$$

where $f(a)$ is the density of grains with size a per size interval da and J_ℓ denotes the nucleation rate. For the present calculations the expression for J_ℓ resulting from classical nucleation theory as given by Gail et al. (1984) was adopted, being aware that the application of classical nucleation theory to grain formation has been critizised, for example by Donn & Nuth (1985).

A perhaps more realistic approach is the formulation of the chemical pathway to carbon soot, which proceeds via formation of polycyclic aromatic hydrocarbons (Keller 1987, Frenklach & Feigelson 1989, Cherchneff et al. 1992). Therefore, wind models with a corresponding preliminary nucleation rate (cf. Goeres et al. 1996) were also calculated. These wind models additionally included a parameterized wave pressure force term (for details cf. Sedlmayr 1989). However, as these modifications merely resulted in a shift of the condensation zone outwards to larger radii and lower temperatures these models will not be presented here.

In writing Eq. (4.19) the source term Q given in Eq. (1.15) which accounts for discontinuous processes arising, for example, from grain-grain collisions was omitted. This is firstly due to our poor understanding of the physics of grain-grain collisions (cf. Seab 1987). Secondly, Dominik et al. (1989) have argued that grain coagulation, for instance, is of minor importance in the context of dust driven winds around late-type stars, because the time scale for grain-grain collisions is too large.

The derivative of $a_r(r_*)$ in Eq. (4.19) is not readily obtained, since $a_r(r_*)$ is actually an integrated quantity (cf. Eq. (4.11)) depending on $a_{r'}(r_*)$ for $r' < r$. The computational multi-component scheme described in Chapter 2 comprises the evaluation of ${\rm d}a_r(r_*)/{\rm d}r_*$ by finite differences on a non-uniform $a_r(r_*)$-grid which is moving in the grain size space. This grid is constructed by following the evolution of the size of a large, variable number of grains originating from appropriately chosen radii $r_i \equiv r_{*,i}$ (cf. Sect. 4.2).

Velocity and temperature of grains

Concerning the momentum balance of the grains it was shown by Krüger et al. (1994) that the grains are closely momentum coupled to the gas and thus move with their respective equilibrium drift velocity relative to the gas. This drift velocity results from balancing $f_{\rm drag}(a)$, the gravitational force and the radiative acceleration force $f_{\rm rad}(a)$ acting on a grain of size a and is given by

$$\begin{aligned} v_{\rm dr}^2(a) = &-\frac{128c_T^2}{18\pi} \\ &+\left[\left(\frac{128c_T^2}{18\pi}\right)^2+\left(\frac{4\pi\kappa_H(a)H}{c}-\frac{4\pi GM_*a^3\rho_{\rm s}}{3r^2}\right)^2(\rho_{\rm g}\pi a^2)^{-2}\right]^{1/2} \end{aligned} \tag{4.20}$$

where $\rho_{\rm s}$ denotes the mass density of the grain material, M_* is the stellar mass, H the frequency integrated Eddington flux (cf. Sect. 4.1.3) and $\kappa_H(a)$ the corresponding mean absorption cross-section of a single grain.

Since the dust component is a pressure-less medium, only the internal energy of the dust is relevant for the energy balance. This energy can be characterized by an internal lattice temperature $T_{\rm d}$ of the grains. It can be shown that the energy exchange rate with the radiation field is several orders of magnitude larger than all other cooling or heating processes for a particular grain (e.g. Gauger et al. 1990). Then the internal dust temperature is simply given by the RE temperature defined in Sect. 4.1.3

$$T_{\rm d} = T_{\rm rad}. \tag{4.21}$$

Derived quantities

Given the size distribution macroscopic quantities like the total dust opacity $\kappa_H^{\rm d}$, the collisional drag force of the grains $f_{\rm drag}$ and the rate of carbon consumption due to grain growth $\mathcal{N}_{\rm C}$ can be calculated by simple integration

$$\kappa_H^{\rm d} = \int_{a_\ell}^{\infty} f(a')\kappa_H(a')\,da' \tag{4.22}$$

$$\begin{aligned} f_{\rm drag} &= f_{\rm rad}^{\rm d} \\ &= \frac{4\pi}{c}\kappa_H^{\rm d}H \end{aligned} \tag{4.23}$$

$$\mathcal{N}_{\rm C} = \int_{a_\ell}^{\infty} f(a')\frac{1}{\tau_{\rm net}(a')}\left(\frac{a'}{a_0}\right)^2 da'. \tag{4.24}$$

4.1.3 Radiative transfer

The stellar flux is generated in regions well below the photosphere. Since the flux of both the kinetic and the thermal energy of the flow is negligible compared to the radiative flux no significant amount of energy is added or substracted from the radiation field[1]. Then the equation of flux conservation can be integrated to give

$$H = \frac{\sigma_{\rm R} T_*^4}{4\pi} \left(\frac{R_*}{r}\right)^2 \tag{4.25}$$

A semi-analytical method to describe radiative transfer in extended circumstellar shells has been developed by Lucy (1971). The basic idea is to close the system of moment equations for the radiation field by splitting the specific intensity $I_\nu(r,\mu)$ of the radiation into two contributions. One part comes directly from the solid angle

$$\mu_* = \sqrt{1 - \frac{R_*^2}{r^2}} \tag{4.26}$$

filled by the stellar photosphere and the other part comes from the corresponding complementary solid angel. Then the first-order moment equation can be solved analytically yielding

$$J = \frac{\sigma_{\rm R} T_*^4}{2\pi} \left(1 - \mu_* + \frac{3}{2}\tau_{\rm L}\right) \tag{4.27}$$

for $r > R_*$, where $\tau_{\rm L}$ is some kind of diluted optical depth variable defined by

$$\frac{{\rm d}\tau_{\rm L}}{{\rm d}r} = -(\kappa_H^{\rm g} + \kappa_H^{\rm d}) \frac{R_*^2}{r^2}. \tag{4.28}$$

Due to the frequency integrated treatment of continuum radiative transfer the spectral distribution of the stellar flux is not known. Therefore the flux mean of the gas opacity is replaced by the Rosseland mean $\kappa_{\rm R}^{\rm g}$ of the gas, which has been interpolated from tables provided by Scholz (Scholz & Tsuji 1984).

In order to model the absorption properties of grains an approximation similar to that presented by Dominik et al. (1989) was implemented

$$\kappa_H(a) = \min\left\{\pi a^3\, 5.9 T_{\rm rad}; 2\pi a^2\right\} \tag{4.29}$$

where the optical constants are adopted from Gail & Sedlmayr (1985) assuming the grains to have amorphous structure. This expression fits the two limit cases of Mie theory when the grains can be assumed either much smaller or larger than the relevant wavelengths involved.

[1]This may not be true in variable objects where shock waves travel through the stellar shell. Here the gas is heated by dissipation of mechanical energy which is at least partially reradiated.

By means of Eq. (4.27) a RE temperature can be defined in the following way

$$T_{\rm rad}^4 = \frac{\pi}{\sigma_{\rm R}}\frac{\kappa_J}{\kappa_B}J \tag{4.30}$$

$$= \frac{T_*^4}{2}\left(1-\sqrt{1-\frac{R_*^2}{r^2}}+\frac{3}{2}\tau_{\rm L}\right)\frac{\kappa_J}{\kappa_B} \tag{4.31}$$

where κ_B is the Planck mean. Assuming $\kappa_J = \kappa_B$ (grey approximation) yields

$$T_{\rm rad}^4 = \frac{T_*^4}{2}\left(1-\sqrt{1-\frac{R_*^2}{r^2}}+\frac{3}{2}\tau_{\rm L}\right) \tag{4.32}$$

4.2 Method of solution

In the previous section the stellar wind has been described by three ordinary differential equations (ODE's) (4.4), (4.9) and (4.28) for the corresponding quantities $v_{\rm g}$, $\epsilon_{\rm C}$ and $\tau_{\rm L}$. These ODE's are subject to the following boundary conditions

$$\epsilon_{\rm C}(R_*) = \epsilon_{\rm C,0} \tag{4.33}$$

$$\tau_{\rm L}(R_*) = 2/3 \tag{4.34}$$

$$\tau_{\rm L}(r\to\infty) = 0. \tag{4.35}$$

Furthermore, an additional internal boundary condition has to be satisfied for the wind equation (4.4) to remain regular at the critical point $r(v_{\rm g} = c_T)$, namely

$$\frac{2c_T^2}{r}-\frac{GM_*}{r^2}+\frac{1}{\rho_{\rm g}}f_{\rm drag}-\frac{{\rm d}c_T^2}{{\rm d}r} = 0. \tag{4.36}$$

In order to determine the grain size distribution according to Eq. (4.19) this system of ODE's is supplemented by a variable number I of ODE's of type (4.10) for the size evolution of sample grains. The corresponding initial conditions at $r_i \equiv r_{*,i}$ are given by

$$a(r_i) = a_\ell. \tag{4.37}$$

In this way a moving, non-uniform grid in grain size space is constructed, its points being identified with the momentary sizes $a_r(r_i)$ of sample grains.

Then, the value of the size distribution at $a_r(r_i)$ for $1 \le i \le I$ can be calculated from Eq. (4.19) where the derivative ${\rm d}a_r(r_*)/{\rm d}r_*$ is approximated by the analytic derivative of the Lagrange interpolating polynomial of degree two passing through the set of points $\{r_j, a_r(r_j)\}$ with $j = i-1, i, i+1$ (cf. Sect. 2.2). By appropriate adjustment of the set of points the size distribution at $a_r(r_1)$ and $a_r(r_I)$ can be calculated in an analogous manner.

During the integration of the flow equations outwards from the stellar surface the number I of ODE's of type (4.10) is successively incremented. This is done in order to achieve a sufficient resolution of the size distribution. A new ODE is added whenever the estimated final size of a grain condensing at the momentary radius r is smaller than a chosen fraction of the estimated final size of the previous sample grain created at r_I:

$$\log a_\infty(r_I) - \log a_\infty(r) > \delta. \tag{4.38}$$

In the limit case of negligible drift the final grain size can be estimated from the local growth conditions and is given by (Dominik et al. 1989)

$$a_\infty(r) = \tau_{\rm net}^{-1} \frac{a_0}{3} \left(\frac{2 v_{\rm g}}{r}\right)^{-1}. \tag{4.39}$$

The value of δ is chosen according to the desired resolution of the grain size distribution at infinity. In order to get a final number $I_{\max}$ of grid points one puts

$$\delta = \frac{\log a_\infty(r_1) - \log a_\ell}{I_{\max} - 1} \tag{4.40}$$

corresponding to a roughly logarithmically equidistant grid in grain size space. Numerical experience has shown that $I_{\max} \sim 100$ yields a fair resolution, although the code is stable for $I_{\max}$ as low as ~ 50. Increasing $I_{\max}$ above ~ 300 results in no additional smoothing of the size distribution or its derived quantities.

These derived quantities of the size distribution (cf. Sect. 4.1.2) are calculated by approximating the integrals by the extended trapezoidal rule (cf. Sect. 2.4).

The system of ODE's (4.4), (4.9), (4.28) and $I_{\max}$ times (4.10) and their initial or boundary conditions (4.36), (4.33), (4.34), (4.35) and $I_{\max}$ times (4.37) constitute a combined eigen- and boundary value problem. It is solved by means of an appropriately modified nested shooting method originally proposed by Gail & Sedlmayr (1985, 1987). The procedure can be summarized as follows

1. The free stellar parameters M_*, L_* and T_*, the initial elemental abundances ϵ_i are fixed and a trial mass loss rate $\dot{M}$ is chosen.

2. The flow equations are integrated outwards from $r = R_*$ with a trial initial gas velocity $v_{\rm g,0}$ which is varied until the internal boundary condition (4.36) is satisfied *at the sonic point*, where $v_{\rm g} = c_T$. As described above the dimension of the system of ODE's is successively incremented after the onset of dust formation.

3. In the immediate neighbourhood of the critical or sonic point the gradient of the gas velocity is calculated according to l'Hospital's rule. This has the consequence that the solution slightly misses the correct sonic point. Nevertheless, this procedure forces the solution to pass from the subsonic to the supersonic region.

4. Just beyond the sonic point the integration is resumed with the wind equation (4.4) and with a slightly incorrect initial condition. Since, however, any solution starting somewhere close to the singular point rapidly approaches the correct solution passing through the singular point, no significant error is introduced by this method of treating the subsonic-supersonic transition (Gail & Sedlmayr 1985). The dimension of the system of ODE's is successively incremented up to $3 + I_{\max}$. At a large but finite radius, typically 30 R_*, the integration is stopped.

5. If the diluted optical depth $\tau_{\mathrm{L}}(30\,R_*)$ differs significantly from zero steps 2. to 4. are repeated with a new trial mass loss rate until convergence is achieved.

In this way the complete system of non-linearily coupled equations describing a two-fluid dust driven wind is solved self-consistently. As a consequence the mass loss rate has not to be fixed *a priori* but follows as an eigenvalue of the problem.

Since one deals with a large number of $3 + I_{\max}$ non-stiff ODE's the flow equations are solved by means of an embedded, explicit fourth order Runge-Kutta scheme (Hairer et al. 1987). A typical model run needs a few hours of computing time on a Silicon Graphics IRIS Indigo R 4000 workstation.

4.3 Results and discussion

The multi-component method for the description of the evolution of the grain size distribution presented in Part I was applied to model spherically symmetric winds around cool carbon stars. A grid of models in the domain of purely dust driven winds in the Hertzsprung-Russel diagram (Dominik et al. 1990) was calculated varying the values of the stellar parameters lumininosity L_*, effective temperature T_*, and initial carbon abundance $\epsilon_{\mathrm{C},0}$. The code has proven to be stable for all adopted values of stellar parameters and it is to be expected that the multi-component method will also work for any other astrophysical context.

In order to demonstrate the influence of grain drift on the size distribution and its derived integral quantities two models of dust driven winds with low and high mass loss rates, respectively, are presented. The adopted parameter values are given in Table 4.1. The initial carbon overabundance of 1.7 is a mean value derived from observations of C-stars (Frantsman & Eglitis 1988). For the chemical abundance of H, He, O, N, Fe, Si, Mg, S and Al solar abundances (Allen 1973) are assumed.

Table 4.1: Fundamental stellar parameters of Model A and B

	Model A	Model B
L_*	$3\,10^4\,L_\odot$	$5\,10^4\,L_\odot$
T_*	2300 K	2100 K
M_*	$1\,M_\odot$	$1\,M_\odot$
$\epsilon_{\rm C,0}$	$1.7\,\epsilon_{\rm O}$	$1.7\,\epsilon_{\rm O}$

For comparison, each model was recalculated with the drift velocity of the grains artificially set equal to zero.

4.3.1 Low mass loss model

Structure of the circumstellar envelope

The assumed values of the parameters for Model A which includes grain drift result in a mass loss rate of

$$\dot{M} = 1.5\,10^{-6}\,M_\odot/\mathrm{yr}. \tag{4.41}$$

The hydrodynamic structure of the stellar envelope is presented in Fig. 4.1. The results of Model A neglecting drift are also plotted and indicated by dashed lines. In the upper panel the expansion velocity $v_{\rm g}$ of the gas, the isothermal sound velocity c_T and the drift velocities $v_{{\rm dr},i}$ of the grains are shown. These mean drift velocities $v_{{\rm dr},i}$ are defined by

$$v_{{\rm dr},i} = \frac{\int_{a_\ell}^{\infty} a^i f(a) v_{\rm dr}(a)\, da}{\int_{a_\ell}^{\infty} a^i f(a)\, da} \tag{4.42}$$

and were introduced, since the depiction of the grain drift velocity is somewhat difficult due to the fact that this drift velocity varies with grain size. For $i = 0$ Eq. (4.42) yields the mean drift velocities averaged over all grains. For $i = 1, 2, 3$ the $v_{{\rm dr},i}$ can be interpreted as radius, surface or volume weighted drift velocities, respectively. Consequently, $v_{{\rm dr},3}$ is the drift velocity associated with the center of mass of the dust component.

Near the stellar photosphere the gas velocity is only several cm/s, the atmosphere nearly is in hydrostatic equilibrium. The gas velocity rises steeply with the increasing drag force and at $r = 1.7 R_*$ exceeds the isothermal sound velocity which varies only weakly and is of the order of 2 km/s. Beyond the sonic point radiation pressure on dust first causes the gas velocity to further increase. Because of the decrease of

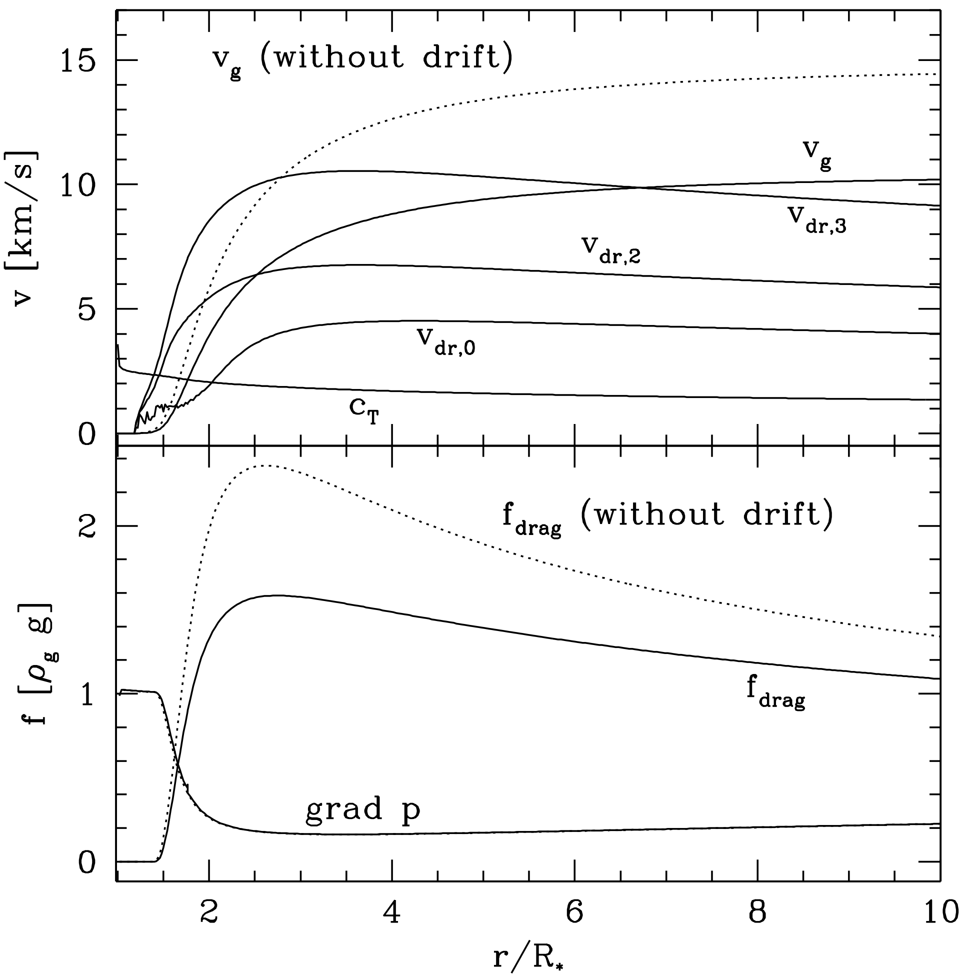

Figure 4.1: Dynamical structure and acting forces of Model A (dashed lines indicate the results neglecting drift). The upper panel shows the radial course of the gas velocity v_g, the isothermal sound velocity c_T, and the mean drift velocities $v_{dr,i}$ (see text). The pressure gradient and the drag force are depicted in the lower panel.

f_{drag} the gas velocity approaches a constant terminal velocity of $v_{g,\infty} = 10.4$ km/s. This value lies well within the range of 7 to 30 km/s observed for cool stellar winds (Knapp 1987).

The mean grain drift velocities $v_{dr,i}$ are weighted towards larger grains for increasing i. The important point to notice here is that although the mean drift velocity $v_{dr,0}$ is of moderate magnitude and comparable with the thermal sound velocity of the gas the bulk of the dust moves with a drift velocity $v_{dr,3}$ relative to the gas which is of the same order as the gas velocity. In the inner region of the wind $v_{dr,3}$ may even be much higher than the gas velocity.

Apart from the grain size the drift velocity of the dust is mainly dependent on the gas density and varies only slightly beyond the sonic point. At large distance from the star there even is a small decrease of the mean drift velocities, since the radiation pressure on the grains is decreased due to increasing reddening of the radiation field.

The lower panel of Fig. 4.1 depicts the forces acting on the bulk of the gas, i.e. the collisional drag force f_{drag} exerted on the gas due to radiatively accelerated dust grains and the pressure gradient grad p, both normated to the gravitational force. The sharp increase of the drag force is caused by the increasing number of dust grains. Its decrease results from the reddening of the radiation field which diminishes the radiation pressure on the dust. The maximum ratio of the drag force f_{drag} and the gravitational force $\rho_{\mathrm{g}} g$ is α_{max}=1.6. It can be clearly seen that inside the dust shell the wind is accelerated by the pressure gradient whereas beyond the sonic point the pressure gradient contributes only little to the further acceleration of the wind.

The circumstellar dust shell (CDS) is optically thin and thus there is no significant backwarming (cf. Fig. 4.2). In summary, the general hydro- and thermodynamical structure is similar to the RE standard model presented by Gail & Sedlmayr (1987).

In the lower panel of Fig. 4.2 the diluted optical depth τ_{L} and the optical thickness of the dust shell at $\lambda = 1\,\mu$m are depicted. The latter is given by

$$\tau_{1\mu} = \int_{R_*}^{r} \kappa_{1\mu}^{\mathrm{d}}\,\mathrm{d}r. \tag{4.43}$$

The opacity of the dust can be expressed according to the results of Mie theory for small particles ($a < \lambda/2\pi$) by

$$\kappa_{\lambda}^{\mathrm{d}} = \int_{a_\ell}^{\infty} f(a) 4\pi a^2 \frac{2\pi a}{\lambda} \mathrm{Im}\left\{\frac{m_\lambda^2 - 1}{m_\lambda^2 + 2}\right\} \mathrm{d}a \tag{4.44}$$

where m_λ is the complex refractive index of the material. According to experimental results of Maron (1990) $m_\lambda = 1.799 + 0.228i$ for amorphous carbon at $\lambda = 1\,\mu$m.

The chemical composition of the gas phase is shown in Fig. 4.3. Only the most abundant molecules (except H_2) are plotted relative to CO the concentration of which is constant and in which all the oxygen is locked. The remaining carbon is mainly in the form of acetylene, which therefore constitutes the main growth species. It is only marginally consumed by dust formation. For low gas densities beyond the sonic point the chemical equilibrium concentrations of most species decrease rapidly. However, this is an artificial result due to the chemical equilibrium approach. Actually, the densities and temperatures and hence the chemical reaction rates at these distances are too small to allow for efficient conversion of most molecules by kinetic reactions. As has been stated in Sect. 4.1.1 this particular chemical nonequilibrium effect was taken into account for atomic hydrogen. As a result, the H/H_2 ratio (dashed lines) becomes constant for $r > 1.4\,R_*$ while the chemical equilibrium (CE) H/H_2 ratio decreases further.

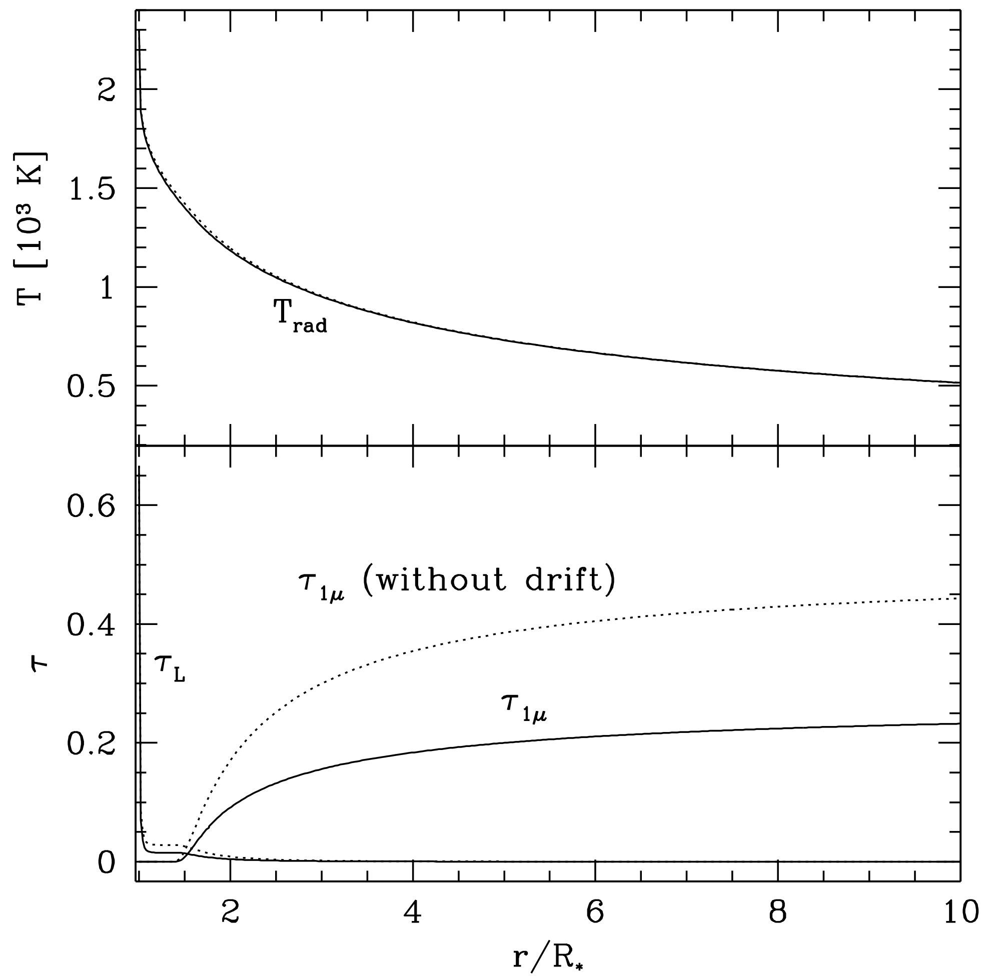

Figure 4.2: Thermodynamical structure and optical depths of Model A (dashed lines indicate the results neglecting drift). The upper panel shows the radial course of the radiative equilibrium temperature. The diluted optical depth τ_{L} and the optical thickness of the dust shell at $\lambda = 1\,\mu$m are depicted in the lower panel.

Grain size distribution

The formation or temporal evolution of the size distribution f in dust driven winds has been discussed in detail by Dominik et al. (1989) for the limit case of neglected drift. Their main results remain valid and will be shortly summarized here

- In the inner, subsonic region the growth conditions are excellent. Moreover, the grains remain in this region for a long time. As later growth further downstream is negligible the grains grow to a large final size almost locally.

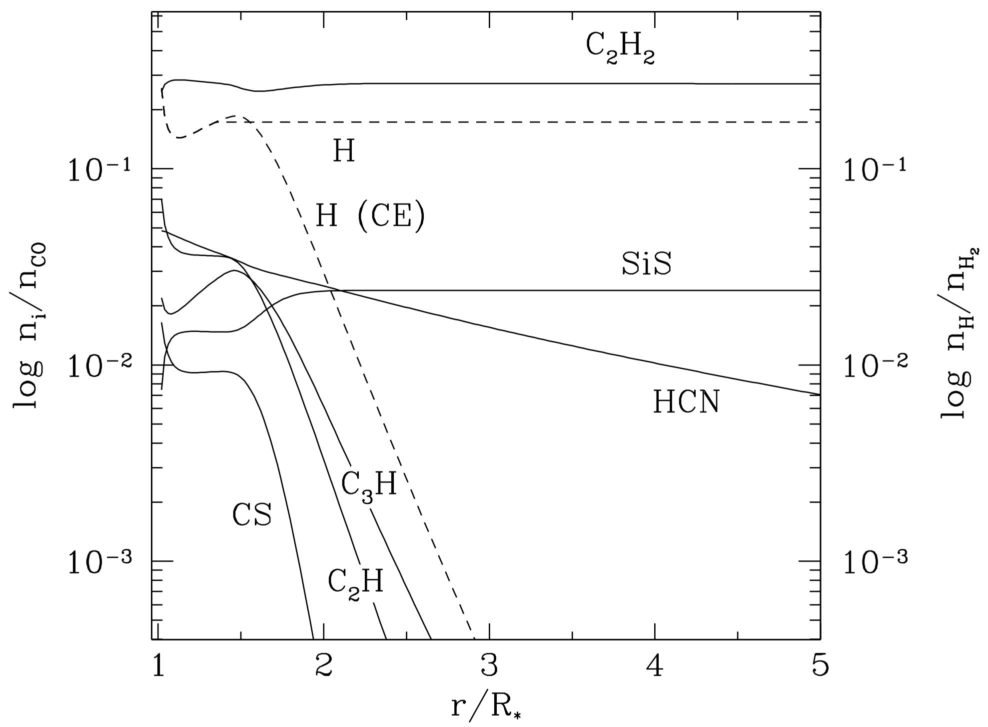

Figure 4.3: Radial course of the densities of selected chemical species and of the H/H_2 ratio (dashed lines, right ordinate) for Model A. The chemical equilibrium (CE) H/H_2 ratio is also depicted.

However, due to comparatively high temperatures close to the star only few grains are formed resulting in the characteristic tail of the distribution function for very large grain sizes.

- In the sonic point region nucleation is very efficient. Most of the grains are created here. They are of medium size since growth conditions have deteriorated due to decreasing gas density and reduced hydrodynamical time scale.
- In the outer, supersonic region the wind becomes increasingly diluted and after some further growth of existing grains the size distribution rapidly approaches the final distribution. Only few new grains are created which do not grow efficiently and form the tail of the size distribution for very small grains.

Turning to a discussion of how the consideration of grain drift affects the final size distribution, five main effects of drift can be distinguished

- Since the flux of grains is conserved the dust becomes increasingly dynamically diluted for high drift velocities (cf. Eq. (4.19) and Krüger et al. 1994).

- The collisional rate between grain and growth species is increased due to larger relative velocities (cf. Eq. (4.14)).
- The dehydrogenation probability p increases, since the activation energy barrier for hydrogen–abstraction is overcome more easily (cf. KPS).
- For drift velocities exceeding $\sim$ 5 km s^{-1} the growth species tends to just bounce off the grain surface, i.e. the sticking efficiency α decreases (cf. Eq. (4.16)).
- As the grain drifts out of the gas element where it has been created, the time of residence in a region of efficient growth is reduced (cf. Eq. (4.10)).

The four latter effects directly influence the growth efficiency of dust grains.

Let us introduce a quantity A_i defined by

$$A_i = \left(1 + \left(\frac{v_{\mathrm{dr},i}}{4\,\overset{\circ}{v}_{\mathrm{C_2H_2}}}\right)^2\right)^{1/2} \cdot \frac{p(v_{\mathrm{dr},i})}{p} \cdot \alpha(v_{\mathrm{dr},i}) \cdot \frac{v_{\mathrm{g}}}{v_{\mathrm{g}} + v_{\mathrm{dr},i}} \tag{4.45}$$

as a measure of the modification of the local growth rate, such that A_i comprises all four effects. Here, $p(v_{\mathrm{dr},i})$ and $\alpha(v_{\mathrm{dr},i})$ are calculated for relative velocities v_{rel}, which are increased according to drift velocities $v_{\mathrm{dr},i}$, while p is calculated for the hypothetical case of purely thermal relative motion. Each of the four factors in Eq. (4.45) corresponds to one of the effects mentioned above: the 'sweeping up' of condensable material, the increased surface density of radical sites, the reduced sticking efficiency and the 'drifting away'. Again, for increasing i the A_i correspond to increasingly larger grains.

Figure 4.4 depicts the radial course of A_i for $i = 0, 2, 3$. In the subsonic regime close to the star the growth efficiency is depressed by a factor of up to 10^2, since the grain velocity, though small compared to the sound velocity, is much larger than the expansion velocity of the gas and grains quickly drift away from their point of creation outwards to regions of less efficient growth.

The majority of the grains is created around the sonic point. Here, the two drift effects of 'sweeping up' and 'drifting away' approximately cancel for these small grains ($a \sim 10$ nm). There is, however, no further growth of large or medium sized grains: Although the large drift velocity of these grains somewhat increases their surface radical density, the sticking efficiency α_3 is virtually zero (cf. Fig. 4.5). In the outer region ($r \gtrsim 4\,R_*$) grain drift continues to inhibit further growth of large grains and somewhat reduces the growth efficiency of small grains.

The resulting size distribution at $r = 30\,R_*$ is shown in the upper panel of Fig. 4.6. The dashed line included for comparison indicates the model with zero drift velocity. By comparison, the size distribution corresponding to the model including

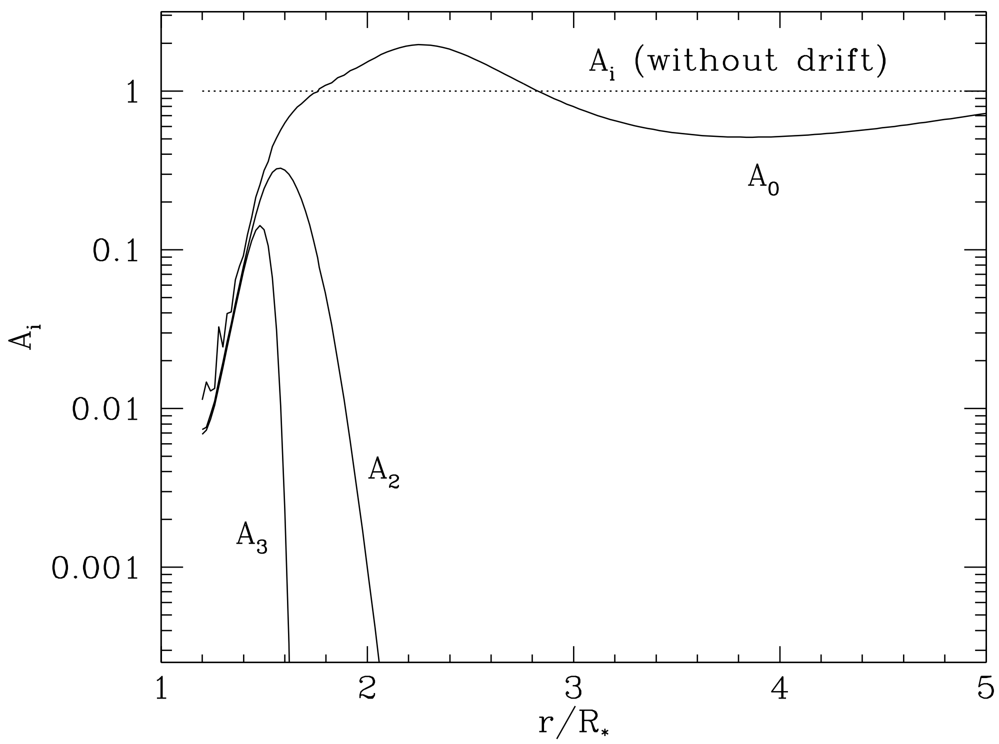

Figure 4.4: Relative change A_0, A_2, A_3 of local growth rate due to drift velocities $v_{\mathrm{dr},0}, v_{\mathrm{dr},2}, v_{\mathrm{dr},3}$ for Model A. Dashed lines indicate the resulting $A_i \equiv 1$ neglecting drift.

grain drift appears distorted. There is a pronounced decrease of the distribution at small grain sizes (1 nm $< a <$ 10 nm).

The cut-off of the distribution function at $a \sim 1$ μm is mainly due nonthermal sputtering. Grains larger than this limit size have very high drift velocities ($v_{\mathrm{dr}}(a) \gtrsim 40\,\mathrm{km\,s^{-1}}$) and are efficiently eroded by collisions with gas particles (mainly He atoms). This cut-off of the distribution function has also been postulated by Jura (1994) in order to explain the observed circumstellar polarisation of IRC+10216 at 2.2 μm (K-band).

To first order, both distribution functions can be fitted piece-wise by power laws of the form a^γ. The spectral indices for the descending branches of the distribution functions (which make up most of the mass of the dust component, see below) are $\gamma \approx -4.2$ for the model where drift was included and $\gamma \approx -4.6$ when drift is neglected. Though tempting in this context, it does not seem apt to compare the obtained spectral indices with the one deduced for the grain size spectrum in the interstellar medium (Mathis et al. 1977) which is $\gamma \sim -3.5$. The latter is bound to result from the superposition of many size distributions originating from distinct dust forming objects, and is furthermore subject to constant processing by

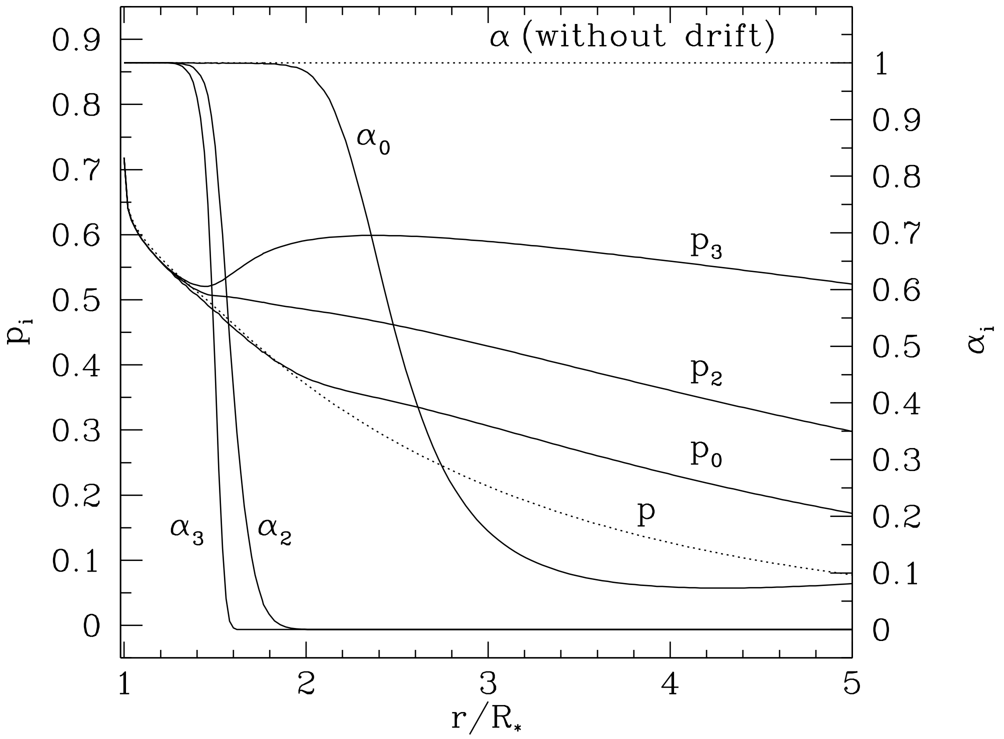

Figure 4.5: Radial course of the dehydrogenation probability $p_i \equiv p(v_{\mathrm{dr},i})$ and the sticking efficiency $\alpha_i \equiv \alpha(v_{\mathrm{dr},i})$ for Model A. Dashed lines indicate the resulting p, α neglecting drift.

interstellar shock waves (e.g. Liffman & Clayton 1989).

Also presented are plots of $f(a)$ multiplied by a and a^4. In Fig. 4.6b the area below the curve for a given size interval $\Delta \log a$ now corresponds to the *number* of grains in this interval. Obviously, without drift the total number of grains is higher than in the case where drift is included, although the position of the maximum, i.e. the most probable or mean grain radius, varies only little. This can also be seen from the radial course of the macroscopic quantities (cf. Fig. 4.7). Depicted are the nucleation rate J_ℓ and the corresponding increase of the number density n_d of dust grains, both normated to the total hydrogen density. The lower panel shows the ratio $\dot{M}_\mathrm{d}/\dot{M}_\mathrm{g}$ of the mass loss rates of the dust and the gas component, the corresponding mass density ratio $\rho_\mathrm{d}/\rho_\mathrm{g}$, which is equal to $\dot{M}_\mathrm{d}/\dot{M}_\mathrm{g}$ only in case of negligible drift, and the mean grain radius $\langle a \rangle$.

This reduction of the grain density due to drift by about 40% can be explained in the following way: First, the dust component is dynamically diluted. Furthermore, there are less grains created in the first place, i.e. the nucleation rate peaks at a lower value. This is due to the fact that comparatively many large grains are formed in the inner region consuming a significant portion of condensable material (and therefore

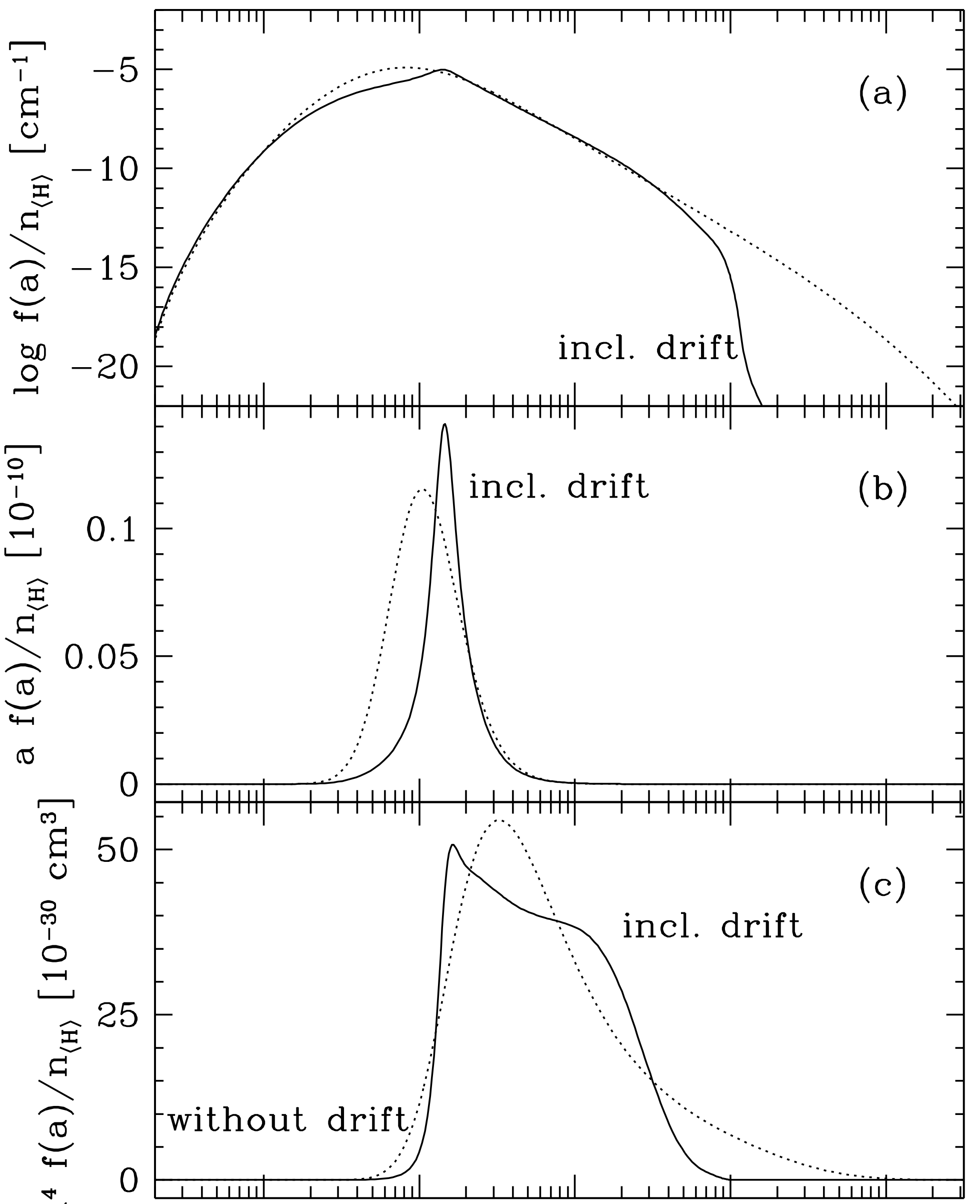

Figure 4.6: **a** Grain size distribution at $r = 30\,R_*$ for Model A. **b** Size distribution multiplied by a. **c** Size distribution multiplied by a^4. All quantities are normated to the total hydrogen density.

suppressing further efficient nucleation, cf. Fig. 4.8) without efficiently driving the wind (since these grains are dynamically diluted). This effect of drift should be quite

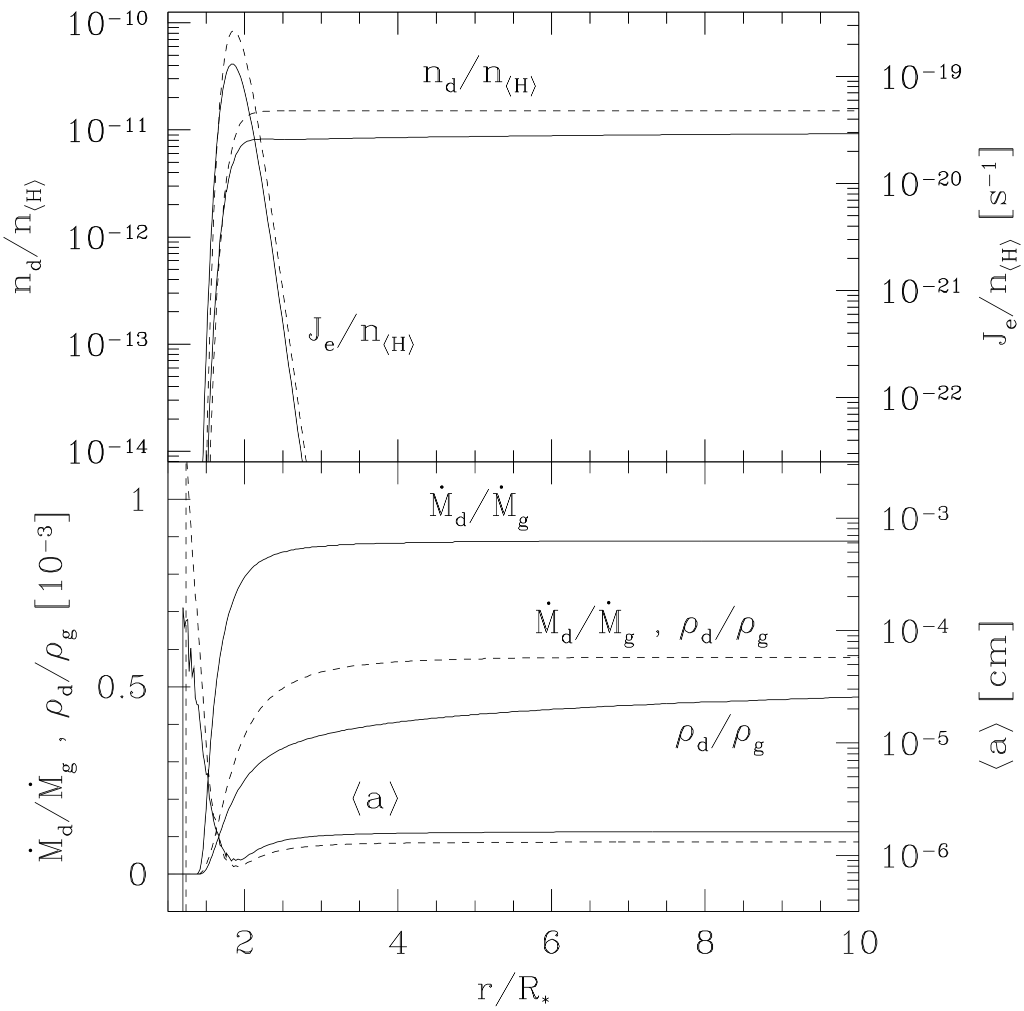

Figure 4.7: Radial course of dust related quantities for Model A (dashed lines indicate the results neglecting drift). The upper panel shows the radial course of the total dust density n_d and the nucleation rate J_ℓ, both normated to the total hydrogen density. The dust-to-gas density and mass loss ratios are depicted in the lower panel along with the mean grain radius $\langle a \rangle$.

independent of the specific nucleation mechanism adopted here, since every realistic expression for the nucleation rate will to *some* degree be dependent on the amount of condensable material.

In Fig. 4.6c the area below the curve corresponds to the *volume* or *mass* contained in the grains. The consideration of drift leads to a considerable distortion of the distribution of condensed matter. The average grain mass is now 40% larger as in the case of neglected drift. Although n_d is reduced, the dust-to-gas mass ratio $\dot{M}_\mathrm{d}/\dot{M}_\mathrm{g}$ injected into the ISM, is increased by about 50% compared to the case of neglected drift (cf. the lower panel of Fig. 4.7). On the other hand, the dust component is

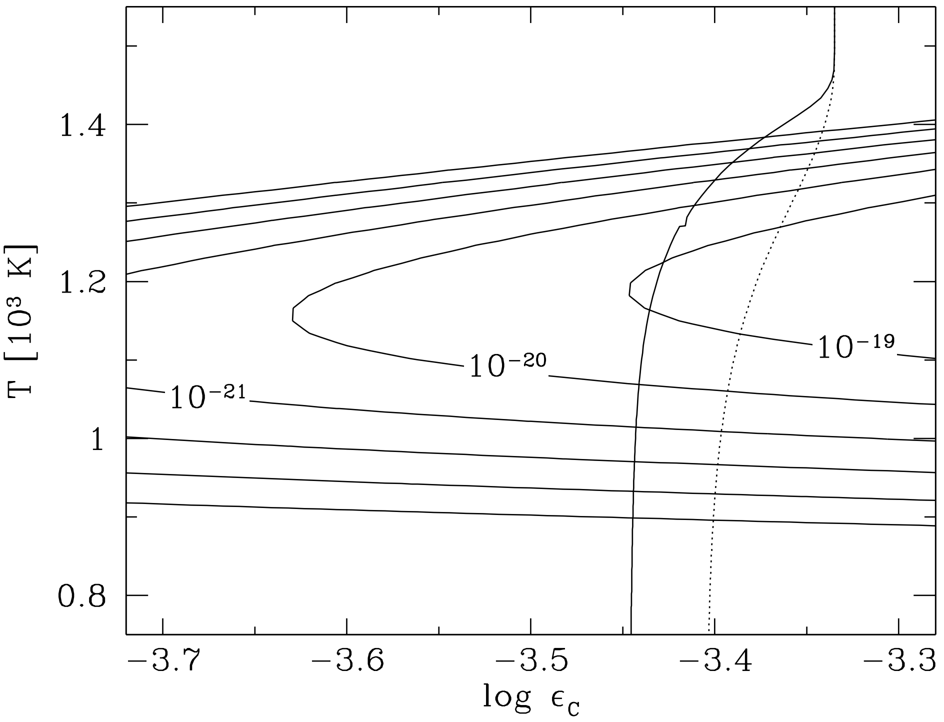

Figure 4.8: Curves of constant nucleation rate J_* per hydrogen atom in the $\log \epsilon_C$-T-plane for Model A. The vertical lines show wind trajectories (dashed lines indicating the results neglecting drift).

dynamically diluted due to the drift increased terminal velocity of the grains and the overall mass density ρ_d actually decreases somewhat (cf. Fig. 4.7).

In this context, it should be emphasized that the commonly employed method of determining $\dot{M}_d$ (e.g. Knapp 1985, Jura 1986) has to be used with care. This has already been noted by Sahai (1990) and Olofsson et al. (1993). In fitting the observed IR-flux of the dust by simple radiative transfer models it is often assumed that the dust velocity is equal to the expansion velocity of the gas. In fact, this procedure only yields the diluted dust density ρ_d and misses a factor of $(v_g + v_{dr,3})/v_g$.

From Fig. 4.6 it can furthermore be seen that grain erosion due to nonthermal sputtering has only a minor influence on the dust component as a whole. The majority of the grains simply is not affected, since they are smaller than the cut-off size (cf. Fig. 4.6b). Only the largest of the mass-bearing grains are subject to sputtering resulting in the comparatively steep right flank of the size distribution in Fig. 4.6a.

4.3.2 High mass loss model

Structure of the circumstellar envelope

The parameters assumed for Model B including grain drift result in a mass loss rate of

$$\dot{M} = 5.5\,10^{-5}\,M_{\odot}/\mathrm{yr}. \tag{4.46}$$

Figure 4.9 depicts the radial course of the sound and expansion velocity of the gas and of the mean drift velocities of the dust. The results of Model B neglecting drift are also plotted and indicated by dashed lines. Due to higher gas densities in Model B compared to Model A the drift velocities are reduced to values $\lesssim 5$ km s^{-1}. However, in the inner region of the wind the grains still move significantly faster than the gas. The terminal velocity of Model B reaches $v_{\mathrm{g},\infty} = 28.3\,\mathrm{km\,s^{-1}}$; the maximum ratio of the drag force f_{drag} and the gravitational force $\rho_{\mathrm{g}} g$ is α_{max}=11.2, which is substantially higher than in the low density model A due to enhanced dust formation.

The circumstellar dust shell is optically thick and gives rise to substantial backwarming (cf. Fig. 4.10). Throughout the circumstellar envelope, the chemical composition of the gas phase is very much the same as in Model A. In summary, the general hydro- and thermodynamical structure is similar to the RE standard model presented by Gail & Sedlmayr (1987).

Grain size distribution

Figure 4.11 depicts the radial course of A_i for $i = 0, 2, 3$. For the high mass loss Model B the growth efficiency is depressed only by a factor of up to 8 in the subsonic regime which is much less than in Model A. In the outer region ($r > 3\,R_*$) growth is enhanced by a factor of up to 4 for the small and medium size grains due to the enhanced dehydrogenation probability of the carbonaceous grain surface (cf. Fig. 4.12) and the 'sweeping up' of condensable material. As in model A, the sticking efficiency α_3 of the growth species on large grains is small beyond the sonic point, and there is little further growth of these grains.

The resulting size distribution at $r = 30\,R_*$ is shown in the upper panel of Fig. 4.13. The dashed line indicates the model with zero drift velocity included for comparison. The consideration of drift now leads to a less significant distortion of the size distribution. However, the amount of ultrasmall particles ($a \lesssim 10$ Å) is increased by nearly an order of magnitude. The existence of such an ultrasmall grain component in the ISM has been suggested on the ground of observations of 1–25 μm infrared emission from interstellar clouds (Sellgren et al. 1983).

The relevant part of the size distribution of Model B including drift can be fitted by power laws with spectral indices $\gamma_1 \approx -2.6$ (20 nm $< a < 0.1\mu$m) and $\gamma_2 \approx -5.3$

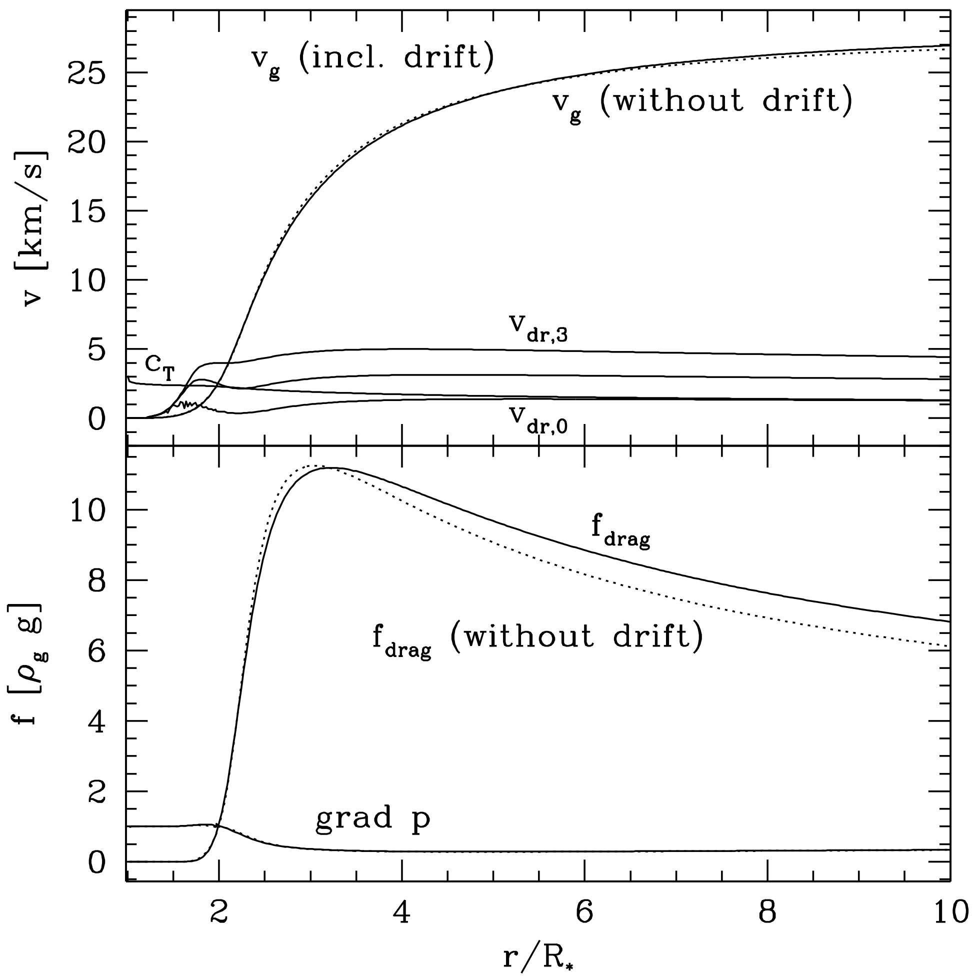

Figure 4.9: Dynamical structure and acting forces for Model B (dashed lines indicate the results neglecting drift). The upper panel shows the radial course of the gas velocity $v_{\rm g}$, the isothermal sound velocity c_T, and the mean drift velocities $v_{{\rm dr},i}$ (see text). The pressure gradient and the drag force are depicted in the lower panel.

($a > 0.1\mu$m), respectively. In the case where drift was neglected the descending branch of the distribution function obeys a power law of the form $a^{-5.1}$.

By analogy with the low mass loss Model A the grain density is reduced by a factor of almost 2 (cf. Figs. 4.13b and 4.14) compared to the case of neglected drift for the same reasons as given in Sect. 4.3.1.

The distribution of condensed material is shifted towards larger grains (cf. Fig. 4.13c). The average grain mass is twice as large, and the relative mass loss rate $\dot{M}_{\rm d}/\dot{M}_{\rm g}$ of the dust component is raised by about 30% compared to the case of

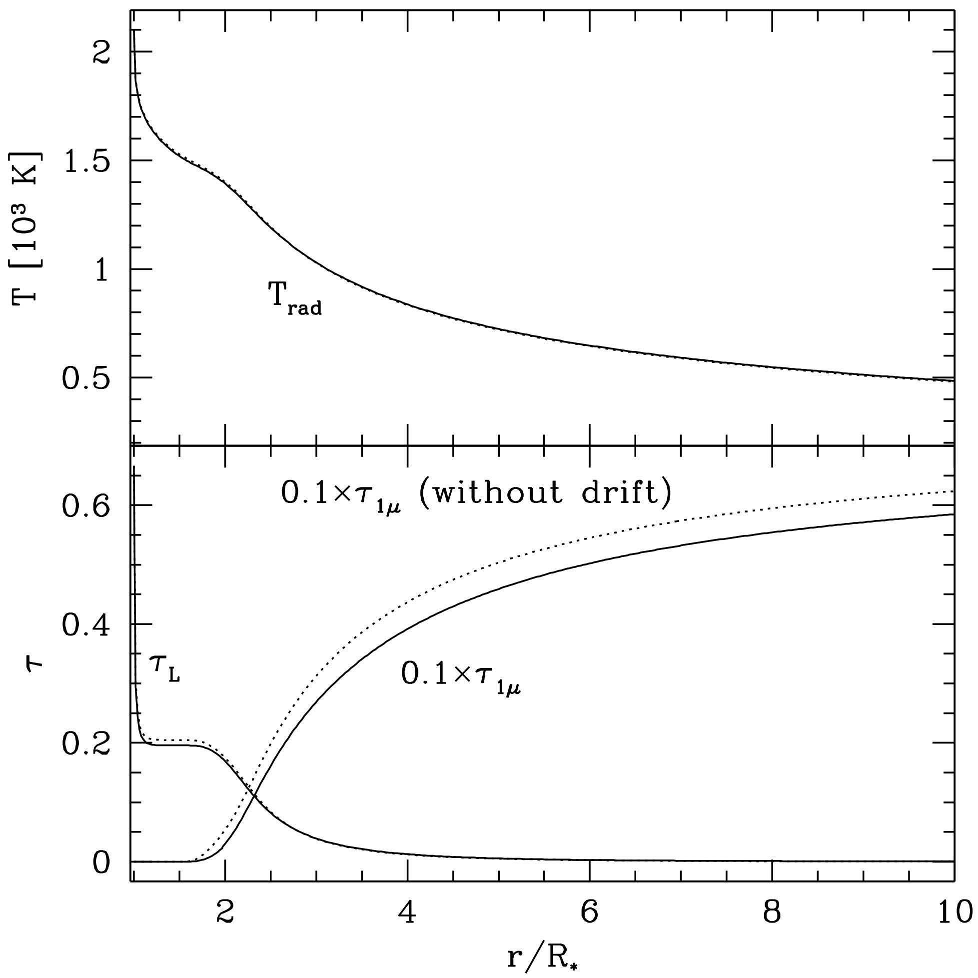

Figure 4.10: Thermodynamical structure and optical depths of Model B (dashed lines indicate the results neglecting drift). The upper panel shows the radial course of the radiative equilibrium temperature. The diluted optical depth $\tau_{\rm L}$ and the optical thickness of the dust shell at $\lambda = 1\,\mu$m are depicted in the lower panel.

neglected drift (cf. Fig. 4.14). Furthermore, although $n_{\rm d}$ is reduced, the overall mass density $\rho_{\rm d}$ of the dust component also somewhat increases (cf. the lower panel of Fig. 4.14).

Because of the moderate drift velocities in Model B nonthermal sputtering has no influence on the shape of the grain size spectrum.

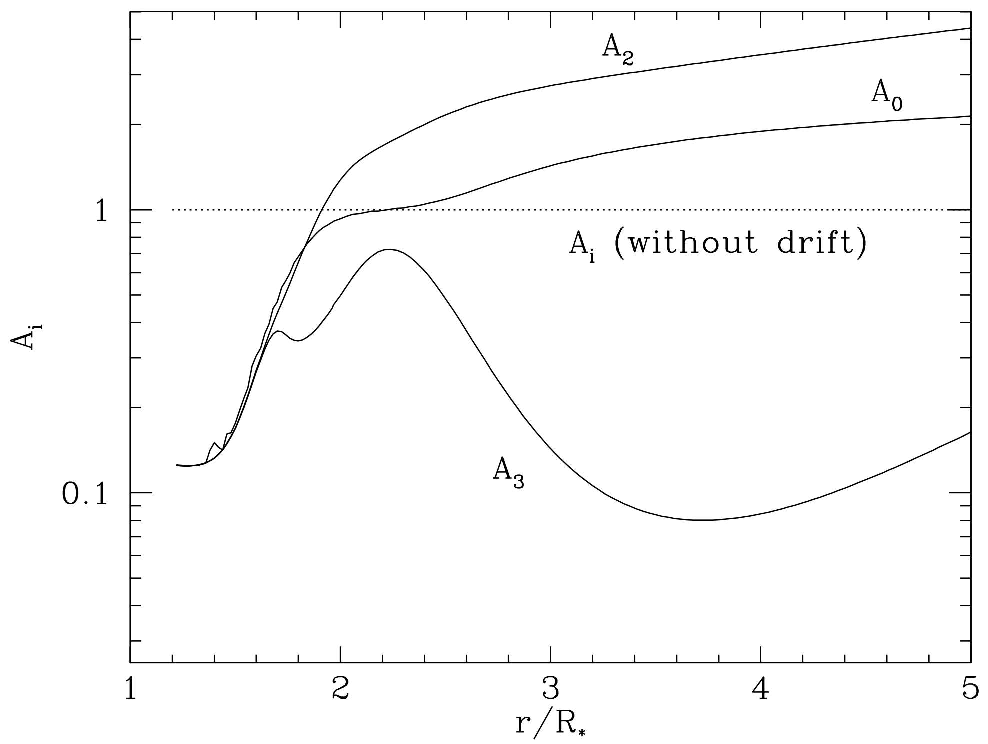

Figure 4.11: Relative change A_0, A_2, A_3 of local growth rate due to drift velocities $v_{\mathrm{dr},0}, v_{\mathrm{dr},2}, v_{\mathrm{dr},3}$ for Model B. Dashed lines indicate the resulting $A_i \equiv 1$ neglecting drift.

4.3.3 The size distribution of stardust injected into the ISM

Eventually the stardust will be injected into the interstellar medium (ISM). As has been shown by Woitke et al. (1993) dust destruction in the transition region of the red giant wind into the ISM is negligible. However, after the grains have come to rest in the ISM and are comoving with the gas, grain densities are increased by a size dependent factor (Krüger & Sedlmayr 1996)

$$\frac{v_{\mathrm{g}}(r_{\max}) + v_{\mathrm{drift}}(a, r_{\max})}{v_{\mathrm{g}}(r_{\max})}.$$

The resulting mass weighted size distribution after injection into the ISM is depicted in Fig. 4.15. As can be seen, the distortion of the distribution of condensed matter when compared to the case of neglected drift is even more pronounced than in the vicinity of the star.

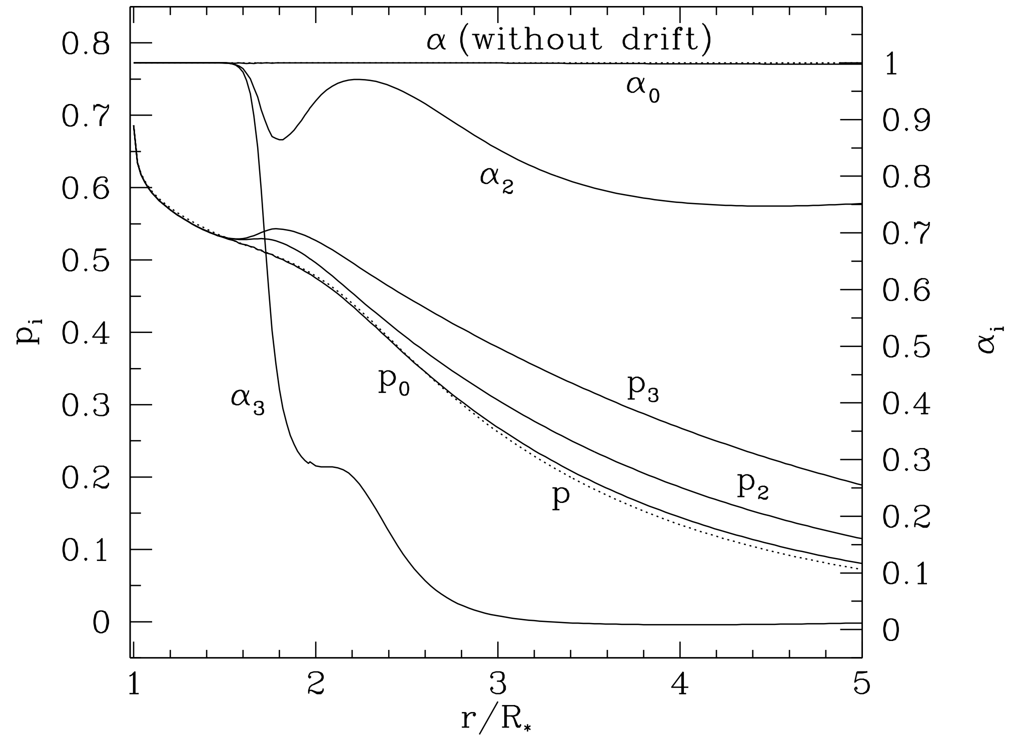

Figure 4.12: Radial course of the dehydrogenation probability $p_i \equiv p(v_{\mathrm{dr},i})$ and the sticking efficiency $\alpha_i \equiv \alpha(v_{\mathrm{dr},i})$ for Model B. Dashed lines indicate the resulting p, α neglecting drift.

4.4 Summary

By means of the multi-component method presented in Part I self-consistent models for dust driven winds in consideration of a size dependent grain drift have been constructed, determining for the first time the shape of the corresponding grain size spectrum. A detailed description of carbonaceous grain growth according to a hydrogen–abstraction/acetylene–addition surface reaction scheme (Krüger et al. 1996) was also included. It was found that although the consideration of grain drift does not greatly affect the resulting general hydro- and thermodynamical structure of the circumstellar envelope it has an decisive influence on the resulting grain size spectrum.

Generally, less but more massive grains are being formed in the models where drift is included. These results are contrary to the preliminary ones obtained by Dominik et al. (1989).

Concerning the microscopic processes, drift mainly reduces the sticking efficiency of the growth species acetylene on large grains with significant drift velocities, although for carbon grains the surface density of radical sites is somewhat increased.

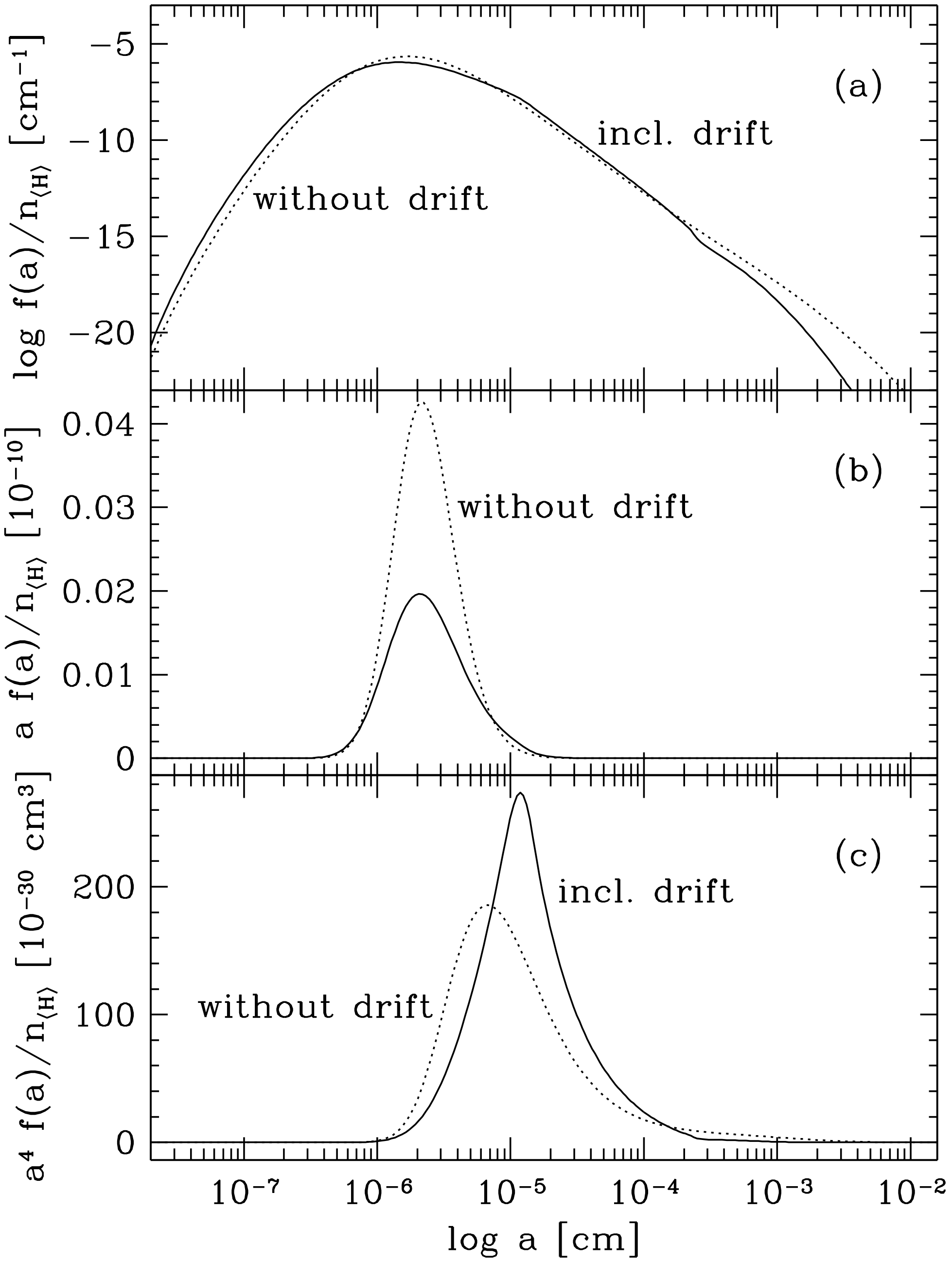

Figure 4.13: **a** Grain size distribution at $r = 30\,R_*$ for Model B. **b** Size distribution multiplied by a. **c** Size distribution multiplied by a^4. All quantities are normated to the total hydrogen density.

Nonthermal sputtering is relevant only for very large grains ($a \gtrsim 1\mu$m) in tenuous winds ($\dot{M} \lesssim 10^{-6}\,M_\odot$/yr).

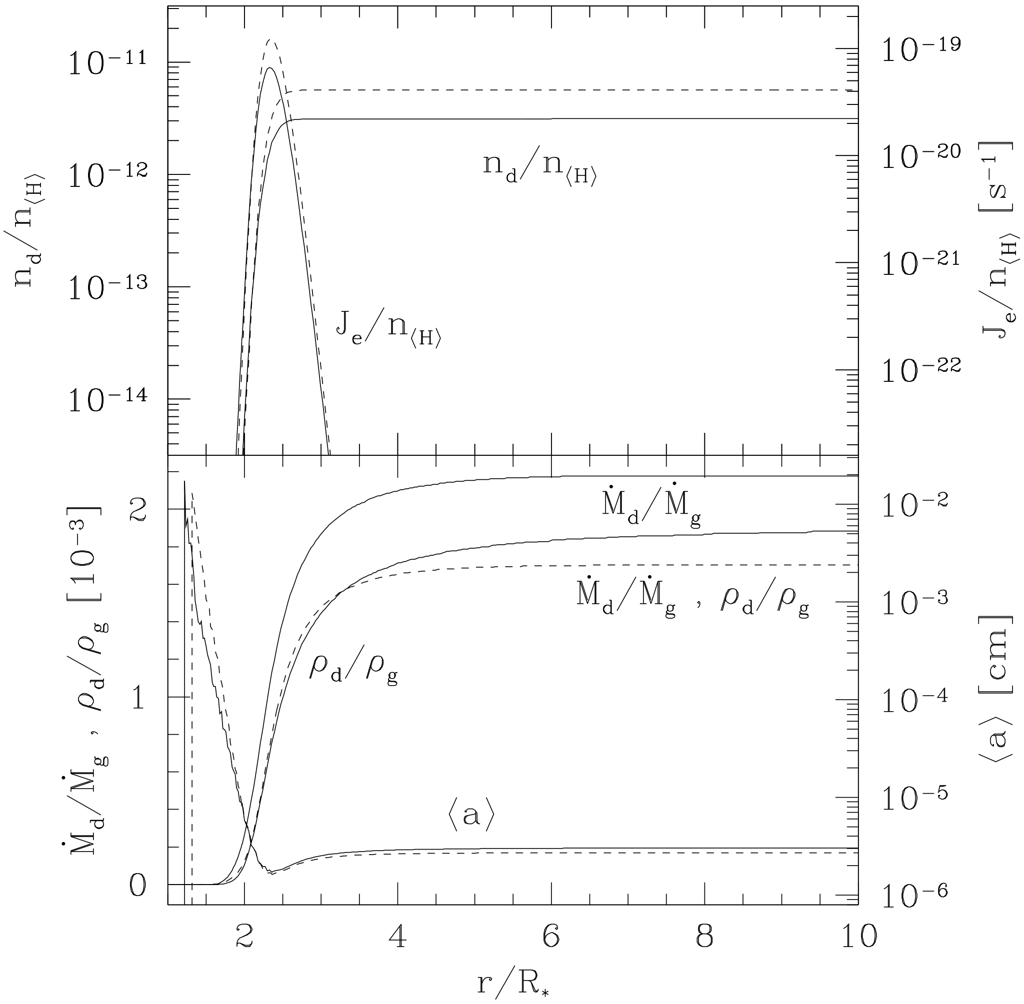

Figure 4.14: Radial course of dust related quantities for Model B (dashed lines indicate the results neglecting drift). The upper panel shows the radial course of the total dust density $n_{\rm d}$ and the nucleation rate J_ℓ, both normated to the total hydrogen density. The dust-to-gas density and mass loss ratios are depicted in the lower panel along with the mean grain radius $\langle a \rangle$.

With regard to stellar diagnostics, grain drift directly affects the prediction of the amount $\dot{M}_{\rm d}$ of dust injected into the interstellar medium. Concerning the modeling of dust driven winds, characteristic quantities like the mass and number density ratios of dust and gas are affected when compared to one-fluid models. The modeling of the optical appearance of circumstellar dust shells should also benefit from a proper consideration of drift, since the resulting spectra depend on the specific shape of the grain size distribution.

The influence of drift gradually increases with decreasing mass loss rate, i.e. decreasing density in the CDS. Thus, the consideration of drift seems to be especially

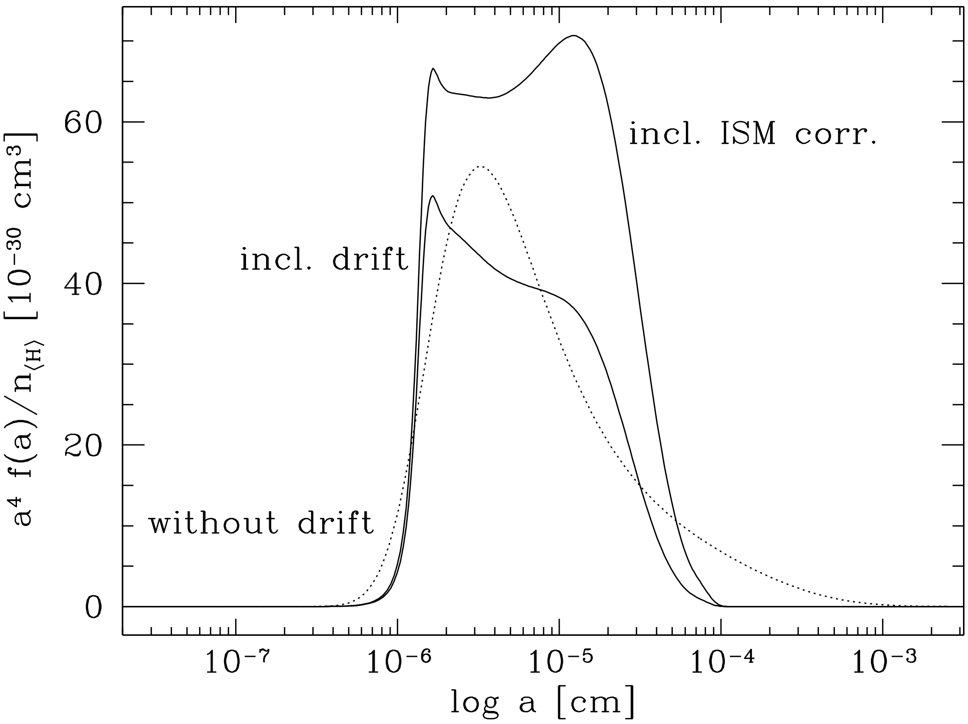

Figure 4.15: Comparison of the grain size distribution function multiplied by a^4 before and after injection into the ISM for Model A. Dashed lines indicate the results neglecting drift

important for our correct understanding of those objects with low to moderate mass loss rates up to about $10^{-5}\ M_\odot$/yr.

Chapter 5

A parameter study of dust coagulation and growth

There is a considerable number of publications dealing with dust coagulation (see the Introduction for some references), especially within dense molecular clouds and protostellar disks. Grain growth due to the accretion of gas particles is usually not treated at the same time, since for the physical conditions prevailing in these astronomical objects this process is completed before dust coagulation begins to affect the size distribution function (e.g. Weidenschilling & Ruzmaikina 1994). Calculations explicitly taking into account both coagulation and growth justify this proceeding for the limited range of physical parameters relevant to the considered dense turbulent clouds (cf. Rossi et al. (1991) and Ossenkopf (1993)). With regard to dust formation in red giant stars, however, Cadwell et al. (1994) concluded that both processes have to be considered at the same time.

A major advantage of the multi-component method presented in Part I of this thesis is the possibility to simultaneously model continuous processes, which slowly change the particle size, and discontinuous processes, which abruptly change the size and/or the number of affected grains (usually as a result of grain-grain collisions). In this chapter concurrent dust coagulation and growth under cosmic conditions is investigated. An extended grid of model calculations is presented in order to determine the domains in the space of relevant parameters where either coagulation or growth become dominant or else both have to be considered in their mutual dependence.

5.1 The scenario

Obviously, a variety of different scenarios can be imagined depending on which astronomical object is considered. It is the aim of this chapter to make some general statements about the relative importance of the two processes of dust coagulation and growth without getting involved in the detailed modeling of a particular object. In order to abstract from these objects, the evolution of the grain size distribution function subjected to dust coagulation and continuous grain growth is studied within the framework of a simple scenario. In this way, the complexity of the problem is reduced to its basic aspects and one can concentrate on the fundamental dependences.

The dust component is assumed to be at rest in a static gas element of constant temperature T_{g} and number density n_{g} of heavy particles, i.e. excluding electrons. The grains are to be in thermal equilibrium with the gas phase, and any radiation fields present shall not affect the process of either grain growth or coagulation.

Dust formation can be conceived as a two-step process (e.g. Sedlmayr 1994). An initial nucleation process is responsible for the gas–solid transformation and provides seed particles. Here, an initial Dirac distribution of spherical dust particles of mass m_0 is adopted

$$f(m,0) = \beta n_{\mathrm{g}} \delta(m - m_0) \tag{5.1}$$

where the free parameter β characterizes the dust-to-gas ratio at $t = 0$. The solid particles are assumed to consist of hypothetical monomers of mass m_{mono}.

These seeds can subsequently grow to macroscopic particles due to the accretion of molecules from the gas phase and/or coagulation (cf. Allamandola et al. 1987). If this formation of macrosopic dust grains in, for instance, a cool stellar envelope is to be investigated the mass m_0 is given by the mass of the small seed particles. If, on the other hand, one is interested in modeling the processing of μm–sized interstellar dust grains, m_0 can also be chosen accordingly. Thus, for purposes of the intended model calculations the basic aspects of either problem can be realized by means of an initial distribution (5.1).

With regard to continuous grain growth, an average growth species of mass m_{mono} and number density

$$n_{\mathrm{mono}}(t) = \epsilon(t) n_{\mathrm{g}} \tag{5.2}$$

will be used for the sake of simplicity. Within this simplifying framework it is again of no principal concern whether homogeneous growth of small seeds is to be described or ice mantle formation on pre-existing grains in, for instance, dense molecular clouds.

The abundance ϵ of the growth species is generally not constant but will decrease as grain growth proceeds and the condensable material in the gas phase is consumed (cf. Eq. (5.6)). The initial abundance at time $t = 0$ is given by

$$\epsilon(0) = \epsilon_0 - \beta m_0 / m_{\mathrm{mono}} \tag{5.3}$$

that means the seed particles are assumed to be made of the same average monomers that are responsible for grain growth.

The particle mass m of a sample grain increases according to (cf. Eq. (1.1))

$$\frac{\mathrm{d}m}{\mathrm{d}t} = m_{\mathrm{mono}}^{1/3} \frac{m^{2/3}}{\tau_{\mathrm{gr}}} \tag{5.4}$$

for the simple growth model adopted here. The characteristic growth time scale τ_{gr} is given by (Gail & Sedlmayr 1988)

$$\begin{aligned} \tau_{\mathrm{gr}}^{-1}(t) &= n_{\mathrm{mono}}(t) v_{\mathrm{th}} 4\pi a_{\mathrm{mono}}^2 \\ &= \epsilon(t) n_{\mathrm{g}} \sqrt{\frac{kT_{\mathrm{g}}}{2\pi m_{\mathrm{mono}}}} 4\pi \left(\frac{3 m_{\mathrm{mono}}}{4\pi \rho_{\mathrm{s}}} \right)^{2/3} \end{aligned} \tag{5.5}$$

where ρ_{s} is the density of the solid material. The sticking efficiency α of the average growth species on the grain is assumed to be unity.

The resulting depletion of condensable material from the gas phase is described by

$$\frac{\mathrm{d}n_{\mathrm{mono}}}{\mathrm{d}t} = - \int_0^\infty \mathrm{d}m\, f(m,t) \tau_{\mathrm{gr}}^{-1}(t) \left(\frac{m}{m_{\mathrm{mono}}} \right)^{2/3} . \tag{5.6}$$

This balance equation is obtained by dividing the r. h. s. of Eq. (5.4) by m_{mono} and convolving with the distribution function $f(m,t)$.

5.2 Fundamental parameters of the problem

In this section, the problem is approached in an analytic way and estimates of the characteristic time scales are derived. In the process of determining the relative importance of continuous growth and coagulation processes the fundamental parameters of the problem are identified.

Considering only continuous growth processes for the moment the time-dependent particle size can be calculated in the regime of negligible depletion $\epsilon(t) \approx \epsilon(0) \approx \epsilon_0$ by integration of Eq. (5.4)

$$m(t) \approx \left(m_{\mathrm{mono}}^{1/3} \frac{t - t_0}{3\tau_{\mathrm{gr}}} + m^{1/3}(t_0) \right)^3 . \tag{5.7}$$

Under the condition of undisturbed growth the time scale t_{gr} for doubling the grain mass $m \equiv m(t_0)$ due to continuous growth is given by

$$t_{\mathrm{gr}}(m) = 3\tau_{\mathrm{gr}} \left(\frac{m}{m_{\mathrm{mono}}} \right)^{1/3} . \tag{5.8}$$

The maximum size reached by the particles of an initial distribution (5.1) is simply $m_{\rm mono}\epsilon_0/\beta$.

Turning to a discussion of coagulation a distribution of spherical particles narrowly peaked around m is considered. The corresponding time scale for doubling the particle mass can be written in terms of the reaction frequency Ω (cf. Eq. (1.17))

$$\begin{aligned} t_{\rm coag}^{-1}(m) &= \beta n_{\rm g}\Omega(m,m,t) \\ &= \beta n_{\rm g} v_{\rm rel} 4\pi \left(\frac{3m}{4\pi\rho_{\rm s}}\right)^{2/3} \end{aligned} \tag{5.9}$$

where $v_{\rm rel}$ denotes the relative velocity of the grains (cf. Sect. 5.3.1 for more details). For purposes of estimating the coagulation time scale a sticking efficiency of unity was assumed for grain-grain collisions (cf. Sect. 5.3.2 for a proper description of dust coagulation).

Equating the time scales for doubling the particle mass due to continuous growth and coagulation, respectively, yields the mass $m_{\rm sep}$ which separates the size space into two regions

$$\frac{m_{\rm sep}}{m_{\rm mono}} = \frac{\epsilon_0}{\beta} \cdot \frac{v_{\rm th}}{3v_{\rm rel}}. \tag{5.10}$$

This equation provides a first estimate of the relative importance of grain growth and coagulation. If the considered particle mass m is smaller than $m_{\rm sep}$, growth dominates over coagulation. In contrast, coagulation is always more important for larger grains.

The first factor on the r. h. s. of Eq. (5.10) specifies the number ratio of accretable monomers in the gas phase and of grains that can coagulate, which normally is much larger than unity. The second factor is essentially the ratio of the respective effective velocities for grain growth and coagulation. These two factors can be regarded as the two fundamental parameters determining the relative importance of the considered processes. The density of the gas does not enter in Eq. (5.10), since the gas can be regarded as a carrier substance which does not take part in the actual processing of the dust (see, however, the discussion of turbulence induced grain velocities in Sect. 5.3.1).

5.3 A realistic description of dust coagulation

The analytical considerations made in the previous section involved several simplifying assumptions, namely size-independent relative velocities and sticking efficencies of unity with regard to the grains. In this section the physical description of grain coagulation will be refined.

5.3.1 Relative grain velocities

There are several different reasons for relative grain motion which have been neatly summarized by Ossenkopf (1993). First, Brownian motion will give grains of mass m a mean thermal velocity $(8kT_{\rm g}/\pi m)^{1/2}$. For the relative motion of two grains due to Brownian motion the mass is substituted by the corresponding reduced mass

$$v_{\rm rel,th}(m,m') = \sqrt{\frac{8kT_{\rm g}(m+m')}{\pi m m'}}. \tag{5.11}$$

Under cosmic conditions large scale random gas motions (turbulence) are a common phenonemon. Depending on their size and also the gas density, grains are coupled more or less efficiently to these chaotic motions by drag forces. For this reason, the grains embedded in the gas exhibit a relative velocity $v_{\rm rel,turb}$ induced by turbulent gas motion. The corresponding drag time scale of the grains (for subsonic motion) is (e.g. Draine 1985)

$$\tau_{\rm drag}(m) = \sqrt{\frac{\pi}{8\mu m_{\rm u} kT_{\rm g}}}\frac{\rho_{\rm s}}{n_{\rm g}}\left(\frac{3m}{4\pi\rho_s}\right)^{1/3}. \tag{5.12}$$

In the limit case of very small particles, the grains are comoving with respect to the local velocity fluctuations of the gas elements, while very large particles remain at rest relative to the center of mass of the bulk of the gas.

Assuming a Kolmogorov spectrum for the turbulent velocity field of the gas, Völk et al. (1980) thoroughly investigated collisions between grains in a turbulent gas. The turbulence velocity in the largest eddy $v_{\rm max}$ is constrained by the sound velocity (cf. Ossenkopf 1993). The corresponding length scale is denoted by $l_{\rm max}$ defining a turnover time

$$\tau_{\rm max} \equiv \frac{l_{\rm max}}{v_{\rm max}} \tag{5.13}$$

which characterizes the cascading of the kinetic energy in the largest eddy into small eddies.

Following an idea of Draine (1985) a rough estimate will be used here in order to approximate the results of the more detailed analysis by Völk et al. (1980). Let m without loss of generality denote the larger mass of m, m'. Then the induced relative velocity $v_{\rm rel,turb}$ between grains can be satisfactorily fit by

$$v_{\rm rel,turb}(m,m') = \left\{ \begin{array}{rcl} v_{\rm max}^{3/2} l_{\rm max}^{-1/2} \tau_{\rm drag}^{1/2}(m) & : & \tau_{\rm drag}(m'), \tau_{\rm drag}(m) \le \tau_{\rm max} \\ v_{\rm max} & : & \tau_{\rm drag}(m') \le \tau_{\rm max} < \tau_{\rm drag}(m) \\ v_{\rm max}^{1/2} l_{\rm max}^{1/2} \tau_{\rm drag}^{-1/2}(m') & : & \tau_{\rm max} < \tau_{\rm drag}(m'), \tau_{\rm drag}(m) \end{array} \right. \tag{5.14}$$

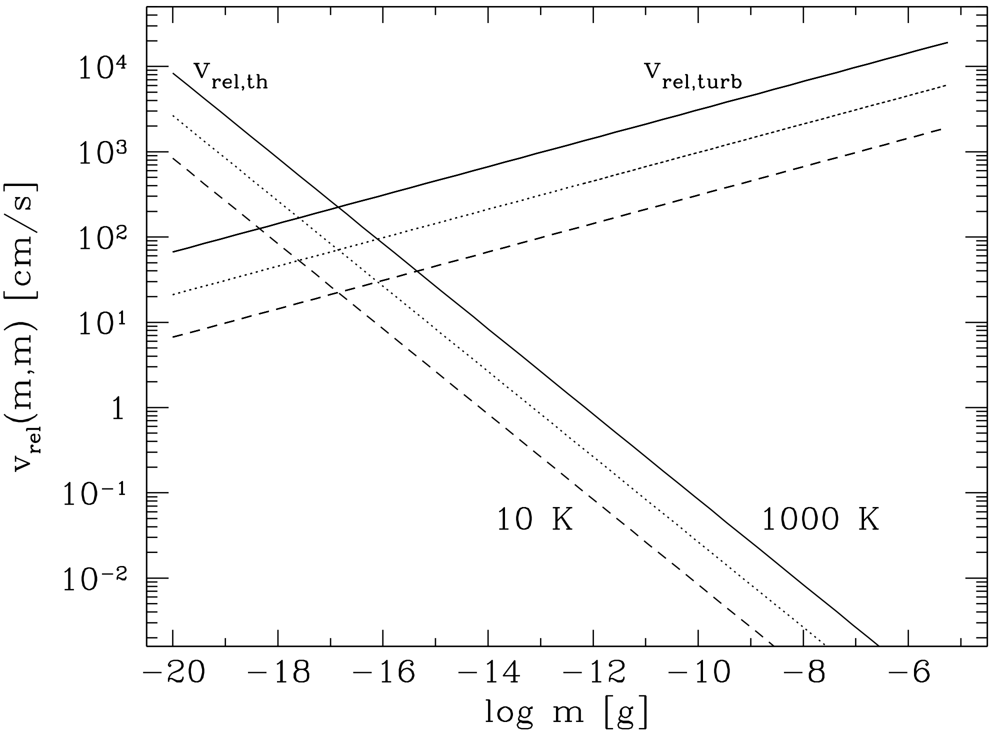

Figure 5.1: Size dependence of the thermal and turbulent velocities, $v_{\mathrm{rel,th}}$ and $v_{\mathrm{rel,turb}}$, between grains of the same size for three different gas temperatures $T_{\mathrm{g}} = 1000$ K (solid lines), 100 K (dotted lines) and 10 K (dashed lines). The turbulence parameters of the largest eddy are $v_{\max} = (kT_{\mathrm{g}}/\mu m_{\mathrm{u}})^{1/2}$ and $(l_{\max} n_g)^{-1/2} = 10^{-12}$ cm.

In the following, it will be assumed that the turbulence velocity $v_{\max}$ in the largest eddy is equal to the sound velocity.

Further causes for relative grain motions such as directed, size-dependent drift velocities due to gravitational forces or radiation pressure are not considered here. The total relative velocity between grains is then simply given by the quadratic mean (cf. Ossenkopf 1994)

$$v_{\mathrm{rel}}(m, m') = \sqrt{v_{\mathrm{rel,th}}(m, m')^2 + v_{\mathrm{rel,turb}}(m, m')^2}. \tag{5.15}$$

Figure 5.1 shows the size dependence of the relative grain velocities for three different gas temperatures. The thermal relative velocities become very small for large grain masses. On the other hand, these particles exhibit considerable turbulence induced relative motion. This suggests that turbulence is an important mechanism to drive efficient dust coagulation. An important point to notice here is that the turbulent

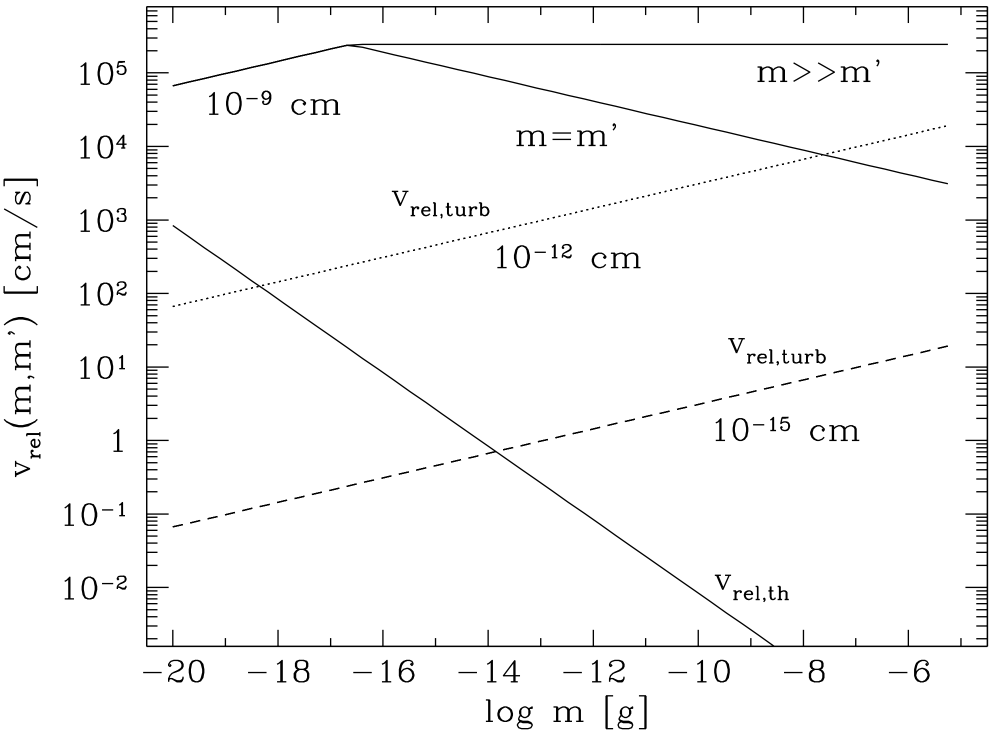

Figure 5.2: Size dependence of the thermal and turbulent velocities, $v_{\rm rel,th}$ and $v_{\rm rel,turb}$, between grains of the same size at $T_{\rm g} = 1000$ K for three different turbulence parameters of the largest eddy $(l_{\rm max} n_{\rm g})^{-1/2} = 10^{-9}$ cm (solid lines), 10^{-12} cm (dotted lines) and 10^{-15} cm (dashed lines). The highest turbulence induced relative velocity is also shown for the case of one of the grains being very small ($m' \ll m$).

velocities are decreasing with $T_{\rm g}$ in the same manner as the thermal velocities. Consequently, the ratio of the effecitive velocities for grain growth and coagulation, i.e. the second factor of the r. h. s. of Eq. (5.10), is independent of the gas temperature.

There is, however, a pronounced dependence of the turbulence induced velocities on the gas density. The ratio of the effective velocities for grain growth and coagulation scales according to $(l_{\rm max} n_{\rm g})^{1/2}$. The size dependence of the relative grain velocities for different turbulence parameters is shown in Fig. 5.2 for the case of two grains of equal grain mass and for the case of one of the grains being very small ($m' \ll m$), respectively.

5.3.2 Sticking efficiencies and the compression of aggregates

Depending on the relative velocity of the grains various outcomes of grain-grain collisions are possible (cf. Tielens 1989). For the low velocities $v_{\rm rel} \lesssim 10^5$ cm/s

Table 5.1: Parameters of the hypothetical grain material

$m_{\rm mono}$	10^{-22} g
$\rho_{\rm s}$	3 g/cm^3
E	10^{11} dyn/cm^2
γ	100 ergs/cm^2

considered here grains either stick or simply bounce elastically.

Recently, Chokshi et al. (1993) made significant progress with regard to determining the sticking efficiencies of colliding grains by using elastic continuum theory for the description of solids. It was found that sticking of two solid spherical grains of radii a, a' will occur if and only if the relative collision velocity is smaller than a critical velocity

$$v_{\rm cr}(a, a') = 1.07 \frac{\gamma^{5/6}}{E^{1/3} \rho_{\rm s}^{1/2}} \left(\frac{a\, a'}{a + a'} \right)^{-5/6} \tag{5.16}$$

which depends on the Young's modulus E and surface energy γ of the material[1]. In this work a hypothetical mean grain material will be considered (cf. Table 5.1).

After a number of grains have coagulated they form a — possibly loose or fluffy — agglomerate (or aggregate). It was pointed out by Chockshi et al. (1993) that with regard to the sticking of these dust aggregates the local radius of curvature of the constituting grains at the contact point will enter into the determination of the critical sticking velocity. The authors also suggested that the collision may lead to slippage or rolling at the individual grain boundaries of the particles making up the aggregates.

In continuation of this work, Dominik & Tielens (1995, 1996) developed theoretical tools to describe in detail the processes involved in the sticking and coagulation of small grains, also accounting for rolling and sliding motions of the aggregate constituents. With this quantitative description of the contact forces they performed dynamical simulations of dust coagulation for several materials and a grid of relative velocities, where the aggregates were not treated as a whole but as a two-dimensional assembly of grains (Dominik & Tielens 1997). The results of these calculations were summarized in a recipe for creating dust aggregates with restructuring effects included, which is the basis for the adopted description of dust aggregate coagulation developed below.

The initial Dirac size distribution of grains will move through the size space due to continuous growth of the grains. Thus, coagulation is at first dominated by collisions

[1]The formula in the original paper was erroneous and was corrected by Dominik & Tielens (1997).

of identical particles and the results of Chockshi et al. (1993) are applicable without modifications, i.e. the critical velocity for sticking is given by Eq. (5.16).

The first small aggregates being formed can be considered as loose agglomerates the constituents of which continue to grow at the same rate as the original single grains. Therefore, it will be assumed that the average mass of the constituting grains, which is an important parameter in the calculation of sticking efficiencies, is equal to the mass $m(t)$ the initial grains of mass m_0 will have grown to at time t according to Eq. (5.4). Dominik & Tielens (1997) found that the critical energy for sticking upon particle–aggregate collisions does not depend on the aggregate size. In fact, the critical velocity for sticking can again be obtained by Eq. (5.16) where the size of the average constituting grain has to be inserted, not the size of the whole aggregate.

After large agglomerates have formed by coagulation, aggregate–aggregate collisions become increasingly likely. The aggregates do not act like elastic solids but rather like compressible solids with the capacity to dissipate large amounts of impact energy internally. The ensueing compression and restructuring upon collision can be quite effective. Clearly, the assumption of an uniform coating of the individual grains due to continuous growth processes is no longer plausible in case of a compact aggregate. Fortunately, it turns out in the numerical calculations that the supply of condensable material will be exhausted before grain agglomerates are present in appreciable concentrations.

Dominik & Tielens (1997) also simulated the collisions of agglomerates of similar size. According to their results the critical velocity for aggregate–aggregate collisions to be sticking without splitting of individual grains in the process is of the same order as the critical velocity for single grains (cf. Eq. (5.16)) inserting the radii of the average constituting particles of the respective aggregates. Unfortunately, no calculations have been performed with regard to the collision of agglomerates with different size. On theoretical grounds it is expected that such collisions tend to permit sticking for even higher relative grain velocities.

In summary, the approach for the description of dust coagulation that will be used in the numerical calculations comprises the following assumptions

- The constituting grains of the aggregates are of equal size. This unique size is given by the mass $m(t)$ a sample grain of the initial mass m_0 will have grown to at time t (cf. Eq. (5.4)).

- The critical velocity for sticking of grain agglomerates and/or remaining single grains in the gas phase can be determined by means of Eq. (5.16) where the grain radii to be inserted are equal to the unique size of the single grains or aggregate constituents, respectively.

- Due to the efficient restructuring and compaction of agglomerates by aggregate–aggregate collisions the resulting agglomerates are treated as spherical compressed aggregates. For the purpose of calculating the drag time scale $\tau_{\rm drag}$ and the collisional cross-section the volume to surface ratio of the dust agglomerates was thus assumed to be the that of a solid sphere.

For mean relative velocities $v_{\rm rel}$ between the grains which are slightly larger than the critical velocity $v_{\rm cr}$ sticking does not cease abruptly, since in reality there is a continuous distribution of relative velocities around the root mean square value $v_{\rm rel}$. According to Ossenkopf (1993) this can conveniently be taken into account by defining an effective relative velocity

$$v_{\rm eff}(m,m') \equiv \alpha_{\rm coag} v_{\rm rel}(m,m') \tag{5.17}$$

where $\alpha_{\rm coag}$ is a hypothetical sticking efficiency for dust coagulation ($\alpha_{\rm coag} \equiv 1$ for $v_{\rm rel} \leq v_{\rm cr}$). With s denoting the ratio

$$s = \frac{2 v_{\rm cr}(a,a')}{\sqrt{\pi} v_{\rm rel}(m,m')} \tag{5.18}$$

the effective relative velocity can be written as

$$v_{\rm eff}(m,m') = (1 - [1-s^2]\exp(-s^2)) v_{\rm rel}(m,m'). \tag{5.19}$$

Figure 5.3 shows the size dependence of the critical velocity $v_{\rm cr}$ for sticking of two single grains of equal size. The corresponding effective collision velocity $v_{\rm eff}$ is depicted for the case of an examplary relative velocity $v_{\rm rel}$ (turbulence parameters of the largest eddy $(l_{\rm max} n_{\rm g})^{-1/2} = 10^{-12}$ cm). As can be seen, sticking becomes increasingly improbable for larger grains. In the case of $v_{\rm rel} > v_{\rm cr}$ the sticking efficiency is further reduced.

With regard to the sticking of agglomerates the emerging picture is somewhat different. The critical velocity $v_{\rm cr}$ does not depend on the aggregate mass but on the size of its average constituent. Figure 5.4 shows the critical velocities for three different constituting grain masses $m_{\rm c}$. The corresponding effective collision velocities $v_{\rm eff}$ refer to an examplary relative velocity $v_{\rm rel}$ (gas temperature $T_{\rm g} = 1000$ K and turbulence parameter of the largest eddy $(l_{\rm max} n_{\rm g})^{-1/2} = 10^{-12}$ cm). For large $m_{\rm c}$ and high relative velocities the sticking efficiency (represented by $v_{\rm eff}$) quickly tends towards zero. On the other hand, sticking of clusters can be very efficient as long as the size of the constituting grains $m_{\rm c}$ remains small.

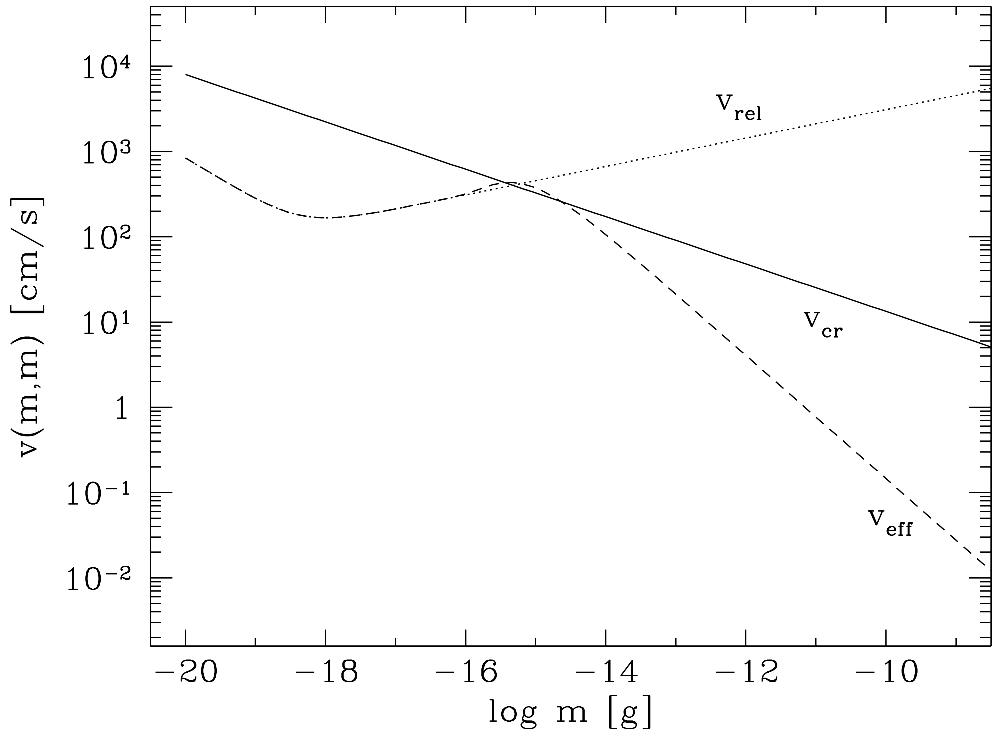

Figure 5.3: Size dependence of the critical and the effective velocity, $v_{\rm cr}$ and $v_{\rm eff}$, for sticking of two single grains of equal size. The adopted relative velocity $v_{\rm rel}$ corresponds to $T_{\rm g} = 1000$ K and turbulence parameter of the largest eddy $(l_{\max} n_{\rm g})^{-1/2} = 10^{-12}$ cm.

5.4 Method of solution

The numerical solution of the problem of simultaneous dust coagulation and growth under cosmic conditions makes use of the computational multi-component method presented in Part I, also taking account of the depletion of condensable material in the gas phase. The fundamental balance equation (1.15) can be slightly simplified, since grain creation or destruction is not treated here. The evolution of a given initial size distribution (5.1) is described by

$$\frac{\mathrm{d}m_t(m_*)}{\mathrm{d}m_*} f(m_t(m_*), t) = f(m_*, 0) + \int_0^t \mathrm{d}t' \, \frac{\mathrm{d}m_{t'}(m_*)}{\mathrm{d}m_*} q(m_{t'}(m_*), t') \tag{5.20}$$

where the independent variable r of the 1D formulation was transformed to the elapsed time t and the particles were chosen to be characterized by their mass m. The mass $m_t(m_*)$ of a sample grain of initial mass m_* can be obtained by integration

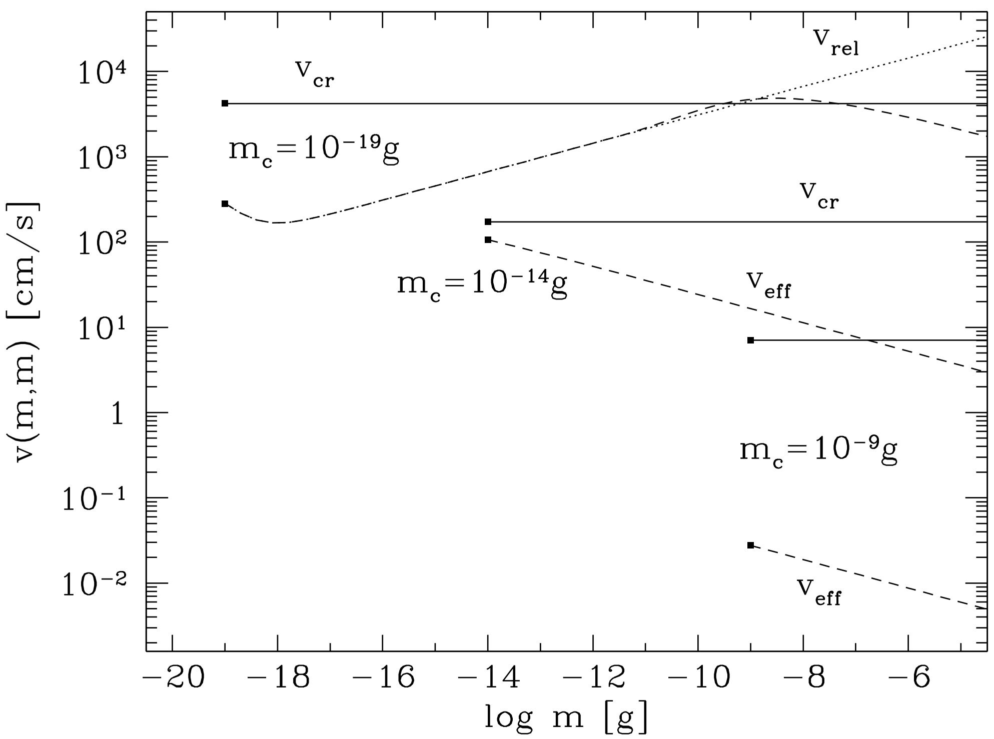

Figure 5.4: Size dependence of the critical and the effective velocity, $v_{\rm cr}$ (solid lines) and $v_{\rm eff}$ (dashed lines), for sticking of two equal dust aggregates of mass m for the case of three different masses $m_{\rm c}$ of the constituting grains. The adopted relative velocity $v_{\rm rel}$ (dotted line) corresponds to $T_{\rm g} = 1000$ K and turbulence parameter of the largest eddy $(l_{\rm max} n_{\rm g})^{-1/2} = 10^{-12}$ cm.

of Eq. (5.4)

$$m_t(m_*) = m_* + m_{\rm mono}^{1/3} \int_0^t \frac{m^{2/3}}{\tau_{\rm gr}} {\rm d}t \tag{5.21}$$

and the source term q describing the effects of coagulation is given by Eq. (2.7) where the reaction frequency Ω is written in terms of the effective collision velocity

$$\Omega(m, m', t) = \pi \left(\frac{3}{4\pi \rho_{\rm s}} \right)^{2/3} (m^{1/3} + m'^{1/3})^2 v_{\rm eff}(m, m'). \tag{5.22}$$

The conservation equation (5.20) can be solved by following the mass evolution of selected sample particles according to Eq. (5.4) and by calculating the accumulated effect of coagulation by means of the computational quantity Q (cf. Chapter 2)

$$\frac{{\rm d}Q(m_t(m_*))}{{\rm d}t} = \frac{{\rm d}m_t(m_*)}{{\rm d}m_*} q(m_t(m_*), t). \tag{5.23}$$

The grid points in particle mass space were distributed logarithmically equidistant

$$m_{*,k} = \begin{cases} m_0/1.4 & : \quad k = 0 \\ 1.4\, m_{*,k-1} & : \quad 1 \leq k \leq 100 \end{cases} \tag{5.24}$$

and the coagulation source term q was discretized as described in Sect. 2.3.1. According to the line of reasoning given in Sect. 5.3.2 the mass m_c of the constituting grains entering in the determination of the critical velocity $v_{\rm cr}$, and hence $v_{\rm eff}$, is equal to $m_t(m_{*,1})$.

In order to check the accuracy of the calculations and to exclude any artificial acceleration of particle coagulation due to coarse mass-coordinate division (cf. Sect. 3.2) some model calculations were repeated with a ratio of 1.2 between consecutive grid points. No significant deviation of the resulting distribution functions was found.

At some time levels during the computation a static rezone procedure is performed in order to avoid an unnecessarily fine resolution of particle size space. A grid point k is eliminated if

$$m_t(m_{*,k+1}) \leq 1.4\, m_t(m_{*,k-1}), \qquad 2 < k < 100. \tag{5.25}$$

At the end of computation the number of grid points may have been reduced to as little as half the original number.

The 202 ordinary differential equations of type (5.4) and (5.23) plus the differential equation (5.6) describing the consumption of the growth species are solved by means of an embedded, explicit fourth order Runge-Kutta scheme (Press et al. 1992). A typical model run (see below) needs between 20 and 50 minutes of computing time on a Pentium PC.

5.5 Results and discussion

In Sect. 5.2 the ratio ϵ_0/β, which corresponds to the final size of the particles provided growth is undisturbed by coagulation, and the ratio $v_{\rm th}/3v_{\rm eff}$ of the effective relative velocities for grain growth and coagulation have been identified as the fundamental parameters of the problem. The latter ratio turns out to be independent of the gas temperature for all grain sizes (cf. Fig. 5.1). The gas density, however, as well as the turbulence parameter $(l_{\rm max} n_{\rm g})^{-1/2}$ of the largest eddy have a selective influence on the turbulent velocity $v_{\rm rel,turb}$ between grains (cf. Fig. 5.2). The second fundamental parameter can be rewritten as

$$\begin{aligned} \frac{v_{\rm th}}{3v_{\rm eff}} &= \frac{v_{\rm th}}{3v_{\rm max}} \left(\frac{l_{\rm max}}{v_{\rm max}\tau_{\rm drag}} \right)^{1/2} \\ &\propto l_{\rm max}^{1/2} n_{\rm g}^{1/2} \end{aligned} \tag{5.26}$$

as long as the drag time scale (5.12) is smaller than the turnover time $\tau_{\max}$ of the largest eddy and the critical velocity for sticking is not exceeded.

Consequently, the evolution of the size spectrum is essentially governed by only two parameters, ϵ_0/β and $l_{\max}^{1/2} n_{\rm g}^{-1/2}$. A two-dimensional parameter study was performed where the parameters were chosen as

$$\begin{array}{rcl} 10^3 \leq & \epsilon_0/\beta & \leq 10^{12} \\ 10^{-16}\,\mathrm{cm} \leq & (l_{\max} n_{\rm g})^{-1/2} & \leq 10^{-7}\,\mathrm{cm} \end{array}$$

The first parameter corresponds to final sizes of the constituting grains of about 20 Å through to 2 μm, while the range of the second parameter is centered around typical values for molecular clouds and protostellar systems. For the remaining parameters the following values have been adopted

$$\begin{aligned} T_{\rm g} &= 1000\,\mathrm{K} \\ \mu &= 1.4 \\ m_0 &= 100\,m_{\rm mono}. \end{aligned}$$

As will be discussed below, the value of the initial grain size m_0 has no significant influence on the evolution of the size distribution function.

The time scale for doubling the particle mass due to either continuous growth or dust coagulation can be regarded as a characteristic time scale of the system. Inserting the characteristic mass $m_{\rm mono}\epsilon_0/\beta$ into Eqs. (5.8) and (5.9) it turns out that the respective time scales are both proportional to

$$\tau \equiv \beta^{-1/3} \epsilon_0^{-2/3} n_{\rm g}^{-1} \left(\frac{4\pi\rho_{\rm s}}{3m_{\rm mono}} \right)^{2/3} \frac{\mathrm{s}}{\mathrm{cm}}. \tag{5.27}$$

For a typical model run the integration was stopped at $t = \tau$.

In the following, two model calculations will be presented in detail. The fundamental parameters are summarized in Table 5.2 and correspond to low and high final masses $m_{\rm c}$ or final radii $a_{\rm c}$, respectively, of the constituting grains. These final constituent masses have a decisive influence with regard to the sticking efficiencies and, hence, the effective velocities between large dust aggregates (cf. Fig. 5.4).

5.5.1 Low final grain mass model

Fig. 5.5 shows the evolution of the size distribution function for Model A (low final mass $m_{\rm c}$). It is convenient to plot the distribution function multiplied by m^2. As can be seen, the peaked intial distribution is shifted through size space as the

Table 5.2: Fundamental parameters and derived quantities of low and high final grain mass model

	Model A	Model B
ϵ_0/β	10^5	10^{10}
$(l_{\max} n_{\rm g})^{-1/2}$ [cm]	10^{-12}	10^{-14}
$\tau n_{\rm g}$ [s cm^{-3}]	1.2 10^{21}	5.4 10^{22}
$m_{\rm c}$ [g] (final)	10^{-17}	10^{-12}
$a_{\rm c}$ (final)	90 Å	0.4 μm

grains accrete material from the gas phase. At the same time a broad distribution of larger particles starts to form due to coagulation. This broad distribution also translates through size space since the constituents of the corresponding loose aggregates continue to grow, just as the remaining single grains. After the supply of condensable material in the gas phase is exhausted at $t \sim 10^{-4}\tau$ the particles keep on coagulating forming progressively larger aggregates and significantly deplete the initial population of single grains[2]. An asymptotic form of the distribution function emerges which advances towards larger particle masses. This distribution function can be fitted piece-wise by power laws of the form $f(m) \propto m^\gamma$. The average slope changes from $\gamma \approx -5/3$ at medium particle masses to $\gamma \approx -1.2$ just before the cut-off.

The above interpretation is confirmed by a plot of the temporal evolution of macroscopic quantities derived from the distribution function. The total number density $n_{\rm d}$ of the dust particles, the total mass $M_{\rm d}$ of the dust component and the average mass $\bar{m}$ of the particles can be obtained by integration and are depicted in Fig. 5.6. Each of these quantities has a characteristic meaning with regard to the interpretation of the processes affecting the size distribution function. For example, continuous growth leads to an increase of the total dust mass $M_{\rm d}$. On the other hand, coagulation is responsible for the decrease of the number of particles represented by $n_{\rm d}$. The mean particle mass $\bar{m}$ is a measure of how far the center of the distribution function has advanced through size space towards larger particle masses. If there are many single grains left the mean value $\bar{m}$ will remain rather low.

This discussion implies that continuous growth processes become negligible as soon as the increase in $M_{\rm d}$ levels off, while coagulation is not effective as long as $n_{\rm d}$ remains constant for small t. Consequently, the time when the curve of $\bar{m}$ leaves that of $M_{\rm d}/\beta n_{\rm g}$, with which is coincides initially, can be regarded as the point where coagulation starts to be dominant ($t \sim 10^{-4}\tau$). The asymptotic value of the total

[2]The seemingly erratic course of the distribution function for $m \sim m_t(m_0)$ is in fact caused by a resonance of the coagulation process which creates particles with integer multiples of the constituent masses $m_t(m_0)$.

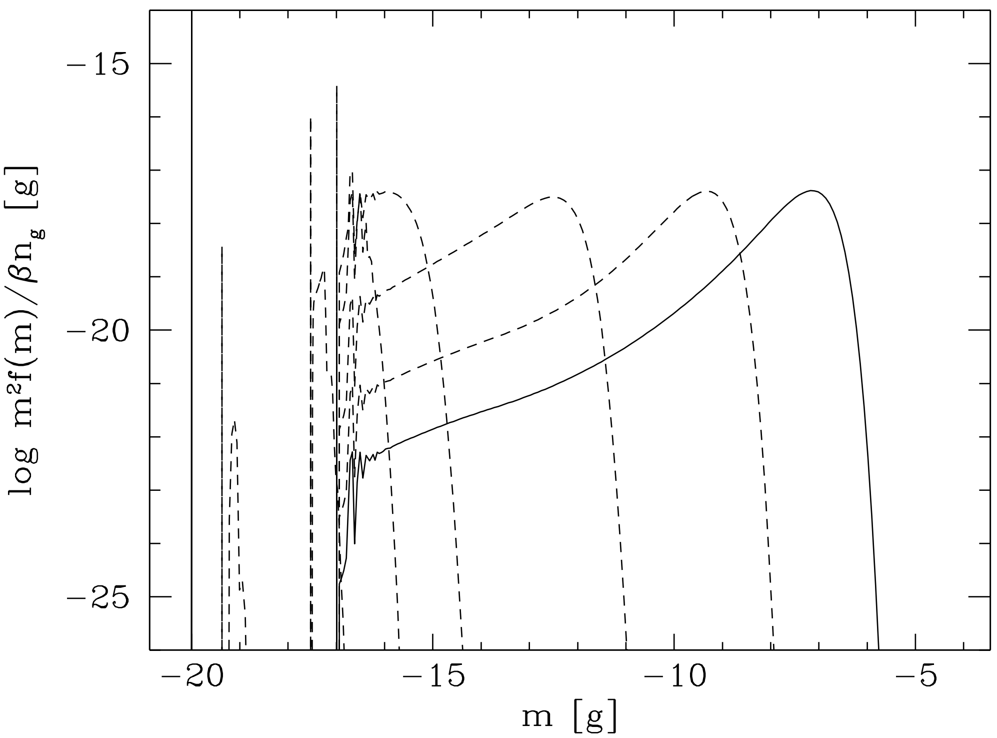

Figure 5.5: The size distribution function multiplied by m^2 for Model A (low final mass of the constituting grains) at various instants of time. The initial and final ($t = \tau$) distributions are indicated by solid lines. Dashed lines correspond to $t/\tau = 10^{-6}, 10^{-5}, \ldots, 10^{-1}$.

dust mass M_d is given by $\epsilon_0 n_\mathrm{g}$ corresponding to complete depletion of the growth species from the gas phase.

5.5.2 High final grain mass model

The evolution of the particle distribution function for Model B (high final mass of the constituting grains) is depicted in Fig. 5.7 in the same manner as for Model A. The important difference to Model A is that more condensable material per seed cluster is available in the gas phase. Thus, the peaked distribution of single grains can move to larger grain masses before continuous growth ceases. The resulting high final mass m_c leads to a reduction of the critical velocities for aggregate–aggregate sticking (cf. Fig. 5.4). Hence, dust coagulation, i.e. the formation of particles larger than m_c, is less efficient than in Model A.

On the other hand, the mean aggregate mass (cf. Fig. 5.8) in Model B is higher, since the original constituents have been much more massive in the first place. The initial slope of the curve of $\bar{m}$, where undisturbed growth can be presumed, is equal

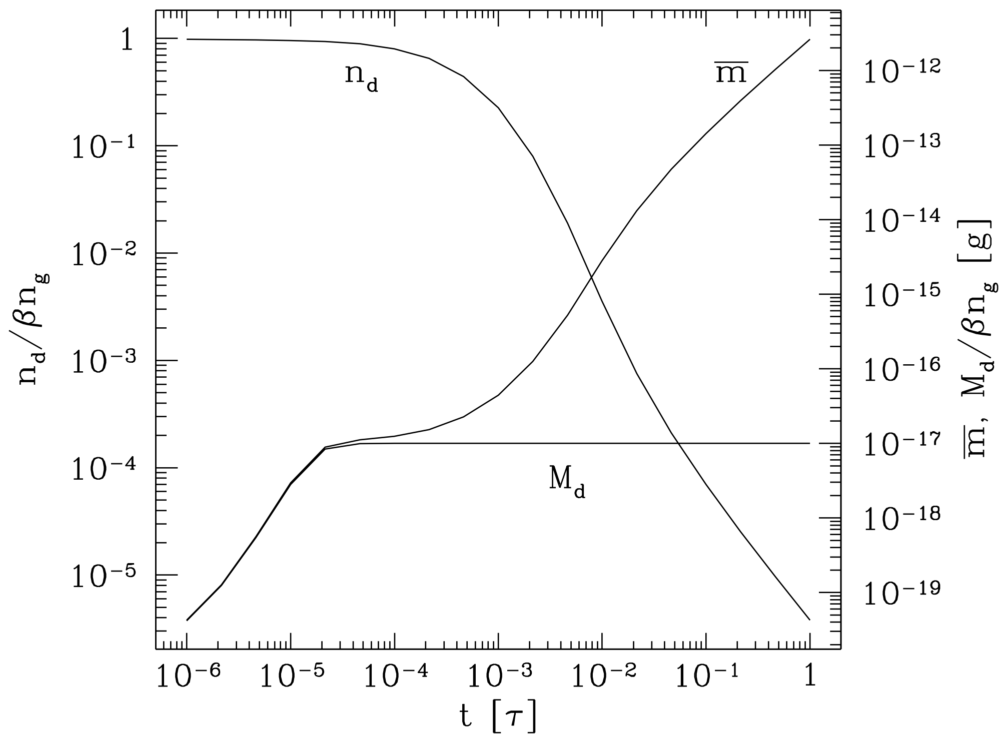

Figure 5.6: Temporal evolution of macroscopic quantities for Model A. Depicted are the total dust density n_d, the total mass M_d of the dust component, and the mean grain mass $\bar{m}$.

to 3 in the log-log-plot as was to be expected from Eq. (5.7). The mean grain mass reaches the correct value of $m_\mathrm{mono}\epsilon_0/\beta$ as the growth species is depleted ($t \sim 10^{-4}\tau$) and before coagulation sets in. When performing the same model calculation with a higher initial mass m_0, similar results are obtained the only difference being that the curves of M_d, $\bar{m}$ start at a higher level. They quickly approach, however, the corresponding curves of the original model.

Summarizing this discussion of two representative models, it is found that continuous grain growth is very efficient. It is not before most of the condensable material is depleted that coagulation begins to significantly affect the distribution function. The temporal evolution of macroscopic quantities of Model A and B, respectively, is remarkably similar when depicted in appropriately normalized plots (cf. Figs. 5.6 and 5.8). The final value of the total dust mass M_d is defined by the fundamental parameter ϵ_0/β. The second parameter $(l_\mathrm{max}n_\mathrm{g})^{-1/2}$ determines the time when efficient coagulation sets in. Regarding the particle size spectrum an asymptotic distribution function seems to ermerge for $t \gtrsim \tau$.

How fast the particle density is reduced due to coagulation mainly depends on the magnitude of the effective collision velocity v_eff. The latter is determined by the tur-

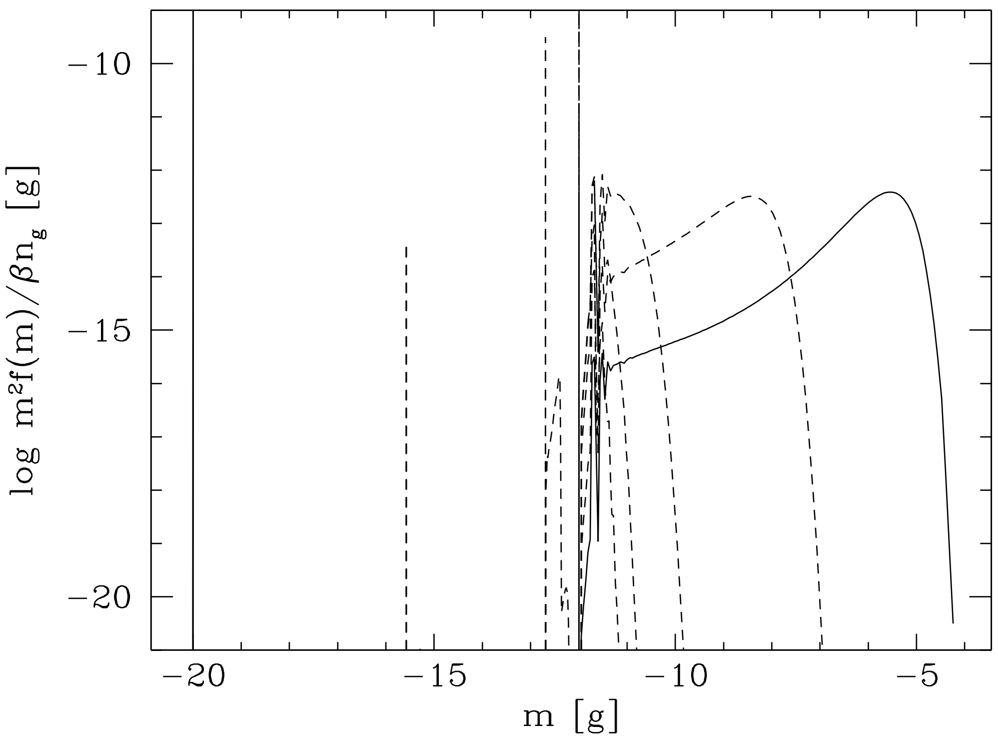

Figure 5.7: The size distribution function multiplied by m^2 for Model B (high final mass of the constituting grains) at various instants of time. The initial and final ($t = \tau$) distributions are indicated by solid lines. Dashed lines correspond to $t/\tau = 10^{-6}, 10^{-5}, \ldots, 10^{-1}$.

bulence induced relative velocity $v_{\rm rel,turb}$ and the mass $m_{\rm c}$ of the constituents of dust aggregates, which is responsible for the sticking properties. The turbulence induced velocity between grains is determined by the fundamental parameter $(l_{\rm max} n_{\rm g})^{-1/2}$, while $m_{\rm c}$ is essentially given by $m_{\rm mono}\epsilon_0/\beta$, since continuous growth is so rapid.

5.5.3 A grid of model calculations

In the investigation of Model A and B it was found that two macroscopic quantities, $n_{\rm d}$ and $\bar{m}$, suffice to indicate the calculated efficiency of the dust coagulation and the growth process. Therefore, these characteristic quantities are chosen here to visualize the results of the model calculations. Both are depicted in dependence of the two fundamental parameters ϵ_0/β and $(l_{\rm max} n_{\rm g})^{-1/2}$. The total density $n_{\rm d}$ is shown in Fig. 5.9 at time $t = 10^{-1}\tau$ and the mean particle mass $\bar{m}$ is plotted in Fig. 5.10 for $t = \tau$.

Obviously, there is a general tendency of $\bar{m}$ to increase with ϵ_0/β, since this ratio is proportional to the final mass of the the constituents $m_{\rm c}$. The dust density also

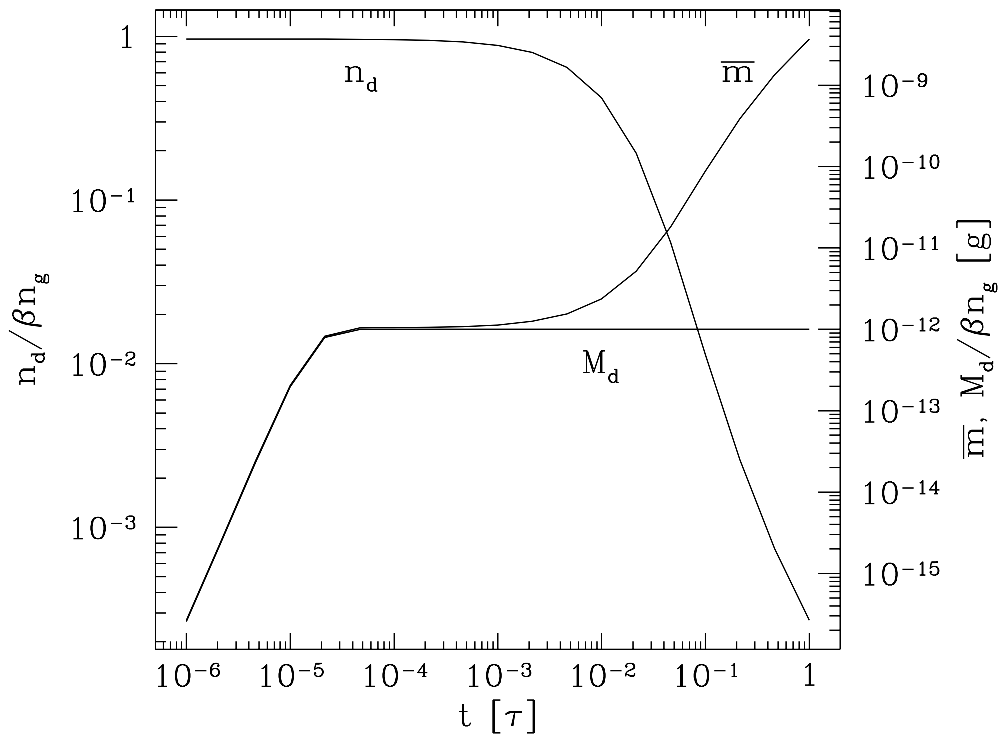

Figure 5.8: Temporal evolution of macroscopic quantities for Model B. Depicted are the total dust density n_d, the total mass M_d of the dust component, and the mean grain mass $\bar{m}$.

increases with ϵ_0/β, but this is due to the reduced sticking probability of aggregates made of larger constituents.

With regard to the dependence on the second fundamental parameter, $(l_\mathrm{max}n_\mathrm{g})^{-1/2}$, there is a feature apparent in the plots of both quantities. For certain combinations of the fundamental parameters the total dust density assumes a local minimum and the mean dust mass a corresponding local maximum representing a region of enhanced coagulation efficiency. These extreme values of the characteristic quantities n_d and $\bar{m}$ occur for a combination of fundamental parameters that can be approximated by a straight line in the log-log-plane, namely

$$\log \epsilon_0/\beta + 3\log(l_\mathrm{max}n_\mathrm{g})^{-1/2} = -30 \tag{5.28}$$

or

$$\frac{\epsilon_0}{\beta}(l_\mathrm{max}n_\mathrm{g})^{-3/2} = 10^{-30}\,\mathrm{cm}^3. \tag{5.29}$$

It will be shown that relation (5.28) or (5.29), respectively, can also be derived analytically. In fact, it is found to be equivalent to the condition that the relative

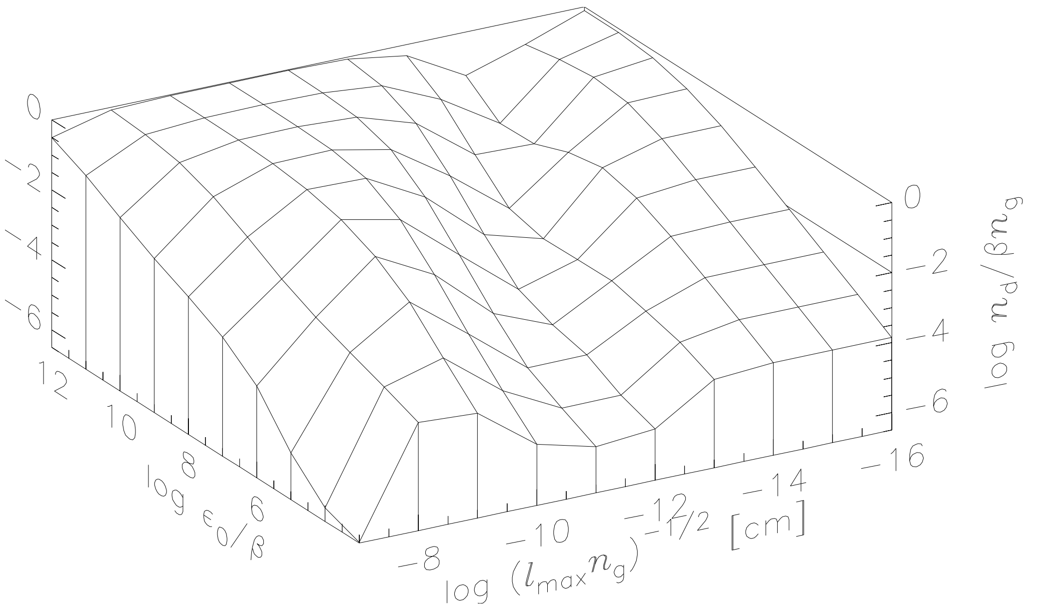

Figure 5.9: Dependence of the particle density $n_{\rm d}$ at $t = 10^{-1}\tau$ on the fundamental parameters $(l_{\rm max}n_{\rm g})^{-1/2}$ and ϵ_0/β.

velocitiy $v_{\rm rel}$ between grains of equal size is of the same order as the critical velocity $v_{\rm cr}$ where both velocities are to be evaluated for masses $m_{\rm mono}\epsilon_0/\beta$, i.e. for the final masses of the constituting grains and any remaining single grains.

$$\begin{aligned} & v_{\rm rel}(m_{\rm c}, m_{\rm c}) = v_{\rm cr}(a_{\rm c}, a_{\rm c}) \\ \Leftrightarrow\quad & v_{\rm max}^{3/2} l_{\rm max}^{-1/2} \tau_{\rm drag}^{1/2}(m_{\rm c}) = 1.07 \frac{\gamma^{5/6}}{E^{1/3}\rho_{\rm s}^{1/2}} \left(\frac{a_{\rm c}}{2}\right)^{-5/6} \\ \Leftrightarrow\quad & \left(\frac{\epsilon_0}{\beta}\right)^{4/3} (l_{\rm max}n_{\rm g})^{-3/2} = 6.93 \frac{\gamma^{5/2}}{E\rho_{\rm s}^3} \left(\frac{8\mu m_{\rm u} k T_{\rm g}}{\pi}\right)^{3/4} v_{\rm max}^{-9/2} \left(\frac{4\pi\rho_{\rm s}}{3m_{\rm mono}}\right)^{4/3} \end{aligned} \tag{5.30}$$

The first thing to note is that relation (5.30) has indeed a form very similar to the fit (5.29) of fundamental parameters of those model calculations in which dust coagulation is most efficient. Inserting the parameters of the hypothetical grain material and $\mu T_{\rm g} = 1400$ K Eq. (5.30) yields a ratio ϵ_0/β of 8.4 10^8 for an examplary turbulence parameter of the largest eddy $(l_{\rm max}n_{\rm g})^{-1/2} = 10^{-13}$ cm. It is for the final mass $m_{\rm c}$ corresponding to this ratio that the sticking efficiency of single grains and aggregates made of them approaches its maximum value. The derived value is in good agreement with $\epsilon_0/\beta = 10^9$ obtained from the fit (5.29) of the model calculations, so the proposition made above is proven.

In the derivation of Eq. (5.30) the relative velocity between grains of equal size was calculated for the case that the drag time scale $\tau_{\rm drag}$ is smaller than the turnover

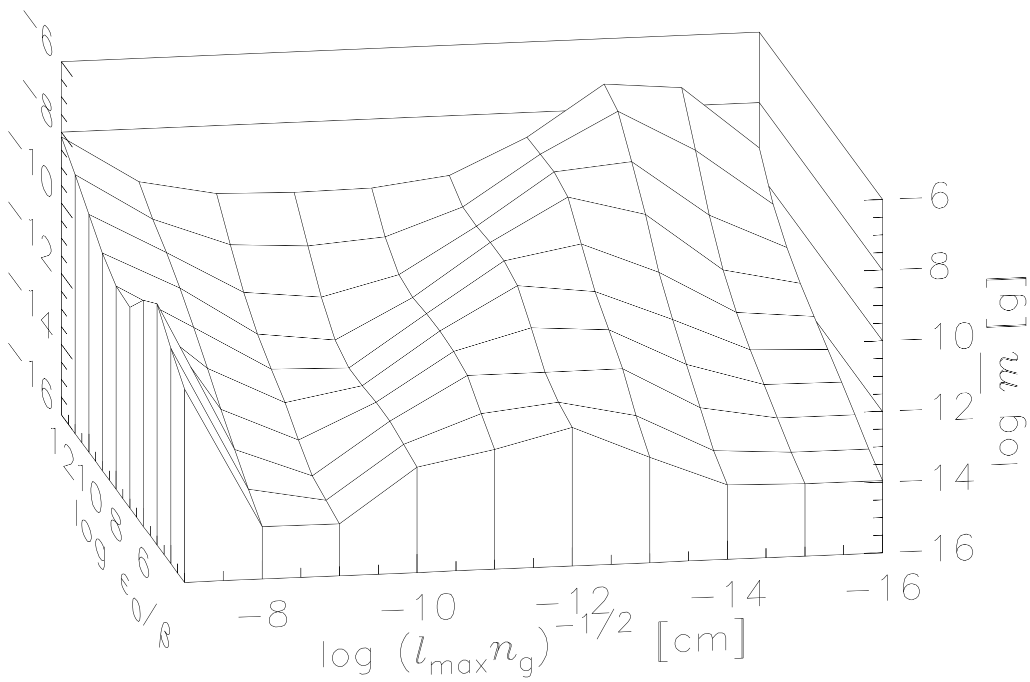

Figure 5.10: Dependence of the mean dust mass $\bar{m}$ at $t = \tau$ on the fundamental parameters $(l_{\rm max} n_{\rm g})^{-1/2}$ and ϵ_0/β.

time $\tau_{\rm max}$ of the largest eddy (cf. Eq. (5.14)). Considering the case $\tau_{\rm drag}(m) > \tau_{\rm max}$ a relation similar to Eq. (5.30) can be obtained in an analogous manner. However, it can be satisfied only for an extreme choice of the fundamental parameters. This alternative region of maximum coagulation efficiency corresponds to the decrease of $n_{\rm d}$ for $(l_{\rm max} n_{\rm g})^{-1/2} = 10^{-7}$ cm and $\epsilon_0/\beta < 10^6$.

5.6 Summary

Simultaneous growth and coagulation of grains under cosmic conditions was investigated. First, two fundamental parameters could be identified by means of a simple analytical approach. They determine the principal evolution of the dust component on normated time scales. Detailed numerical calculations were performed for a wide range of these parameters employing realistic expressions for the description of the sticking properties of the dust and for the relative velocities between particles. In this way, one can obtain a rough estimate of the expected mean particle size and total dust density for arbitrary scenarios without conducting time consuming calculations.

It was found that continuous growth processes are very rapid as long as there is condensable material left in the gas phase, while the time scale for coagulation is generally rather large. On the other hand, coagulation can lead to the formation of large aggregates supposing that the product of gas density and available time is sufficiently large. Regarding the maximum efficiency of dust coagulation a rule of thumb was provided that allows to determine favourable combinations of the fundamental parameters. This choice of parameters was shown to be equivalent to the condition that the relative velocity between dust particles is equal to the critical velocity for sticking of the constituting grains of the dust aggregates.

Chapter 6

Dust destruction in a protostellar accretion shock

Shock waves are present in a variety of different astrophysical environments. Interstellar shock waves, for instance, may be driven by supernova explosions or collisions between fast-moving clumps of interstellar gas. The supersonic infall of gas and dust during the collapse of a molecular cloud core to form a protostar is associated with a high-density accretion shock, too, which stands at the protostellar disk (see Fig. 6.1). The accreting dust particles are processed within such shocks by various physical and chemical processes, which generally act differently on grains of different composition, size, and velocity. Consequently, the grain size spectrum is dramatically changed as the dust grains pass through the shock front and enter the protostellar disk. The resulting size distribution of the surviving grains can be regarded as initial condition for calculations concerning the subsequent formation of planetesimals and, ultimately, planets.

Adopting the dissociative accretion shock model of Neufeld and Hollenbach (1994) an application of the computational multi-component method for the modeling of dust grain processing (cf. Part I) is presented. Thereby, insight is gained of how exactly the grain size distribution function evolves as it is being affected by the evaporation

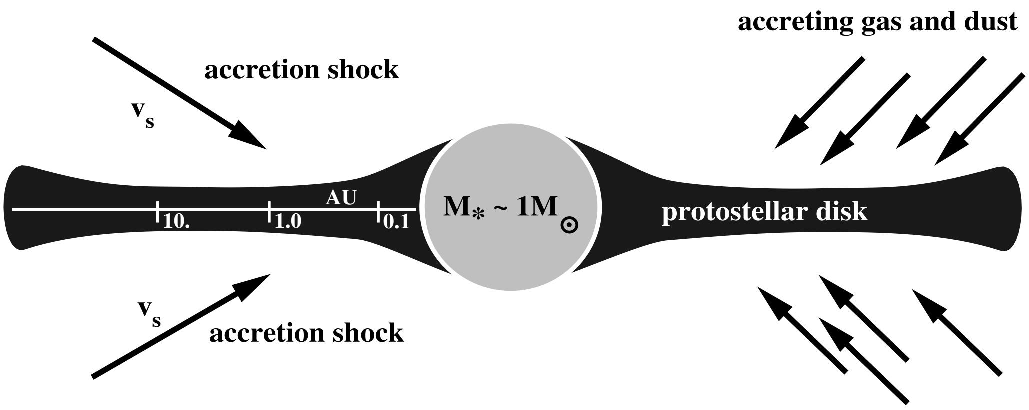

Figure 6.1: Schematic representation of a protostellar accretion shock (adopted from Neufeld & Hollenbach (1994))

of heated grains and by grain sputtering. The multi-component method treats all these important grain destruction mechanisms simultaneously, which are applied here to dust particles composed of several different materials, namely silicate, iron and water ice.

6.1 Adopted shock structure

Since this investigation is mainly concerned with the processing of dust grains, a protostellar accretion shock model is adopted here, namely the "standard model" presented by Neufeld & Hollenbach (1994) for a dense, dissociative J-shock of shock velocity $v_{\rm s} = 50$ km/s, and preshock density of H nuclei $n^0_{\langle\rm H\rangle} = 10^9$ cm^{-3}. These shock parameters correspond to a protostellar accretion model with a mass accretion rate of $10^{-8} M_{\odot}$/yr and median infall radius of 0.1 astronomical units. The sole independent variable of this plane-parallel shock wave model is the distance from the shock front which is designated by the column density

$$N_{\rm H} = \int n_{\langle\rm H\rangle}\,{\rm d}l. \tag{6.1}$$

The shocked molecular gas is treated as a single fluid, in which the gas (neutrals, ions, electrons, but *not* the dust grains) has one common temperature and velocity.

In single fluid J-shocks the gas is heated to high temperatures immediately behind the shock front. The total flux of radiation emitted by the shock, either upstream or downstream, is about half the flux of the kinetic energy density (Hollenbach & McKee 1979)

$$F_{\rm s} = \frac{1}{4} 1.41 m_{\rm u} n^0_{\langle\rm H\rangle} v_{\rm s}^3 \tag{6.2}$$

much of which is initially emitted in the ultraviolet ($m_{\rm u}$ denotes the atomic mass unit). The frequency integrated mean intensity of the UV field $J_{\rm UV}$, which determines the grain heating rate, is given approximately by (Hollenbach & McKee 1979)

$$J_{\rm UV} \approx \frac{F_{\rm s}}{4\pi} \frac{e^{-\tau_{\rm UV}}}{1/3 + \tau_{\rm UV}} \tag{6.3}$$

where $\tau_{\rm UV}$ is the UV optical depth, due primarily to dust (cf. Eq. (6.19)).

After the initial jump of the temperature, the gas cools radiatively. For the "standard" shock model of Neufeld & Hollenbach (1994) the temperature profile $T_{\rm g}(N_{\rm H})$ can be fit satisfactorily by two temperature plateaus and by two drops of the temperature at column densities $\sim 10^{16}$cm^{-2} and $\sim 10^{21}$cm^{-2} behind the shock front

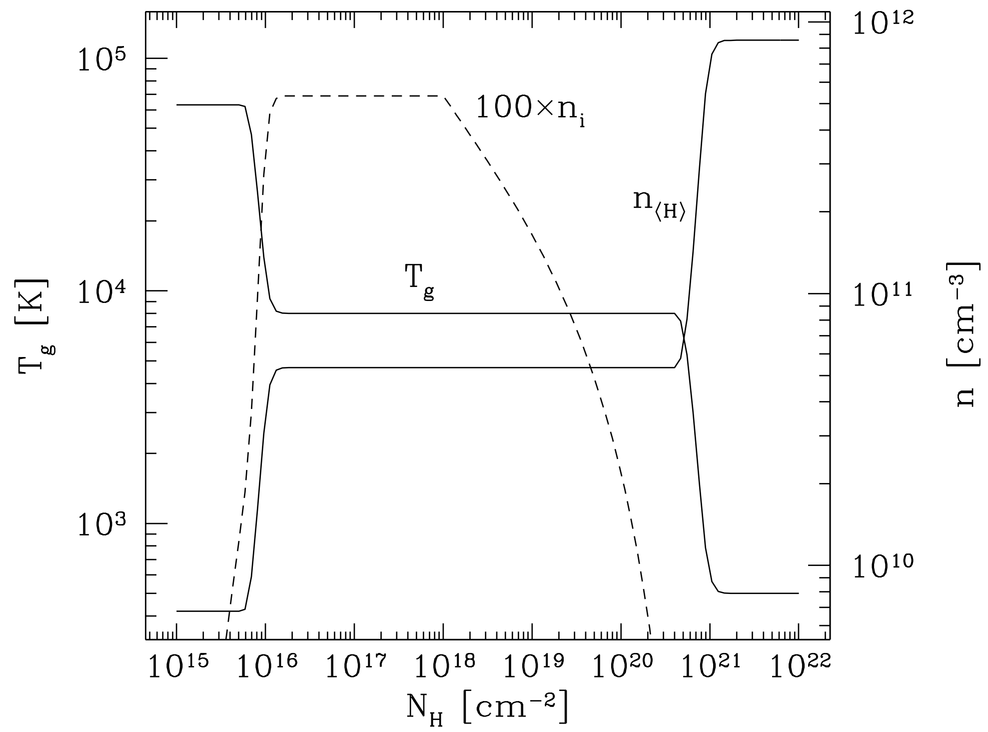

Figure 6.2: Fit of the gas temperature and density profiles behind a shock of velocity of 50 km/s in gas of preshock density 10^9 H nuclei per cm^{-3} (Neufeld & Hollenbach 1994). Also shown is a fit of the density of H^+ ions n_i (dashed line).

(cf. Fig. 6.2). For the case of strong shocks, the thermal pressure in the postshock region is approximately constant and equal to the initial ram pressure. Thus, the gas further compresses as it cools, and the gas density structure can be approximately calculated from the temperature profile by

$$n_{\langle\mathrm{H}\rangle}(N_\mathrm{H}) = \frac{p(N_\mathrm{H})}{kT_\mathrm{g}(N_\mathrm{H})} = \frac{n^0_{\langle\mathrm{H}\rangle}1.41m_\mathrm{u}v_\mathrm{s}^2}{kT_\mathrm{g}(N_\mathrm{H})} \tag{6.4}$$

exploiting the fact that in dissociative shocks the number density of the gas can be approximated by $n_{\langle\mathrm{H}\rangle}$. The adopted structure of the gas density $n_{\langle\mathrm{H}\rangle}$ is also depicted in Fig. 6.2.

Due to mass conservation the velocity v_g of the gas can be calculated from the density structure

$$v_\mathrm{g}(N_\mathrm{H}) = v_\mathrm{s}\frac{n^0_{\langle\mathrm{H}\rangle}}{n_{\langle\mathrm{H}\rangle}(N_\mathrm{H})}. \tag{6.5}$$

6.2 Equations for the dust

The fundamental differential balance or conservation equation (1.15) for the value of the grain size distribution function accounts for both discontinuous processes, e.g. coagulation and shattering, and continuous processes, e.g. sputtering. There are several simplifications arising from the application to the shock model adopted here. First, the processing of a given size spectrum of spherical grains is investigated (cf. Sect. 6.2.3). Thus, dust particles of radius a_* are injected at the base of the flow, where the calculation starts, with an initial velocity $v_\mathrm{d}(a, N_\mathrm{H}^0) = v_\mathrm{s}$ (cf. the discussion in Sect. 3.1.1). Dust *formation* behind the shock front is not considered, i.e. possible nucleation or grain growth is neglected.

Secondly, regarding the flow geometry a plane-parallel shock wave is considered. The velocity component of a dust particle of radius a in N_H-direction is denoted by $v_\mathrm{d}(a, N_\mathrm{H})$. For a grain of initial radius a_* at the base of the flow N_H^0 the radius $a_{N_\mathrm{H}}(a_*)$ at position N_H is given by (cf. Eq. (1.5))

$$a_{N_\mathrm{H}}(a_*) = a_* + \frac{a_0}{3}\int_{N_\mathrm{H}^0}^{N_\mathrm{H}} \left[n_{\langle\mathrm{H}\rangle} v_\mathrm{d}(a_{N'_\mathrm{H}}(a_*), N'_\mathrm{H})\tau_\mathrm{net}(a_{N'_\mathrm{H}}(a_*), N'_\mathrm{H})\right]^{-1} \mathrm{d}N'_\mathrm{H} \qquad (6.6)$$

where a_0 is the hypothetical radius of a monomer and τ_net^{-1} is the net rate of change in grain size. In the context of protostellar accretion shocks vaporization of heated grains as well as thermal and mechanical sputtering will be considered (cf. Sect. 6.2.2).

Under these assumptions the general balance equation simplifies to the following special form

$$-v_\mathrm{d}(a_*, N_\mathrm{H}^0) f(a_*, N_\mathrm{H}^0) + \frac{\mathrm{d}a_{N_\mathrm{H}}(a_*)}{\mathrm{d}a_*} v_\mathrm{d}(a_{N_\mathrm{H}}(a_*), N_\mathrm{H}) f(a_{N_\mathrm{H}}(a_*), N_\mathrm{H}) = 0 \qquad (6.7)$$

6.2.1 Grain dynamics

The velocity of a particular sample grain has to be determined by solving an additional ordinary differential equation, namely the equation of motion. By estimating the time scale for magnetic deflection Neufeld & Hollenbach (1994) have shown that betatron acceleration (Spitzer 1976) is negligible at high densities. The typical grain follows a nearly linear trajectory and is stopped before it can be significantly accelerated by the betatron mechanism. The equation of motion may then be written in terms of the time scales for collisional and Coulomb drag deceleration, τ_coll and τ_Coul, respectively

$$\frac{\mathrm{d}v_\mathrm{d}(a)}{\mathrm{d}N_\mathrm{H}} = -\frac{v_\mathrm{d}(a) - v_\mathrm{g}}{n_{\langle\mathrm{H}\rangle} v_\mathrm{d}(a)} \left(\frac{1}{\tau_\mathrm{coll}} + \frac{1}{\tau_\mathrm{Coul}}\right). \qquad (6.8)$$

The deceleration due to direct collisions with atoms and ions has already been treated in Sect. 3.1.2 yielding an inverse time scale

$$\tau_{\rm coll}^{-1} = \frac{3(v_{\rm d}(a) - v_{\rm g})1.4 m_{\rm u} n_{\langle{\rm H}\rangle}}{4a\rho_{\rm s}}. \tag{6.9}$$

where $\rho_{\rm s}$ denotes the density of the grain material.

When the fractional ionization of the gas exceeds a few percent the last term in Eq. (6.8) may dominate. Moving through a medium of H^+ density $n_{\rm i}$ (cf. Fig. 6.2) a charged grain experiences a Coulomb drag deceleration of a characteristic time scale (Neufeld & Hollenbach 1994)

$$\tau_{\rm Coul}\,[{\rm s}] = 1.67\,10^{18} \frac{a\rho_{\rm s}}{n_{\rm i}T_{\rm g}^{1/2}} \frac{1 + 0.355\,10^{-12}(v_{\rm d}(a) - v_{\rm g})^3 T_{\rm g}^{-3/2}}{1 + 0.064\ln[10^5 T_{\rm g}/(n_{\rm i}a^2)]} \tag{6.10}$$

where all quantities are to be inserted in cgs units.

6.2.2 Heating and destruction of grains

The size evolution of a sample grain is given by (cf. Eq. (1.4))

$$\frac{{\rm d}a}{{\rm d}N_{\rm H}} = \frac{1}{v_{\rm d}(a) n_{\langle{\rm H}\rangle}\tau_{\rm net}}\frac{a_0}{3} \tag{6.11}$$

where $\tau_{\rm net}$ comprises the time scales for mechanical sputtering due to the drift motion of the grains, for thermal sputtering by (thermally) impacting gas particles and for grain vaporization.

$$\tau_{\rm net}^{-1} = -\tau_{\rm sp}^{-1} - \tau_{\rm th}^{-1} - \tau_{\rm vap}^{-1}. \tag{6.12}$$

Each of these contributions will now be discussed in turn.

Mechanical sputtering is described according to Eq. (3.3) of Sect. 3.1.3

$$\tau_{\rm sp}^{-1} = \pi a_0^2 n_{\langle{\rm H}\rangle}(v_{\rm d}(a) - v_{\rm g})\overline{Y}_{\rm sp} \tag{6.13}$$

while thermal sputtering is treated using fifth-order polynomial fits for $\tau_{\rm th}$ provided by Tielens et al. (1994).

The vaporization of heated grains is treated similarly to Neufeld & Hollenbach (1994). Because of the efficient coupling to the radiation field the time scale for

Table 6.1: Grain vaporization parameters

Material	$T_{\rm vap}$ [a] [K]	10^{-5} $\bar{Q}(T_{\rm vap})/a$ [b] [cm^{-1}]	$E_{\rm L}$ [c] [erg/g]
Iron	1395	4.9 10^{-2}	6.69 10^{10}
Silicate	1331	2.9 10^{-3}	2.41 10^{10}
Water ice	180	8.1 10^{-3}	3.35 10^{9}

[a] Pollack et al. 1994

[b] Neufeld & Hollenbach 1994

[c] Weast et al. 1988

grains to reach an equilibrium temperature is very small. Thus, the grain temperature $T_{\rm d}$ can be determinated by balancing the sum of the various heating rates q_i against the cooling rate due to IR-emission $q_{\rm IR}$

$$\sum_i q_i = q_{\rm IR}. \tag{6.14}$$

The latter is given by

$$\begin{aligned} q_{\rm IR}(T_{\rm d}) &= 4\pi \int \kappa_\nu(a) B_\nu(T_{\rm d})\, {\rm d}\nu \\ &= 4\sigma T_{\rm d}^4 \bar{Q}(T_{\rm d}) \pi a^2 \end{aligned} \tag{6.15}$$

where B_ν is the Planck function, κ_ν denotes the spectral absorption coefficient and $\bar{Q}$ is the dimensionless Planck mean absorption efficiency ($\bar{Q} \equiv 1$ for a blackbody).

Of course, the grain temperature calculated from the equilibrium condition (6.14) can not exceed the vaporization temperature $T_{\rm vap}$ of the grain material. Therefore, the maximum energy that can be radiated away is

$$q_{\rm IR}(T_{\rm vap}) = 4\sigma T_{\rm vap}^4 \bar{Q}(T_{\rm vap}) \pi a^2. \tag{6.16}$$

If the total heating rate is larger than $q_{\rm IR}(T_{\rm vap})$ the excess energy is available to vaporize the grain. The corresponding grain size reduction rate is

$$\tau_{\rm vap}^{-1} = \frac{3}{a_0 \rho_{\rm s} E_{\rm L} \pi a^2} \max\left\{0, \sum_i q_{\rm i}(T_{\rm vap}) - q_{\rm IR}(T_{\rm vap})\right\} \tag{6.17}$$

with $E_{\rm L}$ representing the specific latent heat of vaporization. The relevant parameters for silicate, ice and iron grains are summarized in Table 6.1.

Regarding the *heating* of the grains, several important mechanisms have to be distinguished in protostellar accretion shocks. In the very hot region immediately behind the shock front an intense ultraviolet radiation field is generated. It is assumed that absorption of this UV radiation can be treated in the large particle limit of Mie theory ($\lambda < 300$ Å $\lesssim 2\pi a$). By means of Eq. (6.3) it follows for the respective heating rate

$$\begin{aligned} q_{\rm UV} &= 4\pi J_{\rm UV}\pi a^2 \\ &= F_{\rm s}\frac{e^{-\tau_{\rm UV}}}{1/3+\tau_{\rm UV}}\pi a^2 \end{aligned} \tag{6.18}$$

where the UV optical depth τ_{UV} is mainly due to dust absorption

$$\tau_{\rm UV}(N_{\rm H}) = \int_0^{N_{\rm H}} {\rm d}N'_{\rm H} \int_{a_\ell}^{\infty} {\rm d}a\, f(a, N'_{\rm H})\pi a^2. \tag{6.19}$$

Furthermore, a certain fraction α of the gas particles is scattered inelastically (diffuse reflection) by the grains. This means that impinging gas particles are adsorbed, heating the grains by the kinetic energy of the impact. Furthermore, after thermal accomodation, the particles evaporate with a velocity distribution corresponding to the internal dust temperature $T_{\rm d}$. Thus, there is an additional heating (or cooling) rate as internal lattice energy of the grain is transformed into thermal energy of the evaporating gas particle or vice versa, dependent on $T_{\rm g}$ being smaller or larger than $T_{\rm d}$. The total collisional grain heating rate is given by (Draine 1980)

$$\begin{aligned} q_{\rm coll} &= \alpha n_{\langle {\rm H}\rangle}\pi a^2 \sqrt{\frac{8kT_{\rm g}}{\pi\mu m_{\rm u}} + (v_{\rm d}(a)-v_{\rm g})^2} \\ &\quad \cdot \left[0.5\,\mu m_{\rm u}(v_{\rm d}(a)-v_{\rm g})^2 + 2k(T_{\rm g}-T_{\rm d})\right]. \end{aligned} \tag{6.20}$$

The thermal accomodation coefficient α for neutral hydrogen, which is the most abundant species in the gas phase, has been calculated according to the formula reported by Hollenbach & McKee (1979)

$$\alpha = (1-\alpha_0)e^{-\sqrt{2kT_{\rm g}/D}} + \alpha_0 \tag{6.21}$$

where

$$\alpha_0 = \frac{2m_{\rm u}m_{\rm gr}}{(m_{\rm u}+m_{\rm gr})^2} \tag{6.22}$$

is the high-temperature hard-sphere limit, $m_{\rm gr}$ is the mass of the average grain *atom* struck, and D is the depth of the adsorption potential (taken from Burke & Hollenbach 1983).

IR heating of the dust due to thermal emission of grains far downstream or UV-illuminated grains is of minor importance and can be neglected (cf. Neufeld & Hollenbach 1994).

6.2.3 Grain model and properties

As initial condition for the grain size distribution function an MRN power-law distribution of spherical silicate grains (Mathis et al. 1977) was adopted

$$f(a) = 10^{-25.21} n^0_{\langle \mathrm{H} \rangle}\, a^{-3.5}\, \mathrm{cm}^{5/2}, \qquad 5\,10^{-7}\,\mathrm{cm} \leq a \leq 2.5\,10^{-5}\,\mathrm{cm}. \tag{6.23}$$

In addition, test calculations for Fe and for water ice, i.e. small refractory cores coated by a thick ice layer, were performed. For the sake of simplicity, the same initial distribution functions as in the case of silicate grains were assumed.

For purposes of determining the total UV optical depth of the dust according to Eq. (6.19), the size distribution was multiplied by a somewhat arbitrary factor 2 in order to account for other components of the interstellar dust (e.g. graphite).

6.3 Method of solution

The essential idea of the computational approach to evaluate the differential balance equation (6.7) is the discretization of the size distribution on a Lagrange-like grid in grain size space which moves according to the size evolution of selected sample grains. In this way, the grid is self-adapting according to the evolution of the size distribution, which seems more appropriate than the use of a static grid. The initial grid of grain radii $a_{*,i}$ $(i = 1, \ldots, I)$ is chosen to be logarithmically equidistant in the size interval $5\,10^{-7}$ cm $\leq a \leq 2.5\,10^{-5}$ cm.

Further details of the numerical scheme, grid generation, derivation of macroscopic quantities of the dust component etc. are outlined in Chapter 2.

The grid point equations (6.11), the corresponding equations of motions (6.8) for the sample grains and an additional ordinary differential equation for the UV optical depth (cf. Eq. (6.19)) form a system of $2I + 1$ ODE's. They are solved by means of an embedded, explicit fourth order Runge-Kutta scheme (Hairer et al. 1987). The calculations have been performed on a Silicon Graphics IRIS Indigo R 4000 workstation. The results presented below have been calculated with $I = 100$. This takes about five minutes of computing time.

6.4 Results and discussion

Adopting the "standard model" of Neufeld & Hollenbach (1994) for a protostellar accretion shock the evolution of the grain size distribution was investigated by means of the computational multi-component method for the description of dust grain processing. Three model calculations were conducted for initial power-law size distributions of silicate, ice and iron grains, respectively.

6.4.1 Effectiveness of the destructive processes

As was to be expected from previous calculations (e.g. Hollenbach & McKee 1979, Neufeld & Hollenbach 1994), vaporization of heated grains turns out to be the dominant mechanism of silicate grain destruction. There is only little mechanical sputtering of the grains due to grain drift motion, amounting to a radius change of approximately 0.5%. Due to the moderate gas temperature thermal sputtering does not affect the grains.

Grain vaporization sets in, if the heating rate per unit grain area exceeds a limit value

$$q_{\mathrm{IR}}(T_{\mathrm{vap}})/\pi a^2 = 4\sigma T_{\mathrm{vap}}^4 \bar{Q}(T_{\mathrm{vap}})$$

This limit value characterizes the maximum IR emissivity of the grain at the vaporization temperature. It is approximately proportional to the grain radius, i.e. small grains are heated to their vaporization temperature more easily. As an example, $q_{\mathrm{IR}}(T_{\mathrm{vap}})/\pi a^2$ is depicted in Fig. 6.3 for an examplary grain size of $a = 0.1\,\mu$m together with the relevant heating rates (cf. also Sect. 6.2.2).

Clearly, absorption of UV-radiation is an efficient heating process. Heating due to collisions with gas particles is also of significance, since according to Eq. (6.21) a minimum fraction $\alpha_0 \sim 0.1$ of gas particles is always scattered inelastically transferring kinetic energy upon impact.

For grains smaller than the examplary size 0.1 μm in Fig. 6.3 deceleration, and hence the decrease of the collisional heating rate (coll), takes place at smaller column densities. The onset of vaporization (vap) occurs at smaller heating rates leading to efficient grain destruction.

6.4.2 Evolution of the grain size distribution

The evolution of the grain size distribution $f(a, N_{\mathrm{H}})$ is presented in Fig. 6.4 by a sequence of snapshots taken at various column densities N_{H} behind the shock front. Two alterations of f have to be distinguished here. The small grains are completely vaporized, which causes a drastic reduction of the value of the size distribution for small radii $a < a_{\mathrm{vap}} \sim 5\,10^{-6}$ cm.

The second effect is the compression of the dust fluid which subsequently follows the compression of the radiatively cooling gas (at $N_{\mathrm{H}} \sim 10^{16}$ cm^{-2} and 10^{21} cm^{-2}, cf. Fig. 6.2) with a specific time lag due to the size dependent distance required to slow down a grain. This results in a successive upward shift of f, where sections of the size distribution correponding to smaller grain sizes rise first.

From the obtained size distribution macroscopic dust quantities can be easily derived by integration. For example, the absorption coefficient κ_{d} of the dust component in

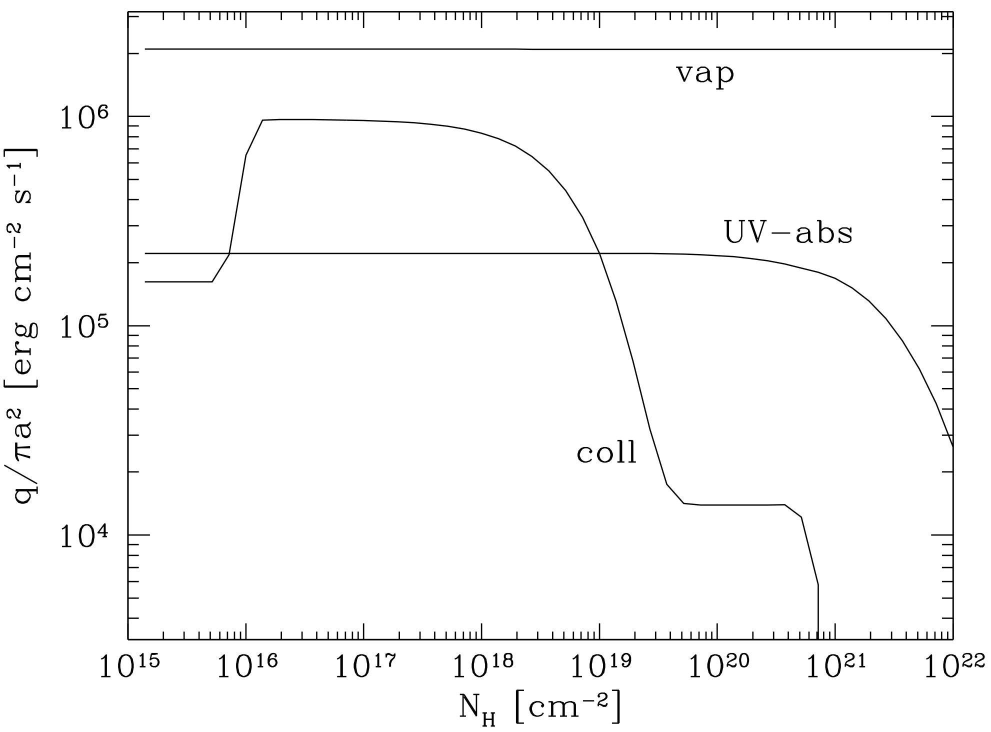

Figure 6.3: Grain heating rates per unit grain cross-sectional area ($a = 0.1\,\mu$m) for absorption of UV radiation (UV-abs) and gas-grain collisions (coll). Also shown for comparison is the heating rate at which the onset of vaporization occurs (vap).

the large particle limit of Mie theory is shown in Fig. 6.5. The initial decline of $\kappa_{\rm d}$ is due to the complete evaporation of small grains (cf. also Fig. 6.4). At column density $N_{\rm H} \sim 10^{19}$ cm^{-2} behind the shock there is a continuous increase of the absorption efficiency, when most of the remaining grains are decelerated and the compression of the dust fluid follows that of the gas. The same effect occurs at column density $N_{\rm H} \sim 10^{21}$ cm^{-2} where another jump of the gas density takes place (cf. Fig. 6.2).

Also depicted in Fig. 6.5 is the UV optical depth $\tau_{\rm UV}$ corresponding to $\kappa_{\rm d}$. It turns out that $\tau_{\rm UV}$ is quite small, and it is not before the final compresssion of the dust fluid that efficient absorption of the UV field sets in. The optical depth of the dust component is responsible for the weakening of the UV radiation, which in turn determines the grain temperatures and thus the vaporization of grains. In the presented calculation this interaction between the optical depth of the surviving dust grains and the remaining intensity of the UV radiation causing further vaporization was consistently accounted for.

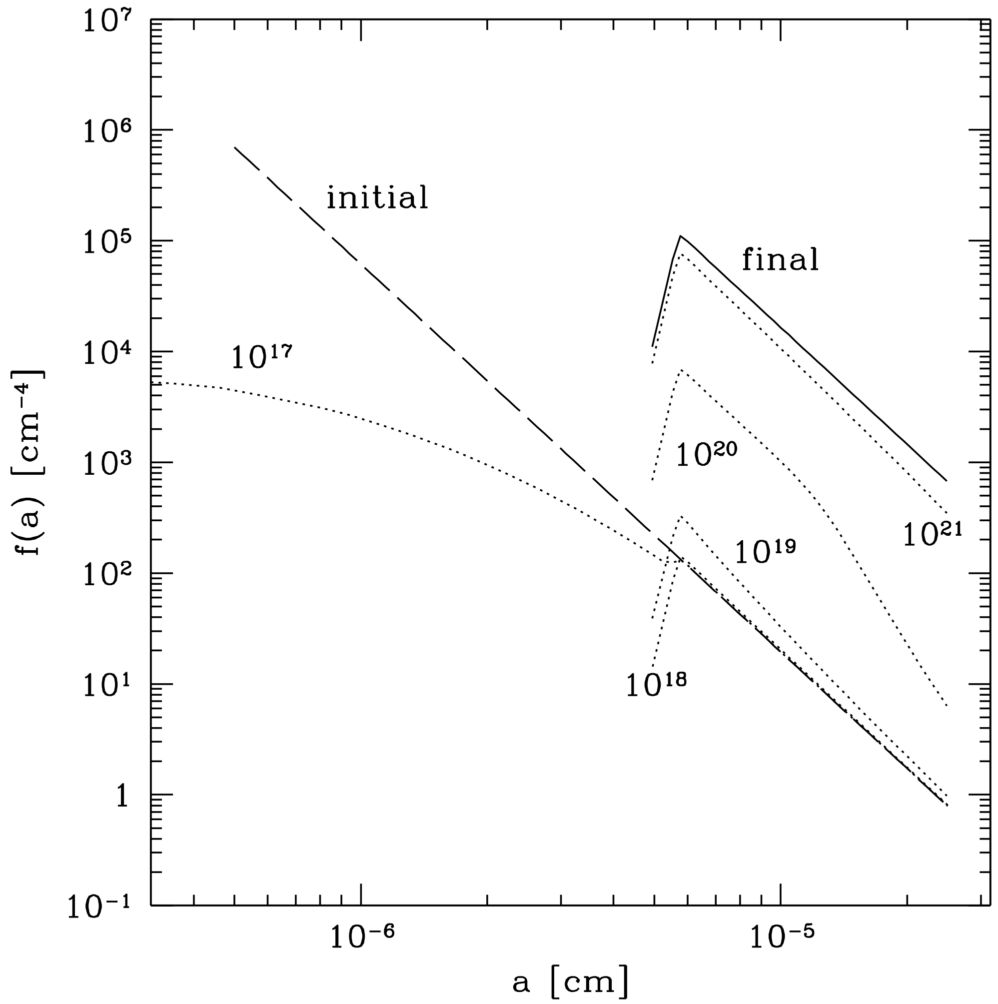

Figure 6.4: Evolution of the grain size distribution as function of the particle radius a. $f(a)$ is depicted at various column densities $N_{\rm H} = 10^m$ cm^{-2} behind the shock front. The dashed line indicates the initial MNR distribution (Mathis et al. 1977). The solid line designates the final grain distribution after all grains have come to rest with respect to the bulk motion of the gas.

6.4.3 Other grain materials

The results presented above apply to silicate grains. Test calculations for other grain materials have also been performed. The results are summarized in Table 6.2 for some characteristic quantities. In the case of pure iron grains no vaporization takes places. This is due to the high emission efficiency of this conductive material. Ice mantles, on the other hand, will vaporize very quickly regardless of their thickness. Obviously, low surface binding energy and IR emissivity of the material leads to poor resistance against vaporization.

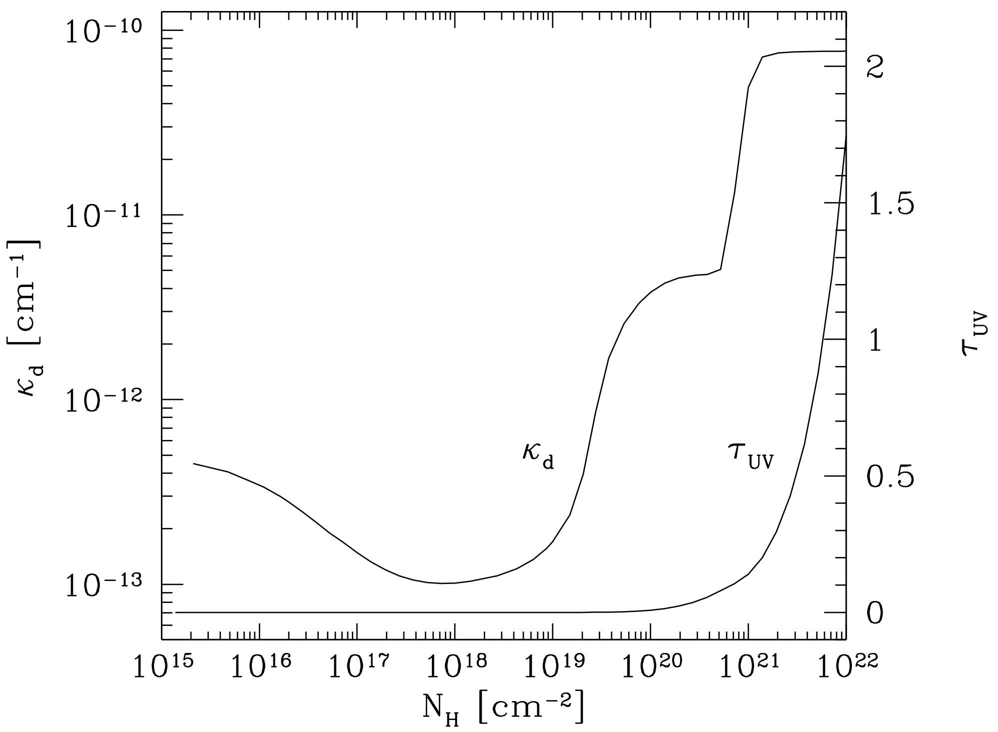

Figure 6.5: Dust opacity κ_d in the large particle limit of Mie theory and corresponding UV optical depth τ_{UV} behind the shock front.

Table 6.2: Summary of the results for several grain materials

	silicate	iron	ice
total dust mass lost	38%	0%	100%
fraction of grains lost	99.7%	0%	100%
fraction of radius sputtered	0.5%	0.5%	n. a.
a_{vap} [cm]	$5\ 10^{-6}$	$< 5\,10^{-7}$	$> 2.5\,10^{-5}$

6.5 Summary

By applying the general method presented in Part I to a protostellar accretion shock, the various processes acting on the grains could be treated simultaneously, taking furthermore into account that grains of different size may move and be processed differently. In this way, a more detailed treatment of such effects as the size dependence of grain deceleration and grain temperature on the processing of the distribution function was achieved.

It was possible not only to compute the final grain size distribution after processing by the shock but also to determine the shape of inbetween size distributions during grain processing, which cannot be described by a power–law. Essentially, it has been found that large grains above a certain limit size $a_{\rm vap}$ remain almost unscathed while those below $a_{\rm vap}$ completely vaporize. In the case of silicate grains 38% of the total dust mass is returned to the gas phase. It seems plausible that most of this material will recondense on the few remaining grains as they settle towards the quiescent midplane of the accretion disk.

Concluding remarks

Realizing the necessity of a general method for describing dust formation and processing without making prior assumptions about the particular physical processes involved, a new computational scheme was derived for modeling the evolution of size distribution functions in stationary one-dimensional flows. Various physical and chemical processes acting differently on particles of different size can be treated simultaneously. Furthermore, a fundamental shortcoming inherent in previous approaches to this subject has been surmounted, that is the particles are not assumed to be comoving but are allowed to exhibit size-dependent hydrodynamical velocities.

The numerical method was applied to several test problems where analytical solutions are known. It is found to be both highly accurate and computationally efficient. This is because the size distribution is discretized on a Lagrange-like grid which moves in size space according to the evolution of selected sample particles. Therefore, the grid is self-adapting to the way the size distribution is evolving. Furthermore, a suitable discretization of the source term for particle coagulation guarantees that physical conservation laws like mass conservation are strictly obeyed.

In Part II of this thesis, the multi-component method was applied to model the formation and processing of cosmic dust grains considering three different astrophysical scenarios. First, dust formation in the cool envelopes around carbon stars was investigated within the framework of a self-consistent model of a stationary dust driven wind. Special attention was paid to a physical description of carbonaceous grain growth according to a hydrogen-abstraction/acetylene-addition surface reaction scheme and to the influence of grain drift motion on the shape of the resulting grain size spectrum. It is found that the consideration of drift results in a considerable distortion of the size distribution as compared to the case of zero drift velocity. Generally, there are less but larger grains if drift is included. The difference in characteristic quantities such as the increase of the mean grain mass and the dust-to-gas ratio injected into the ISM or the decrease of the dust optical depth due to dynamical dilution may amount to 50% for low mass loss models. Concerning the microscopic processes, several effects come into play the most important being the suppression of further growth of large grains with significant drift velocities due to the reduced sticking efficiency of the growth species acetylene.

In a second application, dust growth and coagulation were treated in their mutual dependence. This simultaneous treatment of continuous and discontinuous processes exploits a major advantage of the multi-component method. After identifying the two fundamental parameters determining the relative importance of either process under cosmic conditions a grid of model calculations was presented employing realistic expressions for the description of the sticking properties of the dust and for the turbulence induced relative velocities between particles. In this way, one can obtain a rough estimate of the expected mean particle size and total dust density for arbitrary scenarios without performing time consuming calculations. It is found that continuous growth processes always are very rapid as long as there is condensable material left in the gas phase, while the time scale for coagulation is generally rather long. On the other hand, coagulation can lead to the formation of massive aggregates provided that the product of gas density and available time is sufficiently large. The efficiency of dust coagulation is maximum when the relative velocity between dust particles is equal to the critical velocity for sticking of the constituting grains of the dust aggregates.

Last not least, dust destruction in a protostellar accretion shock was investigated adopting the published structure of a dense molecular shock. The final grain size distribution after processing by the shock was computed as well as the shape of inbetween size distributions during grain processing. Essentially, it is found that large grains above a certain limit size a_{vap} remain almost unscathed while those below a_{vap} completely vaporize. In the case of an MRN distribution of silicate grains (Mathis et al. 1977) 38% of the total dust mass is returned to the gas phase for a shock velocity of 50 km/s.

In summary, it can be said that a powerful tool has been devised and successfully applied to several astrophysical problems. It has to be emphasized though that the multi-component method is in no way restricted to the description of cosmic dust grains. In fact, there is a wide range of promising candidates that can be cast in a form such that this new method is applicable.

Consider, for instance, the solution polymerization in homogeneous reactors (e.g. Ray 1981). The polymer size distribution is affected both by continuous growth of the individual particles and by coalescence of polymers. At a first glance, this problem requires the consideration of a very large number of reaction steps and intermediates. However, the growth process takes the form of a repetitive sequence of reactions which can be lumped together into net reactions between polymers of different size. The problem then is completely analogous to the case considered in Chapter 5. Other potential applications include the modeling of aerosol dynamics, colloidal aggregation, soot formation in laminar premixed flames (Colket & Hall 1994), even RNA replication kinetics in biochemistry (e.g. Biebricher et al. 1987).

An example making full use of the capabilities of the multi-component method is the modeling of the combined coalescence, breakup and evaporation processes occuring in raindrop formation (Brown 1993). Here, the consideration of vertical differential advection due to sedimentation of the drops (Le Cam & Isaka 1989) would exploit the main advantage of the method which was specifically designed to account for size-dependent particle velocities.

Bibliography

[Allamandola *et al.* 1987] Allamandola, L. J., Tielens, A. G. G. M., and Barker, J. R., 1987. The IR emission feature: emission from PAH molecules and amorphous carbon particles. In Léger, A., d'Hendecourt, L. B., and Boccarra, N., editors, *Polycyclic Aromatic Hydrocarbons and Astrophysics*, pages 255–271. D. Reidel Publ. Comp.

[Allen 1973] Allen, C. W., 1973. *Astrophysical Quantities.* The Athlone Press, London.

[Baulch *et al.* 1992] Baulch, D. L., Cobos, C. J., Cox, R. A., Esser, C., Frank, P., Just, T., Kerr, J. A., Pilling, M. J., Troe, J., Walker, R. W., and Warnatz, J., 1992. Evaluated kinetic data for combustion modelling. *J. Phys. Chem. Ref. Data*, **21**, 411–734.

[Beck *et al.* 1992] Beck, H. K. B., Gail, H.-P., Henkel, R., and Sedlmayr, E., 1992. Chemistry in circumstellar shells. I. Chromospheric radiation fields and dust formation in optically thin shells of M-giants. *A&A*, **265**, 626–642.

[Bernstein *et al.* 1995] Bernstein, M. P., Sandford, S. A., Allamandola, L. J., Chang, S., and Scharberg, M. A., 1995. Organic compounds produced by photolysis of realistic interstellar and cometary ice analogs containing methanol. *ApJ*, **454**, 327–344.

[Biebricher *et al.* 1987] Biebricher, C. K., Eigen, M., Gardiner Jr., W. C., Husimi, Y., Keweloh, H.-C., and Obst, A., 1987. Modeling studies of RNA replication and viral infection. In Warnatz, J. and Jäger, W., editors, *Complex chemical reaction systems*, pages 17–38, Springer–Verlag, Berlin.

[Bohren and Huffman 1983] Bohren, C. F. and Huffman, D. R., 1983. *Absorption and Scattering of Light by Small Particles.* John Wiley & Sons, New York.

[Bowen 1988] Bowen, G. H., 1988. Dynamical modelling of long-period variable star atmospheres. *ApJ*, **329**, 299–317.

[Brown 1993] Brown, P. S., Jr., 1993. Analysis and parameterization of the combined coalescence, breakup, and evaporation processes. *J. of the Atmosph. Sci.*, **50**, 2940–2951.

[Cadwell *et al.* 1994] Cadwell, B. J., Wang, H., Feigelson, E. D., and Frenklach, M., 1994. Induced nucleation of carbon dust in red giant stars. *ApJ*, **429**, 285–299.

[Cherchneff *et al.* 1992] Cherchneff, I., Barker, J. R., and Tielens, A. G. G. M., 1992. Polycyclic Aromatic Hydrocarbon formation in carbon-rich stellar envelopes. *ApJ*, **401**, 269–287.

[Chokshi *et al.* 1993] Chokshi, A., Tielens, A. G. G. M., and Hollenbach, D., 1993. Dust coagulation. *ApJ*, **407**, 806–819.

[Colket and Hall 1994] Colket, M. B. and Hall, R. J., 1994. Successes and uncertainties in modeling soot formation in laminar, premixed flames. In Bockhorn, H., editor, *Soot formation in combustion*, pages 442–468, Springer-Verlag, Berlin.

[Daniels and Hughes 1981] Daniels, A. and Hughes, W., 1981. The mass distribution of an accreting system of dust particles – a Monte Carlo simulation. *MNRAS*, **195**, 205–212.

[Dominik 1992] Dominik, C., 1992. *Formation of dust grains in the winds of cool giants.* PhD thesis, Technische Universität, Berlin, FRG.

[Dominik and Tielens 1995] Dominik, C. and Tielens, A. G. G. M., 1995. Resistance to rolling in the adhesive contact of two elastic spheres. *Phil. Mag. A*, **72**, 783–803.

[Dominik and Tielens 1996] Dominik, C. and Tielens, A. G. G. M., 1996. Resistance to sliding on atomic scales in the adhesive contact of two elastic spheres. *Phil. Mag. A*, **73**, 1279–1302.

[Dominik and Tielens 1997] Dominik, C. and Tielens, A. G. G. M., 1997. The Physics of Dust Coagulation and the Structure of Dust Aggregates in Space. *ApJ*, **480**, 647–673.

[Dominik *et al.* 1989] Dominik, C., Gail, H.-P., and Sedlmayr, E., 1989. The size distribution of dust particles in a dust-driven wind. *A&A*, **223**, 227–236.

[Dominik *et al.* 1990] Dominik, C., Gail, H.-P., Sedlmayr, E., and Winters, J. M., 1990. HR diagrams for dust driven winds around C-stars. *A&A*, **240**, 365–375.

[Dominik *et al.* 1993] Dominik, C., Sedlmayr, E., and Gail, H.-P., 1993. Dust formation in stellar winds. VI. Moment equations for the formation of heterogeneous and core-mantle grains. *A&A*, **277**, 578–594.

[Donn and Nuth 1985] Donn, B. and Nuth, J. A., 1985. Does nucleation theory apply to the formation of refractory circumstellar grains? *ApJ*, **288**, 187–190.

[Dorschner 1982] Dorschner, J., 1982. Interstellar grain size spectrum and circumstellar grain-grain collisions. *Ap&SS*, **81**, 323–328.

[Draine 1980] Draine, B. T., 1980. Interstellar shock waves with magnetic precursors. *ApJ*, **241**, 1021–1038.

[Draine 1985] Draine, B. T., 1985. Tabulated optical properties of graphite and silicate grains. *ApJS*, **57**, 587–594.

[Draine 1995] Draine, B. T., 1995. Grain destruction in interstellar shock waves. *Ap&SS*, **233**, 111–123.

[Fleischer *et al.* 1992] Fleischer, A. J., Gauger, A., and Sedlmayr, E., 1992. Circumstellar Dust shells around Long-period Variables. I. Dynamical models of C-stars including dust formation, growth and evaporation. *A&A*, **266**, 321–339.

[Frantsman and Eglitis 1988] Frantsman, Y. L. and Eglitis, I. E., 1988. The [C/O] ratio in N stars: observations and theory. *SvA*, **14**, L109–L111.

[Frenklach and Feigelson 1989] Frenklach, M. and Feigelson, E. D., 1989. Formation of polycyclic aromatic hydrocarbons in circumstellar envelopes. *ApJ*, **341**, 372–384.

[Fulle 1992] Fulle, M., 1992. A dust-tail model based on Maxwellian velocity distribution. *A&A*, **265**, 817–824.

[Gail and Sedlmayr 1984] Gail, H.-P. and Sedlmayr, E., 1984. Formation of crystalline and amorphous carbon grains. *A&A*, **132**, 163–167.

[Gail and Sedlmayr 1985] Gail, H.-P. and Sedlmayr, E., 1985. Dust formation in stellar winds. II. Carbon condensation in stationary, spherically expanding winds. *A&A*, **148**, 183–190.

[Gail and Sedlmayr 1987] Gail, H.-P. and Sedlmayr, E., 1987. Dust formation in stellar winds. III. Self-consistent models for dust-driven winds around C-stars. *A&A*, **171**, 197–204.

[Gail and Sedlmayr 1988] Gail, H.-P. and Sedlmayr, E., 1988. Dust formation in stellar winds. IV. Heteromolecular carbon grain formation and growth. *A&A*, **206**, 153–168.

[Gail *et al.* 1984] Gail, H.-P., Keller, R., and Sedlmayr, E., 1984. Dust formation in stellar winds. I. A rapid computational method and application to graphite condensation. *A&A*, **133**, 320–332.

[Gauger *et al.* 1990] Gauger, A., Gail, H.-P., and Sedlmayr, E., 1990. Dust formation, growth and evaporation in a cool pulsating circumstellar shell. *A&A*, **235**, 345–361.

[Gehrz 1989] Gehrz, R. D., 1989. Sources of stardust in the galaxy. In Allamandola, L. J. and Tielens, A. G. G. M., editors, *Interstellar Dust*, pages 445–453, Kluwer Academic Publishers, Dordrecht.

[Goeres *et al.* 1988] Goeres, A., Henkel, R., Sedlmayr, E., and Gail, H.-P., 1988. Nonequilibrium Chemistry in Circumstellar Shells. *Rev. Mod. Astron.*, **1**, 231–248.

[Goeres *et al.* 1996] Goeres, A., Keller, R., Sedlmayr, E., and Gail, H.-P., 1996. Circumstellar Carbon Condensation: I. Low-p,T stabilities of Polyatomic Hydrocarbons. *Polycyclic Aromatic Compounds*, **8**, 129–165.

[Hairer *et al.* 1987] Hairer, E., Nørsett, S. P., and Wanner, G., 1987. *Solving Ordinary Differential Equations I.* Springer–Verlag, Berlin.

[Hayakawa and Hayakawa 1988] Hayakawa, H. and Hayakawa, S., 1988. Power-law size distribution of dust grains. *PASJ*, **40**, 341–345.

[Hayashi and Nakagawa 1975] Hayashi, C. and Nakagawa, Y., 1975. Size distribution of grains growing by thermal grain–grain collisisions. *Prog. Theor. Phys.*, **54**, 93–103.

[Head-Gordon and Tully 1992] Head-Gordon, M. and Tully, J. C., 1992. Competition between static and dynamical effects in adsorption: sticking of Ar on Ar-covered Ru(001). *Surf. Sci.*, **268**, 113–126.

[Hollenbach and McKee 1979] Hollenbach, D. and McKee, F., 1979. Molecule formation and infrared emission in fast interstellar shocks. I. Physical processes. *ApJS*, **41**, 555–592.

[Jenniskens *et al.* 1993] Jenniskens, P., Baratta, G. A., Kouchi, A., de Groot, M. S., Greenberg, J. M., and Strazulla, G., 1993. Carbon dust formation on interstellar grains. *A&A*, **273**, 583–600.

[Jones *et al.* 1994] Jones, A. P., Tielens, A. G. G. M., Hollenbach, D. J., and McKee, C. F., 1994. Grain destruction in shocks in the interstellar medium. *ApJ*, **433**, 797–810.

[Jones *et al.* 1996] Jones, A. P., Tielens, A. G. G. M., and Hollenbach, D. J., 1996. Grain shattering in shocks: The interstellar grain size distribution. *ApJ*, **469**, 740–764.

[Jura 1986] Jura, M., 1986. Mass loss from carbon stars. *ApJ*, **303**, 327–332.

[Jura 1994] Jura, M., 1994. The particle–size distribution in the dust ejected from IRC +10216. *ApJ*, **434**, 713–718.

[Keller 1987] Keller, R., 1987. Polyaromatic hydrocarbons and the condensation of carbon in stellar winds. In Léger, A., d'Hendecourt, L., and Boccara, N., editors, *Polycyclic Aromatic Hydrocarbons and Astrophysics*, pages 387–397, D. Reidel Publ. Comp., Dordrecht.

[Kessel'man and Frolov 1986] Kessel'man, V. S. and Frolov, A. B., 1986. The grain-size spectrum in a protostellar cloud. *SvA*, **30**, 284.

[Knapp 1985] Knapp, G. R., 1985. Mass Loss from evolved stars. IV. The dust-to-gas ratio in the envelopes of Mira variables and carbon stars. *ApJ*, **293**, 273–280.

[Knapp 1987] Knapp, G. R., 1987. Mass loss from carbon stars – Observations of the CO millimeter wavelength rotational lines. In Kwok, S. and Pottasch, S. R., editors, *Late Stages of Stellar Evolution*, pages 103–118, D. Reidel Publ. Comp., Dordrecht.

[Kozasa *et al.* 1984] Kozasa, T., Hasegawa, H., and Seki, J., 1984. Grain formation in the expanding gas flow around cool luminous stars. *Ap&SS*, **98**, 61–79.

[Krüger and Sedlmayr 1996] Krüger, D. and Sedlmayr, E., 1996. The size distribution of stardust injected into the ISM. In Kress, M. E., Tielens, A. G. G. M., and Pendleton, Y. J., editors, *From Stardust to Planetesimals: Contributed Papers*, pages 77–80, Moffett Field.

[Krüger and Sedlmayr 1997] Krüger, D. and Sedlmayr, E., 1997. Two–fluid models for stationary dust driven winds. II. The size distribution of dust grains in consideration of drift. *A&A*, **321**, 557–567.

[Krüger *et al.* 1994] Krüger, D., Gauger, A., and Sedlmayr, E., 1994. Two–fluid models for stationary dust–driven winds. I. Momentum and energy balance. *A&A*, **290**, 573–589.

[Krüger *et al.* 1996] Krüger, D., Patzer, A. B. C., and Sedlmayr, E., 1996. On the growth of carbonaceous grains in circumstellar envelopes. *A&A*, **313**, 891–896.

[Kwok 1975] Kwok, S., 1975. Radiation pressure on grains as a mechanism for mass loss in red giants. *ApJ*, **198**, 583–591.

[Lafon and Berruyer 1991] Lafon, J.-P. and Berruyer, N., 1991. Mass loss mechanisms in evolved stars. *A&AR*, **2**, 249–289.

[Le Cam and Isaka 1989] Le Cam, M. N. and Isaka, H., 1989. Numerical simulation of raindrop spectra: effects of vertical differential advection of raindrops. *J. of Atmosph. Res.*, **22**, 307–321.

[Lenzuni *et al.* 1995] Lenzuni, P., Gail, H.-P., and Henning, T., 1995. Dust evaporation in protostellar cores. *ApJ*, **447**, 848–862.

[Liffman 1990] Liffman, K., 1990. The effect of catastrophic collisional fragmentation and diffuse medium accretion on a computational medium. *ApJ*, **355**, 518–535.

[Liffman and Clayton 1989] Liffman, K. and Clayton, D. D., 1989. Stochastic evolution of refractory interstellar dust during the chemical evolution of a 2-phase interstellar medium. *ApJ*, **340**, 853–868.

[Lissauer and Stewart 1993] Lissauer, J. J. and Stewart, G. R., 1993. Growth of planets from planetesimals. In Levy, E. H. and Lunine, J. I., editors, *Protostars and Planets III*, pages 1061–1088, The University of Arizona Press, Tucson.

[Lucy 1971] Lucy, L. B., 1971. The formation of resonance lines in extended atmospheres. *ApJ*, **163**, 95–110.

[MacGregor and Stencel 1992] MacGregor, K. B. and Stencel, R. E., 1992. On the interaction between dust and gas in late-type stellar atmospheres and winds. *ApJ*, **397**, 644–651.

[Maron 1990] Maron, N., 1990. Optical properties of fine amorphous carbon grains in the infrared region. *Ap&SS*, **172**, 21–28.

[Mathis *et al.* 1977] Mathis, J. S., Rumpl, W., and Nordsieck, K. H., 1977. The size distribution of interstellar grains. *ApJ*, **217**, 425–433.

[McKee *et al.* 1987] McKee, C. F., Hollenbach, D. J., Seab, C. G., and Tielens, A. G. G. M., 1987. The structure of time-dependent interstellar shocks and grain destruction in the interstellar medium. *ApJ*, **318**, 674–701.

[Mihalas and Weibel Mihalas 1984] Mihalas, D. and Weibel Mihalas, B., 1984. *Foundations of Radiation Hydrodynamics*. Oxford University Press.

[Millar *et al.* 1991] Millar, T. J., Rawlings, J. M. C., Bennett, A., Brown, P. D., and Charnley, S. B., 1991. Gas phase reactions and rate coefficients for use in astrochemistry. The UMIST ratefile. *A&AS*, **87**, 585–619.

[Mizuno *et al.* 1988] Mizuno, H., Markiewicz, W. J., and Völk, H. J., 1988. Grain growth in turbulent protoplanetary accretion disks. *A&A*, **195**, 183–192.

[Nejad and Millar 1987] Nejad, L. A. M. and Millar, T. J., 1987. Chemical modelling of molecular sources V. IRC + 10216. *A&A*, **183**, 279–286.

[Netzer and Elitzur 1993] Netzer, N. and Elitzur, M., 1993. The dynamics of stellar outflows dominated by interaction of dust and radiation. *ApJ*, **410**, 701–713.

[Neufeld and Hollenbach 1994] Neufeld, D. A. and Hollenbach, D. J., 1994. Dense molecular shocks and accretion onto protostellar disks. *ApJ*, **428**, 170–185.

[Ogmen and Duley 1988] Ogmen, M. and Duley, W. W., 1988. Laboratory synthesis of hydrogenated amorphous carbon films. *ApJ*, **334**, L117–L120.

[Ohtsuki *et al.* 1990] Ohtsuki, K., Nakagawa, Y., and Nakazawa, K., 1990. Artificial acceleration in accumulation due to coarse mass-coordinate divisions in numerical simulation. *Icarus*, **83**, 205–215.

[Olofsson *et al.* 1993] Olofsson, H., Eriksson, K., Gustafsson, B., and Carlström, U., 1993. A study of circumstellar envelopes around bright carbon stars. I. Structure, kinematics, and mass loss rate. *ApJS*, **87**, 267–304.

[Ossenkopf 1993] Ossenkopf, V., 1993. Dust coagulation in dense molecular clouds: the formation of fluffy aggregates. *A&A*, **280**, 617–646.

[Ossenkopf 1994] Ossenkopf, V., 1994. *Koagulation und optische Wirkung inhomogener Staubteilchen in dichten Molekülwolken.* PhD thesis, Friedrich-Schiller-Universität, Jena.

[Parker 1960] Parker, E. N., 1960. The hydrodynamic treatment of the expanding solar corona. *ApJ*, **132**, 175–183.

[Pollack *et al.* 1994] Pollack, J., Hollenbach, D., Beckwith, S., Simonelli, D., Roush, T., and Fong, W., 1994. Composition and radiative properties of grains in molecular clouds and accretion disks. *ApJ*, **421**, 615–639.

[Press *et al.* 1992] Press, W. H., Teukolsky, S. A., Vetterling, W. T., and Flannery, B. P., 1992. *Numerical Recipes.* Cambridge University Press, 2nd edition.

[Ray 1981] Ray, W. H., 1981. Dynamic behaviour of polymerization reactors. In Ebert, K. H., Deuflhard, P., and Jäger, W., editors, *Modelling of chemical reaction systems*, pages 337–354, Springer–Verlag, Berlin.

[Rossi *et al.* 1991] Rossi, S. C. F., Benevides-Soares, P., and Barbuy, B., 1991. Grain coagulation in contracting protostellar clouds. *A&A*, **251**, 587–596.

[Rowan-Robinson and Harris 1982] Rowan-Robinson, M. and Harris, S., 1982. Radiative transfer in dust clouds — II. Circumstellar dust shells around early M giants and supergiants. *MNRAS*, **200**, 197–215.

[Ruden *et al.* 1990] Ruden, P. S., Glassgold, A. E., and Shu, F. H., 1990. Thermal structure of neutral winds from young stellar objects. *ApJ*, **361**, 546–569.

[Safrononv 1962] Safrononv, V. S., 1962. A particular solution of the coagulation equation. *Doklady Akad. Nauk SSSR*, **147**, 64–66.

[Sahai 1990] Sahai, R., 1990. A new self-consistent model of circumstellar CO emission for deriving mass-loss rates in red giants. I. The carbon-rich star U Camelopardalis. *ApJ*, **362**, 652–662.

[Scholz and Tsuji 1984] Scholz, M. and Tsuji, T., 1984. The effects of spherical extension upon the photospheric structure and spectrum of red giants: comparison of M and C stars. *A&A*, **130**, 11–18.

[Seab 1987] Seab, C. G., 1987. Grain destruction, formation, and evolution. In Hollenbach, D. J. and Thronson, H. A., Jr., editors, *Interstellar processes*, pages 491–512, D. Reidel Publ. Comp., Dordrecht.

[Seab and Shull 1983] Seab, C. G. and Shull, J. M., 1983. Shock processing of interstellar grains. *ApJ*, **275**, 652–660.

[Sedlmayr 1989] Sedlmayr, E., 1989. Dust condensation in stellar outflows. In Allamandola, L. J. and Tielens, A. G. G. M., editors, *Interstellar Dust*, pages 467–477. Kluwer Academic Publishers, Dordrecht.

[Sedlmayr 1994] Sedlmayr, E., 1994. From molecules to grains. In Jørgensen, U. G., editor, *IAU Colloquium 146: Molecules in the Stellar Environment*, pages 163–185, Springer–Verlag, Berlin.

[Sedlmayr and Dominik 1995] Sedlmayr, E. and Dominik, C., 1995. Dust driven winds. *Space Sci. Rev.*, **73**, 211–272.

[Sellgren *et al.* 1983] Sellgren, K., Werner, M. W., and Dinerstein, H. L., 1983. Extended near-infrared emission from visual reflection nebulae. *ApJ*, **271**, L13–L17.

[Smoluchowsky 1916] Smoluchowsky, M., 1916. Drei Vorträge über Diffusion, Brownsche Molekularbewegung und Koagulation von Kolloidteilchen. *Phys. Zeits.*, **17**, 557–571,585–599.

[Smoluchowsky 1917] Smoluchowsky, M., 1917. Versuch einer mathematischen Theorie der Koagulationskinetik kolloidaler Lösungen. *Z. Phys. Chemie*, **92**, 129–168.

[Spitzer 1976] Spitzer, L., 1976. High-velocity interstellar clouds. *Comments on Astrophys. and Sp. Phys.*, **6**, 177–187.

[Tielens 1983] Tielens, A. G. G. M., 1983. Stationary flows in the circumstellar envelopes of M giants. *ApJ*, **271**, 702–716.

[Tielens 1989] Tielens, A. G. G. M., 1989. Dust in dense clouds. In Allamandola, L. J. and Tielens, A. G. G. M., editors, *Interstellar Dust*, pages 239–262, Kluwer Academic Publishers, Dordrecht.

[Tielens *et al.* 1994] Tielens, A. G. G. M., McKee, C. F., Seab, C. G., and Hollenbach, D. J., 1994. The physics of grain–grain collisions and gas–grain sputtering in interstellar shocks. *ApJ*, **431**, 321–340.

[Völk *et al.* 1980] Völk, H. J., Jones, F. C., Morfill, G. E., and Röser, S., 1980. Collisions between grains in a turbulent gas. *A&A*, **85**, 316–325.

[Weast *et al.* 1988] Weast, R. C., Astle, M. J., and Beyer, W. H., editors, 1988. *CRC Handbook of Chemistry and Physics*. CRC Press, Inc., Boca Raton, Florida, 69^{th} edition.

[Weidenschilling and Ruzmaikina 1994] Weidenschilling, S. J. and Ruzmaikina, T. V., 1994. Coagulation of grains in static and collapsing protostellar clouds. *ApJ*, **430**, 713–726.

[Wetherill 1990] Wetherill, G. W., 1990. Comparison of analytical and physical modeling of planetesimal accumulation. *Icarus*, **88**, 336–354.

[Wetherill and Stewart 1989] Wetherill, G. W. and Stewart, G. R., 1989. Accumulation of a swarm of small particles. *Icarus*, **77**, 330–357.

[Winters *et al.* 1994] Winters, J. M., Dominik, C., and Sedlmayr, E., 1994. Theoretical spectra of circumstellar dust shells around carbon-rich asymptotic giant branch stars. *A&A*, **288**, 255–272.

[Woitke 1992] Woitke, P., 1992. Staubbildung in der Supernova 1987 A. Master's thesis, Technische Universität, Berlin.

[Woitke *et al.* 1993] Woitke, P., Dominik, C., and Sedlmayr, E., 1993. Dust destruction in the transition region between stellar wind and interstellar medium. *A&A*, **274**, 451–464.

Danksagung

Die Zeit der Promotion war ein langer Weg, der ohne die Hilfe vieler Leute ungleich steiniger gewesen wäre. Ich bedanke mich besonders bei Prof. Dr. Sedlmayr, der mir überhaupt erst die Möglichkeit eröffnete, als Assistent ans Institut zu kommen und meine wissenschaftlichen Forschungen auch nach dem Diplom fortzusetzen. Ich habe in dieser Zeit viel mehr gelernt als "nur" Astrophysik. Stets durfte ich meinen eigenen Ideen folgen. Dieses Vertrauen weiß ich sehr zu schätzen.

Diese Arbeit wäre nicht zustandegekommen ohne die durch offene Türen geprägte Arbeitsatmosphäre, in der *jeder* Kollege sofort bereit war, mit seinem Fachwissen auszuhelfen, Fragen zu beantworten und vorhandene Daten und Computerprogramme zur Verfügung stellen. Uwe Bolick bringe ich für seinen ehrenamtlichen Einsatz als Sys-Op die größte Hochachtung entgegen.

Vielen Dank auch an den P-N 801. Eure "aufmunternden" Kommentare haben mich in den ersten Jahren immer wieder angestachelt, nicht aufzugeben und meine Anstrengungen zu verstärken.

Mein ehemaliger Schreibtischnachbar Holger Beck hat dafür gesorgt, daß auch zwischendurch ein kleines Schwätzchen über ganz banale Themen möglich war. Unser steter Austausch beim Konzipieren des Numerikums war mir ebenfalls sehr wichtig.

Ein steter Quell der Inspiration und wichtigster Ansprechpartner in wissenschaftlichen Fragen war Peter Woitke, dem ich insbesondere auch für das Korrekturlesen dieser Dissertation danke. Unsere Zusammenarbeit war sehr fruchtbar, und Du hast mit Deinen unbequemen Fragen dazu beigetragen, daß unsere gemeinsame Idee des Mehrkomponentenverfahrens reifen konnte. Schön, daß Du und Jürgen mich auch in den letzten Wochen vor der Abgabe ertragen habt.

Meiner Kollegin Beate Patzer, der guten Seele des Instituts, gilt mein besonderer Dank. Auch in meiner schwersten Zeit hast Du mir kompromißlos beigestanden und geholfen wo Du konntest — ohne zu fragen und ohne gefragt worden zu sein. Und das ganz selbstlos, auch wenn es nicht um unsere gemeinsamen Forschungsprojekte ging.

Lebenslauf

Daniel Krüger

24.8.1966	geboren in Berlin
Familienstand	ledig

Ausbildung:

August 1973 – Juli 1977	Scharmützelsee-Grundschule, Berlin
September 1977 – Juli 1983	Goethe-Gymnasium, Berlin
August 1983 – Juli 1986	Oberstufenzentrum für Chemie, Physik und Biologie, Berlin Erfolgreiche Teilnahme an zahlreichen Schülerwettbewerben, darunter Landessieg im Wettbewerb "Jugend forscht" 1986 Allgemeine Hochschulreife 19.7.1986
Oktober 1986 – Oktober 1988	Grundstudium Physik an der TU Berlin Vordiplom 13.10.88
Oktober 1988 – Juli 1989	Auslandsstudium am King's College London
Oktober 1989 – August 1993	Hauptstudium Physik an der TU Berlin Studienschwerpunkte Astrophysik und Numerik Diplom 6.8.93
Seit Oktober 1993	Wissenschaftlicher Mitarbeiter mit Lehraufgaben am Institut für Astronomie und Astrophysik der TU Berlin

Berufsrelevante Tätigkeiten:

Frühjahr und Sommer 1988	13-wöchiges Industriepraktikum bei der Fa. Siemens AG Berlin
Seit März 1994	Teilnahme an Workshops und Sommerschulen aus dem Bereich Scientific Computing
Seit April 1994	Veröffentlichung diverser Fachartikel und Tagungsbeiträge
Seit Oktober 1995	Mitarbeit in Universitätsgremien (Ausbildungskommission, Rat des Zentralen Rechenzentrums)
Seit Mai 1996	Aufbau und Installation des institutseigenen PC-Pools unter Windows 95

Besondere Kenntnisse:

Englisch fließend in Wort und Schrift
Schulkenntnisse in Französisch (vertieft durch Weiterbildungskurse an der TU Berlin)
Langjährige Programmiererfahrung in FORTRAN sowie erweiterte Grundkenntnisse in C/C++
Erfahrung in der Anwendung von Standardsoftware unter UNIX und MS-Windows

Außeruniverstäre Aktivitäten:

Baseball (Spieler auf Verbandsliga-Ebene, Schiedsrichtertätigkeit)

Berlin, 2. Juli 1997